JAERI-Data/Code
98-018

CASKET:
A COMPUTER CODE SYSTEM FOR THERMAL AND STRUCTURAL ANALYSES OF RADIOACTIVE MATERIAL TRANSPORT AND/OR STORAGE CASK

May 1998

Takeshi IKUSHIMA

日本原子力研究所
Japan Atomic Energy Research Institute

本レポートは，日本原子力研究所が不定期に公刊している研究報告書です。
入手の問合わせは，日本原子力研究所研究情報部研究情報課（〒319-1195　茨城県那珂郡東海村）あて，お申し越しください。なお，このほかに財団法人原子力弘済会資料センター〒319-1195　茨城県那珂郡東海村日本原子力研究所内）で複写による実費頒布をおこなっております。

This report is issued irregularly.
Inquiries about availability of the reports should be addressed to Research Information Division, Department of Intellectual Resources, Japan Atomic Energy Research Institure, Tokai-mura, Naka-gun, Ibaraki-ken 319-1195, Japan.

編集兼発行　日本原子力研究所

JAERI−Data/Code 98−018

CASKET : A Computer Code System for Thermal and Structural Analyses of Radioactive Material Transport and/or Storage Cask

Takeshi IKUSHIMA

Department of Fuel Cycle Safety Research
Nuclear Safety Research Center
Tokai Research Establishment
Japan Atomic Energy Research Institute
Tokai-mura, Naka-gun, Ibaraki-ken

(Received April 3, 1998)

A computer code system CASKET (CASK thermal and structural analyses and Evaluation code system) for the thermal and structural analyses which are indispensable for radioactive material transpot and/or storage cask designs has been developed. The CASKET is a simplified computer code system to perform parametric analyses on sensitivity evaluations in designing a cask and conducting its safety analysis. Main features of the CASKET are as follow: (1) it is capable to perform impact analysis of casks with shock absorbers, (2) it is capable to perform impact analysis of casks with fins. (3) puncture analysis of casks is capable, (4) rocking analysis of casks during seismic load is capable, (5) material property data library are provided for impact analysis of casks, (6) material property data library are provided for thermal analysis of casks, (7) fin energy absorption data library are provided for impact analysis of casks with fins are and (8) not only main frame computers (OS MSP) but also work stations (OS UNIX) and personal computers (OS Windows 3.1) are available. In the paper, brief illustrations of calculation methods are presented. Some calculation results are compared with experimental ones to confirm the computer programs are useful for thermal and structural analyses.

Keywords: Computer Program, Impact Analysis, Drop Impact, Fin Impact Analysis, Rocking Analysis, Data Library, Transport Cask, Storage Cask

JAERI－Data/Code 98－018

CASKET：放射性物質輸送・貯蔵容器の熱・構造安全解析コードシステム

日本原子力研究所東海研究所安全性試験研究センター燃料サイクル安全工学部
幾島　毅

（1998年4月3日受理）

放射性物質輸送・貯蔵容器の安全解析において重要な部分である熱・構造解析のためのコードシステムCASKETを開発した。CASKETは設計や安全解析における感度解析をパラメトッリクに容易に実施するための簡易解析コードシステムである。CASKET主要な特徴は次の通りである。(1) ショックアブソーバ付き輸送容器の衝突解析が可能である。(2) フィン付き輸送容器の衝突解析が可能である。(3) 輸送容器の貫通解析が可能である。(4) 輸送・貯蔵容器の地震時のロッキング解析が可能である。(5) 衝突解析用の材料特性データライブラリが用意されている。(6) 熱伝導解析用の材料特性データライブラリーが用意されている。(7) フィン吸収エネルギーデータライブラリーが用意されている。(8) 大型計算機（OS MSP）以外にもワークステーション（OS UNIX）およびパーソナルコンピュータ(OS Windows 3.1)によっても使用できる。本報告書は計算手法の解説及び解析結果を実験結果と比較してプログラムの妥当性を検討したものである。

東海研究所：〒319-1195　茨城県那珂郡東海村白方白根2-4

Contents

目　　次

1. Introduction

Radioactive material transport casks(IAEA regulatory standard type B pckages, type A fissile packages and so on) are required to maintain integrity against the nine meters free drop test onto unyield target, the puncture test dropped onto a 150 mm diameter mild steel bar from a height of one meter and so on.

In the drop analyses for radioactive transport casks, it has become possible to perform them in detail calculation by using interaction evaluation computer programs, DYNA2D[1], DYNA3D[2], NIKE2D[3], NIKE3D[4], PISCES[5] and HONDO[6]. However, the considerable cost and the computer time are necessitated to perform analyses by these programs. To decrease the cost and the time, a simplified computer code system CASKET shown in Fig. 1.1 has been developed[7],[8]. The CASKET is a static calculation code system. The CASKET is capable of evaluating the acceleration and the deformation of cask bodies and the stress and the deformation of puncture bars.

Main features of the computer program CASKET are as follows:

(1) it is capable to perform impact analysis of casks with shock absorbers,

(2) it is capable to perform impact analysis of casks with fins,

(3) puncture analysis of casks is capable,

(4) rocking analysis of casks during seismic load is capable,

(5) material property data library are provided for impact analysis of casks,

(6) material property data library are provided for thermal analysis of casks,

(7) fin energy absorption data library are provided for impact analysis of casks with fins and

(8) not only main frame computers (OS MSP) but also work stations (OS UNIX) and personal computers (OS Windows 3.1) are available for use of CASKET.

In the paper, brief descriptions, calculation methods, benchmark calculations and data libraries of the CASKET, are presented.

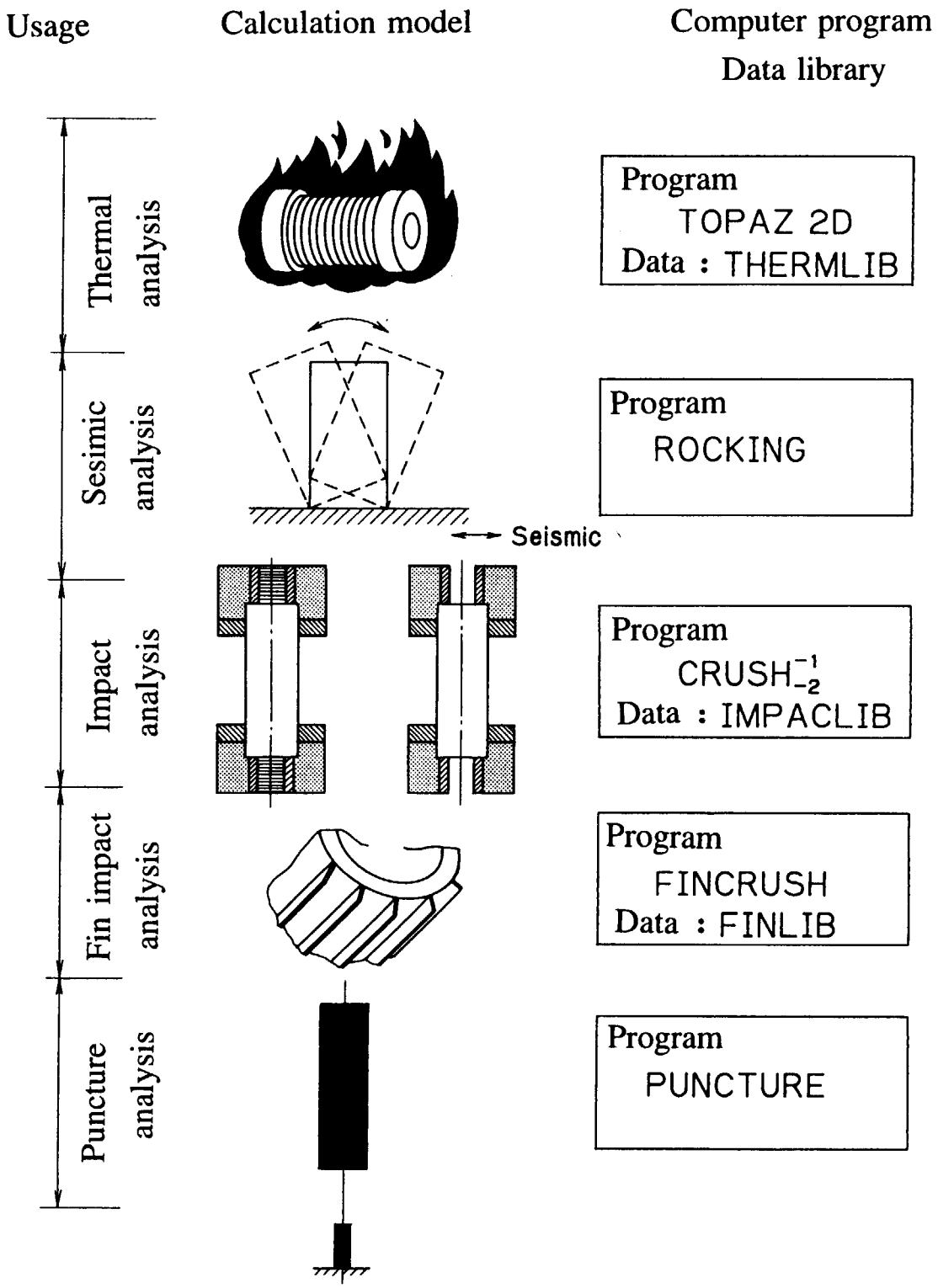

Fig. 1.1 Thermal and structural safety analysis code system CASKET

2. TOPAZ2D

A heat conduction computer program TOPAZ2D[9] is based on a two-dimensional implicit finite element method. The TOPAZ2D has been developed by Shapiro in LLNL.

The TOPAZ2D can be used to solve for the steady state or transient temperature field on two-dimensional planar or axisymmetric geometries. Material properties may be temperature dependent and either isotropic or orthotropic. A variety of time and temperature dependent boundary conditions can be specified including temperature, flux, convection and radiation. By implementing the user subroutine feature, users can model chemical reaction kinetics and allow for any type of functional representation of boundary conditions and internal heat generation. The TOPAZ2D can solve problems of diffuse band radiation in an enclosure coupled with conduction in the material surrounding the closure. Additional features include thermal contact resistance across an interface, bulk fluids, phase change and energy balances.

Thermal stresses can be calculated using the solid mechanics computer programs SAP4[10], NIKE2D or so on. The TOPAZ2D has no general mesh generation capability. Rows of evenly spaced nodes and rows of sequential elements may be generated. For complex zoning, the mesh generation program and preprocessor MAZE[11] should be used. The ORION[12] interactive post-processor can be used to provide temperature contour, temperature-time history and various geometry plots.

3. CRUSH

3.1 Description of CRUSH program

In the drop impact analyses for radioactive transport casks, it has become possible to perform them in detail by using interaction evaluation, computer programs. However, the considerable cost and computer time are necessitated to perform analyses by these programs. To meet the above reguirements, simplified computer programs CRUSH1[13] and CRUSH2[14] have been developed. The CRUSH1 and CRUSH2 are static calculation computer programs capable of evaluating the maximum acceleration of cask bodies and the maximum deformation of shock absorbers using a Uniaxial Displacement Method (UDM)[15].

3.2 Calculation equation

3.2.1 Calculation model

In the modeling of shock absorber, it is assumed that the shock absorber consists of three or four species of material as shown in Figs.3.1 to 3.3. In the figures, the symbols of K_i(i=1 ~ 5) indicate boundary condition constants which are estimated by an overpack stiffness and boundary condition of the shock absorber.

When the shock absorber deforms by the displacement $\Delta \ell$ in a corner drop as shown in Fig.3.4, the strain ε of a one-dimensional bar is

$$\varepsilon=\frac{\Delta \ell}{\ell} \quad . \tag{3.1}$$

The force f of the one-dimensional bar is

$$f=K\sigma(\varepsilon)\Delta A \ , \tag{3.2}$$

where ℓ, σ and ΔA are the length, stress and area of the one-dimensional bar. K is the boundary condition constant. The total force F of the shock absorber is

$$F=\sum_i f_i \ . \tag{3.3}$$

The dissipated energy $E(\delta)$ can be also obtained using equation similar to above Eq.(3.3)

$$E(\delta)=\int_0^{\delta} F \ dl \ . \tag{3.4}$$

Therefore, when a cask whose weight of W is dropped from a height H with an oblique angle θ, the maximum displacement of the shock absorber δ and the maximum acceleration of the cask body α are given as follows.

$$E(\delta)= \gamma \cdot W \cdot H \ , \tag{3.5}$$

$$\alpha=\frac{F(\delta)}{M} , \tag{3.6}$$

where γ is the ratio of the energy absorbed in the primary impact to the total energy absorbed in the primary and secondary impacts. M is mass of the cask.

3.2.2 Vertical drop impact

In the modeling a shock absorber in CRUSH, it is assumed that the shock absorber consists of three or four species of shock absorber materials as shown in Fig.3.5. In the figure, the symbols of σ_A, σ_B, σ_C, σ_D indicate their materials determined by the geometries of the cask and the shock absorber.

When the shock absorber deforms by a displacement Z in a vertical drop, the impact load F and the dissipated energy E are given by following equations.

$$F=F_{01}+F_{12}+F_{23}+F_{34}+F_{45} , \tag{3.7}$$

$$E=\int_0^Z F\,dZ , \tag{3.8}$$

where, for the region 0 ~ R_1

$$F_{01}=K_1\ \pi\ \sigma_D\left(\frac{Z}{Z_2}\right)R_1^2 , \tag{3.9}$$

for the region R_1 ~ R_2

$$F_{12}=K_2\ \pi\ \sigma_A\left(\frac{Z}{Z_2}\right)(R_2^2-R_1^2) , \tag{3.10}$$

for the region R_2 ~ R_3

$$F_{23}=K_3\ \pi\ \sigma_B\left(\frac{Z}{Z_2}\right)(R_3^2-R_1^2) , \tag{3.11}$$

for the region R_3 ~ R_4

$$\left.\begin{aligned} F_{34}&=K_4\ \pi\ \sigma_B\left(\frac{\Delta Z_B}{Z_3}\right)(R_4^2-R_3^2);(\text{for } \sigma_B \text{ material}),\\ F_{34}&=K_4\ \pi\sigma_C\left(\frac{\Delta Z_C}{Z_4-Z_3}\right)(R_4^2-R_3^2);(\text{for } \sigma_C \text{ material}),\end{aligned}\right\} \tag{3.12}$$

$$\left.\begin{aligned} &Z=\Delta Z_B+\Delta Z_C, \\ &\sigma_B\left(\frac{\Delta Z_B}{Z_3}\right)=\sigma_C\left(\frac{\Delta Z_C}{Z_4-Z_3}\right), \end{aligned}\right\} \tag{3.13}$$

for the region $R_4 \sim R_5$

$$\left.\begin{aligned} &F_{45}=K_5\ \pi\ \sigma_B\left(\frac{\Delta Z_B}{Z_3}\right)(R_5^2-R_4^2);(\text{for } \sigma_B \text{ material}), \\ &F_{45}=K_5\ \pi\ \sigma_C\left(\frac{\Delta Z_C}{Z_4-Z_3}\right)(R_5^2-R_4^2);(\text{for } \sigma_C \text{ material}), \end{aligned}\right\} \tag{3.14}$$

$$\left.\begin{aligned} &Z=\Delta Z_B+\Delta Z_C, \\ &\sigma_B\left(\frac{\Delta Z_B}{Z_3}\right)=\sigma_C\left(\frac{\Delta Z_C}{Z_4-Z_3}\right), \end{aligned}\right\} \tag{3.15}$$

$$0 \leqq K_i \leqq 1.$$

σ_i (i=A, B, C, D) is stress in these material regions.

3.2.3 Horizontal drop impact

When the shock absorber deforms by the displacement Z in a horizontal drop as shown in Figs.3.6 to3.8, the impact load and the dissipated energy are given by following equations.

$$F=\sum_i F_{ij}=F_{01}+F_{12}+F_{23}+F_{34}+F_{45}+F_{56}+F_{67}+F_{78}+F_{89}\ , \tag{3.16}$$

$$F_{ij}=2\int_0^{R_5}\Delta F\ dx\ , \tag{3.17}$$

$$E=\int_0^{y} F\ dy\ , \tag{3.18}$$

where, for the region $0 \sim Z_1$, and $0 \sim R_1$

$$\left.\begin{aligned} &\Delta F=K_1\ \sigma_D\left(\frac{\Delta y_1}{y_1}\right)dx \cdot Z_1;\ (\text{for } \sigma_D \text{ material})\ , \\ &\Delta F=K_1\ \sigma_A\left(\frac{\Delta y_2}{y_2}\right)dx \cdot Z_1;\ (\text{for } \sigma_A \text{ material})\ , \\ &\Delta F=K_1\ \sigma_B\left(\frac{\Delta y_3}{y_3}\right)dx \cdot Z_1;\ (\text{for } \sigma_B \text{ material})\ , \end{aligned}\right\} \tag{3.19}$$

$$\left.\begin{aligned} y_1&=2\sqrt{R_1^2-x^2}\ ,\\ y_2&=2\left(\sqrt{R_2^2-x^2}-\sqrt{R_1^2-x^2}\right)\ ,\\ y_3&=2\left(\sqrt{R_5^2-x^2}-\sqrt{R_2^2-x^2}\right)\ . \end{aligned}\right\} \tag{3.20}$$

$$\left.\begin{aligned} &U=\Delta y_1+\Delta y_2+\Delta y_3\ ,\\ &\sigma_D\left(\frac{\Delta y_1}{y_1}\right)=\sigma_A\left(\frac{\Delta y_2}{y_2}\right)=\sigma_B\left(\frac{\Delta y_3}{y_3}\right)\ . \end{aligned}\right\} \tag{3.21}$$

$$\left.\begin{aligned} &U=y-h;\left\{\begin{matrix} U\leqq 0, & \text{for } \Delta F=0\\ U>0, & \text{for } \Delta F\neq 0 \end{matrix}\right\},\\ &h=R_5-\sqrt{R_5^2-x^2}\ . \end{aligned}\right\} \tag{3.22}$$

for the region 0 ～ Z_1 and R_1 ～ R_2

$$\left.\begin{aligned} &\Delta F=K_1\ \sigma_A\left(\frac{\Delta y_1}{y_1}\right)dx\cdot Z_1;\ (\text{for } \sigma_A \text{ material})\ ,\\ &\Delta F=K_1\ \sigma_B\left(\frac{\Delta y_2}{y_2}\right)dx\cdot Z_1;\ (\text{for } \sigma_B \text{ material})\ . \end{aligned}\right\} \tag{3.23}$$

$$\left.\begin{aligned} y_1&=2\sqrt{R_2^2-x^2}\\ y&=2\left(\sqrt{R_5^2-x^2}-\sqrt{R_2^2-x^2}\right)\ . \end{aligned}\right\} \tag{3.24}$$

$$\begin{aligned} &U=\Delta y_1+\Delta y_2\ ,\\ &\sigma_A\left(\frac{\Delta y_1}{y_1}\right)=\sigma_B\left(\frac{\Delta y_2}{y_2}\right)\ . \end{aligned} \tag{3.25}$$

for the region 0 ～ Z_1 and R_2 ～ R_3

$$\Delta F=K_1\sigma_B\left(\frac{U}{y}\right)dx\cdot Z_1\ , \tag{3.26}$$

$$y=2\sqrt{R_5^2-x^2}\ . \tag{3.27}$$

For the region Z_1 ～ Z_2 and 0 ～ R_5 equations are similar as eqs. (3.9) through (3.25) when Z_1 changes to (Z_2-Z_1) and K_1 to K_4.

For the region $Z_2 \sim Z_3$ and $0 \sim R_3$

$$\Delta F = K_3 \sigma_B \left(\frac{U}{y} \right) dx \cdot (Z_3 - Z_2) \ , \tag{3.28}$$

where

$$y = \sqrt{r_5^2 - x^2} - \sqrt{R_3^2 - x^2} \ . \tag{3.29}$$

For the region $Z_2 \sim Z_3$ and $R_3 \sim R_5$

$$\Delta F = K_3 \sigma_B \left(\frac{U}{y} \right) dx \cdot (Z_3 - Z_2) \ , \tag{3.30}$$

where

$$y = 2\sqrt{R_5^2 - x^2} . \tag{3.31}$$

For the region $Z_3 \sim Z_4$ and $0 \sim R_3$

$$\Delta F = K_4 \sigma_C \left(\frac{U}{y} \right) dx \cdot (Z_3 - Z_2) \ , \tag{3.32}$$

where

$$y = \sqrt{R_5^2 - x^2} - \sqrt{R_3^2 - x^2} \ . \tag{3.33}$$

For the region $Z_3 \sim Z_4$ and $R_3 \sim R_5$

$$\Delta F = K_4 \sigma_C \left(\frac{U}{y} \right) dx \cdot (Z_4 - Z_3) \ , \tag{3.34}$$

where

$$y = 2\sqrt{R_5^2 - x^2} . \tag{3.35}$$

For the region $Z_5 \sim Z_6$ equations are the same as the region $Z_3 \sim Z_4$, the region $Z_6 \sim Z_7$ the same as the region $Z_2 \sim Z_3$, the region $Z_7 \sim Z_8$ the same as the region $Z_1 \sim Z_2$ and the region $Z_8 \sim Z_9$ the same as the region $0 \sim Z_1$.

3.2.4 Oblique drop impact

In the modeling a shock absorber in the CRUSH at an oblique drop impact, it is assumed that shock absorber consists of one specy of shock absorber materials as shown in Fig.3.3. The stress of a wooden shock absorber can be written as following, including the effect of the wood grain angle θ .

$$\sigma_x = \sigma_A \cos^2\theta + \sigma_B \sin^2\theta \ , \tag{3.36}$$

where σ_A, σ_B and σ_x are stresses in the wood whose grain direction is parallel, perpendicular and angle θ degree to the drop direction, respectively.

Let us consider a cutway section of the shock absorber as shown in Figs.3.9, 3.10 and 3.11. The impact load and the dissipated energy are given by following equations (see Fig.3.11).

$$F_i=2\int_0^{x_M}\Delta F\ dx\ , \tag{3.37}$$

$$F=\int_s F_i\ ds\ , \tag{3.38}$$

$$E=\int_0^y F\ dy\ , \tag{3.39}$$

$$U=y-h_0-h;\left\{\begin{array}{ll} U\leqq 0, & \text{for } \Delta F=0 \\ U>0, & \text{for } \Delta F\neq 0 \end{array}\right\}. \tag{3.40}$$

Sectional figures of the shock absorber in the case of oblique drop are shown in Figs.3.12 and 3.13.

Let us consider S-T coordinate as shown in Fig.3.14.

The coordinates of points $P_1 \sim P_{12}$ and $Q_1 \sim Q_4$ are as follows.

$$\left.\begin{array}{lll}
P_1\{ & -R_5\cos\theta\ , & R_5\sin\theta\ \} \\
P_2\{ & -R_1\cos\theta\ , & R_1\sin\theta\ \} \\
P_3\{ & R_1\cos\theta\ , & -R_1\sin\theta\ \} \\
P_4\{ & R_5\cos\theta\ , & -R_5\sin\theta\ \} \\
P_5\{ & -R_3\cos\theta+Z_2\sin\theta, & R_3\sin\theta+Z_2\cos\theta\} \\
P_6\{ & -R_1\cos\theta+Z_2\sin\theta, & R_1\sin\theta+Z_2\cos\theta\} \\
P_7\{ & R_1\cos\theta+Z_2\sin\theta, & -R_1\sin\theta+Z_2\cos\theta\} \\
P_8\{ & R_3\cos\theta+Z_2\sin\theta, & -R_3\sin\theta+Z_2\cos\theta\} \\
P_9\{ & -R_5\cos\theta+Z_4\sin\theta, & R_5\sin\theta+Z_4\cos\theta\} \\
P_{10}\{ & -R_3\cos\theta+Z_4\sin\theta, & R_3\sin\theta+Z_4\cos\theta\} \\
P_{11}\{ & R_3\cos\theta+Z_4\sin\theta, & -R_3\sin\theta+Z_4\cos\theta\} \\
P_{12}\{ & R_5\cos\theta+Z_4\sin\theta, & -R_5\sin\theta+Z_4\cos\theta\} \\
Q_2\{ & -R_1\cos\theta+Z_1\sin\theta, & R_1\sin\theta+Z_1\cos\theta\} \\
Q_3\{ & R_1\cos\theta+Z_1\sin\theta, & -R_1\sin\theta+Z_1\cos\theta\} \\
Q_0\{ & Z_2\sin\theta, & Z_2\cos\theta\ \} \\
Q_4\{ & R_4\cos\theta+Z_4\sin\theta, & -R_4\sin\theta+Z_4\cos\theta\}
\end{array}\right\} \tag{3.41}$$

The lengths of h_0 as shown in Figs.3.12 and 3.13 are as follows.

when $\sigma_D \neq 0$

$$\left.\begin{aligned} h_0 &= R_5\sin\theta - \frac{\sin\theta}{\cos\theta}S \ ; \ (\text{region } P_1\sim P_2 \text{ and } P_3\sim P_4)\ , \\ h_0 &= \frac{\cos\theta}{\sin\theta}(S - R_5\cos\theta); \ (\text{region } P_4\sim P_{12})\ . \end{aligned}\right\} \tag{3.42}$$

when $\sigma_D=0$

$$\left.\begin{aligned} h_0 &= R_5\sin\theta - \frac{\sin\theta}{\cos\theta}S \ ; \ (\text{region } P_1\sim P_2 \text{ and } P_3\sim P_4)\ , \\ h_0 &= \frac{\cos\theta}{\sin\theta}(S - R_5\cos\theta); \ (\text{region } P_4\sim P_{12})\ , \\ h_0 &= \frac{\cos\theta}{\sin\theta}(S + R_1\cos\theta) + (R_1 + R_5)\sin\theta; \\ &\qquad\qquad (\text{region } P_2\sim Q_2\sim P_6)\ , \\ h_0 &= \infty \ ; \ (\text{region } P_6\sim Q_0\sim P_7)\ . \end{aligned}\right\} \tag{3.43}$$

The lengths of h_1, ℓ_1 and ℓ_2 are as follows.

(a) If ℓ_2 is known ($S<P_5$, $S \leqq 0$, $\ell_1=0$ and $K_h=0$), h_0, h_1 and ℓ_2 are shown in Fig.3.15(a).

$$\left.\begin{aligned} \ell_2 &= \frac{R_5}{\sin\theta} \ ; \ (\text{region } P_1\sim P_9)\ , \\ \ell_2 &= \frac{1}{\sin\theta\cos\theta}(Z_4\sin\theta - S) \ ; \ (\text{region } P_9\sim P_{10})\ . \end{aligned}\right\} \tag{3.44}$$

when $\sigma_D \neq 0$

$$h_1 = -\frac{S}{\sin\theta\cos\theta}\ . \tag{3.45}$$

when $\sigma_D=0$

$$\left.\begin{aligned} h_1 &= -\frac{S}{\sin\theta\cos\theta}; \ (\text{region } P_1\sim P_2)\ , \\ h_1 &= \frac{R_1}{\sin\theta} \ ; \ (\text{region } P_2\sim P_6)\ . \end{aligned}\right\} \tag{3.46}$$

(b) If ℓ_1 and ℓ_2 are known ($S<P_5$, $S>0$, $\sigma_D \neq 0$ $h_1=0$ and $K_h=0$), h_0, ℓ_1 and ℓ_2 are shown in Fig.3.15(b).

$$\left.\begin{aligned} l_2 &= \frac{R_5}{\sin\theta} && ;\ (\text{region } P_1 \sim P_9)\ , \\ l_2 &= \frac{1}{\sin\theta\cos\theta}(Z_4\sin\theta - S) && ;\ (\text{region } P_9 \sim P_{10})\ , \end{aligned}\right\} \tag{3.47}$$

$$\left.\begin{aligned} l_1 &= \frac{S}{\sin\theta\cos\theta} && ;\ (S \leqq P_4,\ \text{region } P_2 \sim P_4 \sim P_{12})\ , \\ l_1 &= \frac{R_5}{\sin\theta} && ;\ (S > P_4,\ \text{region } P_2 \sim P_4 \sim P_{12})\ , \end{aligned}\right\} \tag{3.48}$$

(c) If ℓ_2 is known ($S<P_5$, $S>0$, and $\sigma_D=0$), h_0, h_1 and ℓ_1 are shown in Fig.3.15(c) and are the same as Eqs. (3.42), (3.43) and (3.43).

(d) If ℓ_2 is known ($P_5 \leqq S \leqq Q_0$ and $K_h=1$), h_0, h_1, ℓ_1 and ℓ_2 are shown in Fig.3.16(d).

$$l_2 = \frac{1}{\sin\theta\cos\theta}(Z_1\sin\theta - S)\ . \tag{3.49}$$

when $\sigma_D \neq 0$

$$\left.\begin{aligned} h_1 &= -\frac{S}{\sin\theta\cos\theta}\ , \\ l_1 &= 0\ , \end{aligned}\right\}\ ;\ (\text{for } S \leqq 0)\ , \tag{3.50}$$

$$\left.\begin{aligned} h_1 &= 0\ , \\ l_1 &= \frac{S}{\sin\theta\cos\theta}\ , \end{aligned}\right\}\ ;\ (\text{for } 0 < S \leqq P_4)\ , \tag{3.51}$$

$$\left.\begin{aligned} h_1 &= 0\ , \\ l_1 &= \frac{R_5}{\sin\theta}\ , \end{aligned}\right\}\ ;\ (\text{for } S > P_4)\ . \tag{3.52}$$

when $\sigma_D=0$

$$\left.\begin{aligned} h_1 &= \frac{R_1}{\sin\theta}\ , \\ l_1 &= 0\ , \end{aligned}\right\}\ ;\ (\text{for } S \leqq P_6)\ , \tag{3.53}$$

$$\left.\begin{aligned} h_1 &= \frac{1}{\sin\theta\cos\theta}(Z_2\sin\theta - S)\ , \\ l_1 &= 0\ , \end{aligned}\right\}\ ;\ (\text{for } S > P_6)\ . \tag{3.54}$$

(e) If ℓ_1 is known ($Q_0 \leqq S \leqq P_1$, ℓ_2=0 and K_h=1), h_1, and ℓ_1 are shown in Fig.3.16(e).
For region $Q_0 \sim P_8$

$$h_1=\frac{1}{\sin\theta\cos\theta}(S-Z_2\sin\theta) \ , \tag{3.55}$$

$$\left.\begin{aligned} l_1&=\frac{S}{\sin\theta\cos\theta} \ ; \ (\text{for } S< P_4) \ , \\ l_1&=\frac{R_5}{\sin\theta} \ ; \ (\text{for } S\geqq P_4) \ . \end{aligned}\right\} \tag{3.56}$$

For region $P_8 \sim P_1$

$$h_1=\frac{R_3}{\sin\theta} \ , \tag{3.57}$$

$$\left.\begin{aligned} l_1&=\frac{S}{\sin\theta\cos\theta} \ ; \ (\text{for } S< P_4) \ , \\ l_1&=\frac{R_5}{\sin\theta} \ ; \ (\text{for } S\geqq P_4) \ . \end{aligned}\right\} \tag{3.58}$$

(f) If ℓ_1 is known ($S>P_1$, ℓ_2 =0 and K_h=1), h_1 and ℓ_1 are shown in Fig.3.16(f).

$$h_1=\frac{1}{\sin\theta\cos\theta}(S-Z_4\sin\theta) \ , \tag{3.59}$$

$$\left.\begin{aligned} l_1&=\frac{S}{\sin\theta\cos\theta} \ ; \ (\text{for } S< P_4) \ , \\ l_1&=\frac{R_5}{\sin\theta} \ ; \ (\text{for } S\geqq P_4) \ . \end{aligned}\right\} \tag{3.60}$$

The sectional figure of the shock absorber in the case of the oblique drop impact as shown in Fig.3.17, is an ellipsoid. The equation of the ellipsoid is as follows.

$$\frac{x^2}{R_5^2}+\frac{y^2}{b^2}=1 \ , \tag{3.61}$$

where

$$b=\frac{R_5}{\sin\theta} \tag{3.62}$$

Rearranged eq. (3.61), using $y=h(x_M)$

$$x_M=\sqrt{b^2-h^2}\cdot\sin\theta\ , \tag{3.63}$$

$$y=\frac{1}{\sin\theta}\sqrt{R_5^2-x^2}\ . \tag{3.64}$$

Force ΔF at the sectional area (ΔS, Δx) is as follows.

$$\Delta F=K\cdot\sigma(\frac{U}{l})\Delta S\cdot\Delta x., \tag{3.65}$$

where K is the boundary condition constant as shown in Fig.3.18.

$$0\leqq K_i\leqq 1 \tag{3.66}$$

where

K_1 : for $\sigma_D=0$; region $P_3\sim Q_3$,
for $\sigma_D\neq 0$; region $P_1\sim X_1$,
K_2 : for $\sigma_D=0$; region $Q_3\sim P_7$,
for $\sigma_D\neq 0$; region $X_1\sim X_2$,
K_3 : for region $P_{11}\sim Q_4$,
K_4 : for region $Q_4\sim P_{12}$.

3.2.5 Convergence method

The convergence methods for two or three materials in one dimensional bar in the case of the oblique drop impact, are as follows.

(1) Two materials

According to the stress-strain relation as shown in Fig.3.19, the following equations are derived.

$$\left.\begin{aligned}\sigma_A&=\sigma_A^0+K_A\varepsilon_A=\sigma_A^0+\frac{K_A}{l_A}U_A\ ,\\ \sigma_B&=\sigma_B^0+K_B\varepsilon_B=\sigma_B^0+\frac{K_B}{l_B}U_B\ ,\end{aligned}\right\} \tag{3.67}$$

and

$$\left.\begin{aligned}U_A+U_B&=U\ ,\\ -\sigma_A+\sigma_B&=0\ ,\end{aligned}\right\} \tag{3.68}$$

from above two equations,

$$\begin{bmatrix} 1 & 1 \\ -\frac{K_A}{l_A} & \frac{K_B}{l_B} \end{bmatrix} \begin{Bmatrix} U_A \\ U_B \end{Bmatrix} = \begin{Bmatrix} U \\ \sigma_A{}^0 - \sigma_B{}^0 \end{Bmatrix} . \tag{3.69}$$

By solving Eq. (3.69), we obtain U_A and U_B.

(2) Three materials

$$\begin{bmatrix} 1 & 1 & 1 \\ -\frac{K_A}{l_A} & \frac{K_B}{l_B} & 0 \\ -\frac{K_A}{l_A} & 0 & \frac{K_K}{l_K} \end{bmatrix} \begin{Bmatrix} U_A \\ U_B \\ U_K \end{Bmatrix} = \begin{Bmatrix} U \\ \sigma_A{}^0 - \sigma_B{}^0 \\ \sigma_A{}^0 - \sigma_K{}^0 \end{Bmatrix} . \tag{3.70}$$

(3) Strain, stiffness and stress

Strain

$$\varepsilon_i = \frac{U_i}{l_i} . \tag{3.71}$$

Stiffness (see Fig.3.20)

$$K_i = \frac{\sigma_2 - \sigma_1}{\varepsilon_2 - \varepsilon_1} . \tag{3.72}$$

Stress (see Fig.3.20)

$$\sigma_i = \sigma_1 - K_i \cdot \varepsilon_i . \tag{3.73}$$

3.2.6 Cover Plate of Shock Absorber

Modeling of cover plate as shown in Figs. from 3.21 to 3.23 is the same as shock absorber.

3.3 Benchmark Calculation

In order to demonstrate the adequacy of the simplified computer program CRUSH, the benchmark calculations using experimental results of the 1/4 scale model of NUPAC 125B cask as shown in Fig.3.24 have been performed.

Figure 3.25 is the deformed shapes of the cask after 9 meters drop impact obtained by the detailed computer program DYNA3D. The comparison among the results obtained by the experiments, the simplified computer program CRUSH and the detailed computer program DYNA3D are shown in Table 3.1. The relation among the oblique angles of cask drop attitude, the maximum accelerations and the maximum deformations obtained by CRUSH are shown in Figs. 3.26 and 3.27. According to Table 3.1 and Figs.3.26 and 3.27, the results by the simplified computer program CRUSH agree with both the experimental results and the results of the detailed program DYNA3D.

Table 3.1 Comparison between simplified and detailed analyses and experiment

Attitude	Acceleration (G)				Displacement (mm)			
	Experiment	Simplified analysis		Detailed analysis	Experiment	Simplified analysis		Detailed analysis
		CRUSH1	CRUSH2	DYNA3D		CRUSH1	CRUSH2	DYNA3D
Vertical	200	179	208	271* (200)**	51	52	50	50
Corner	106	125	136	145 (97)	127	151	146	118
Horizontal	180	183	219	240 (182)	61	63	74	57

* Value of low pass filter is 600 Hz.

** Mean value= $\frac{\text{Impact velocity}}{\text{Rebound time}}$.

(NUPAC 125B cask 1/4 scale model).

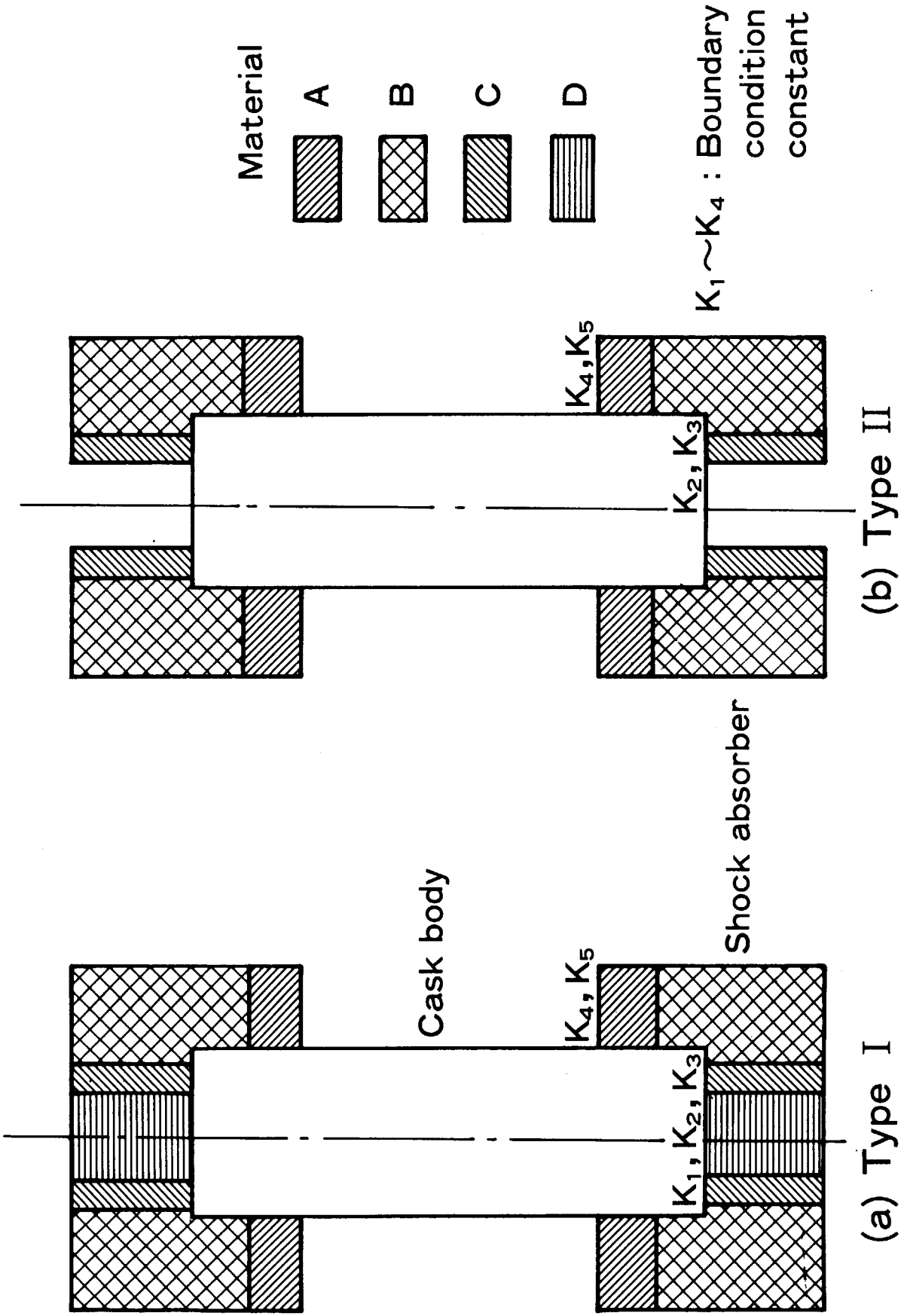

Fig. 3.1 Vertical drop model

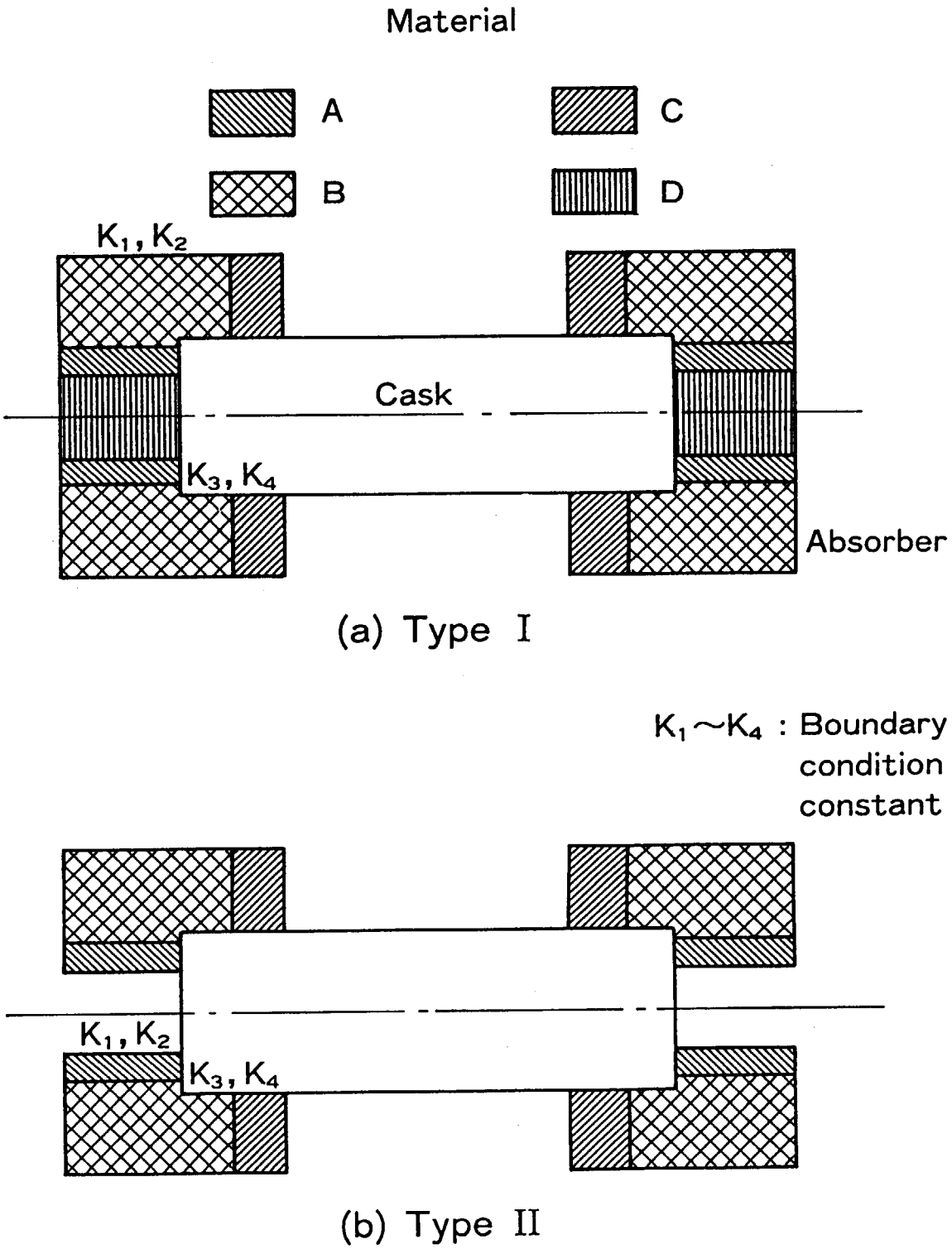

Fig. 3.2 Horizontal drop model

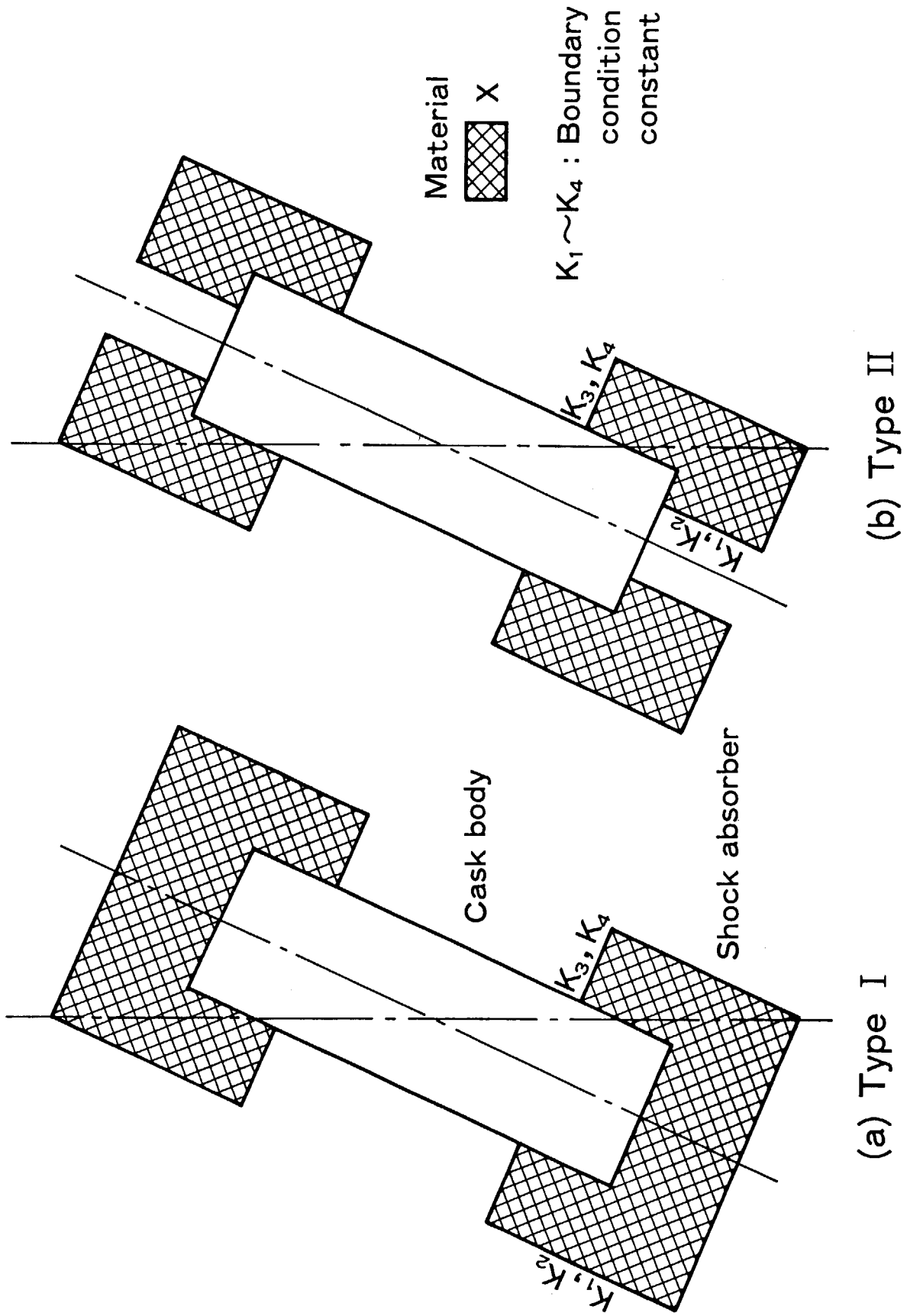

Fig. 3.3 Oblique drop model

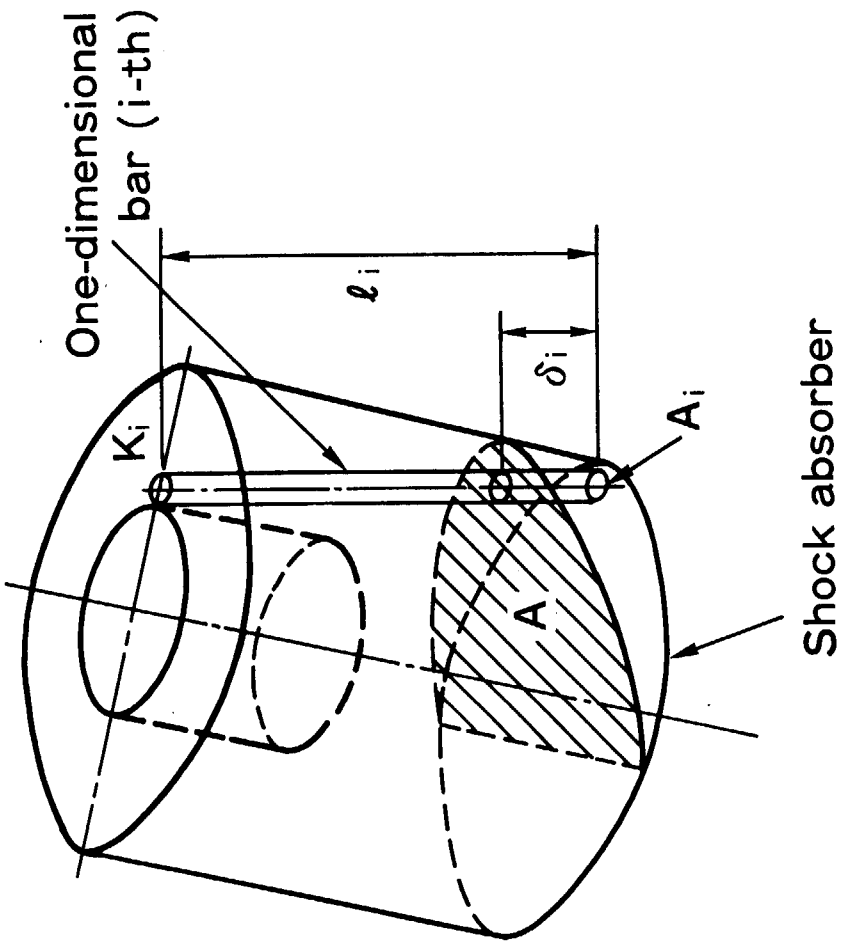

Strain : ε

$$\varepsilon_i = \frac{\delta_i}{\ell_i}$$

Force : F_i

$$F_i = K_i \sigma_i(\varepsilon_i) A_i$$

Total force : F

$$F = \Sigma_i F_i A_i$$

Acceleration : α

$$\alpha = \frac{F}{M}$$

M : Mass, A : Area

σ : Stress, K : Boundary condition constant

Fig. 3.4 Uni-axial displacement method

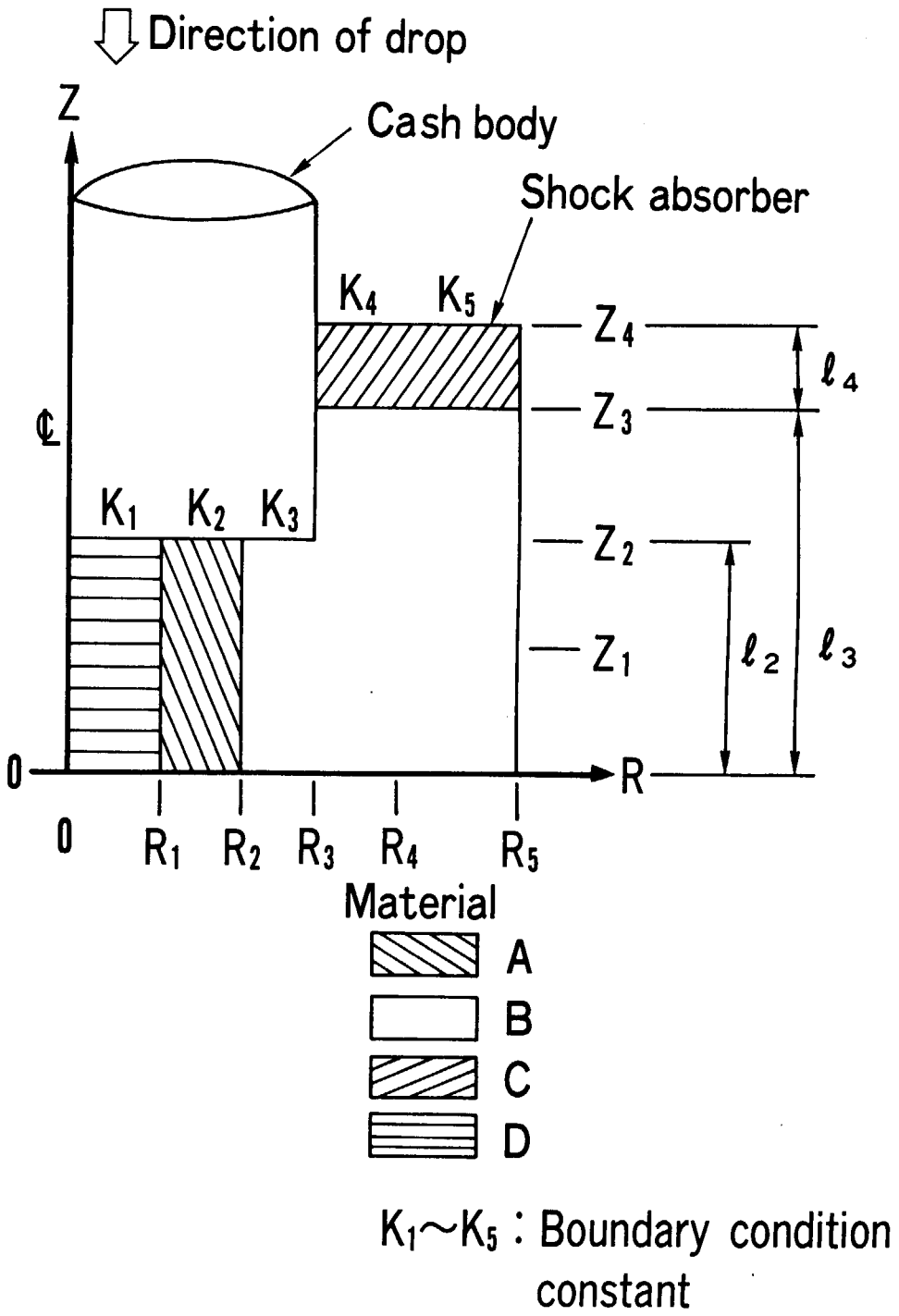

Fig. 3.5 Geometry and material in the case of vertical drop model

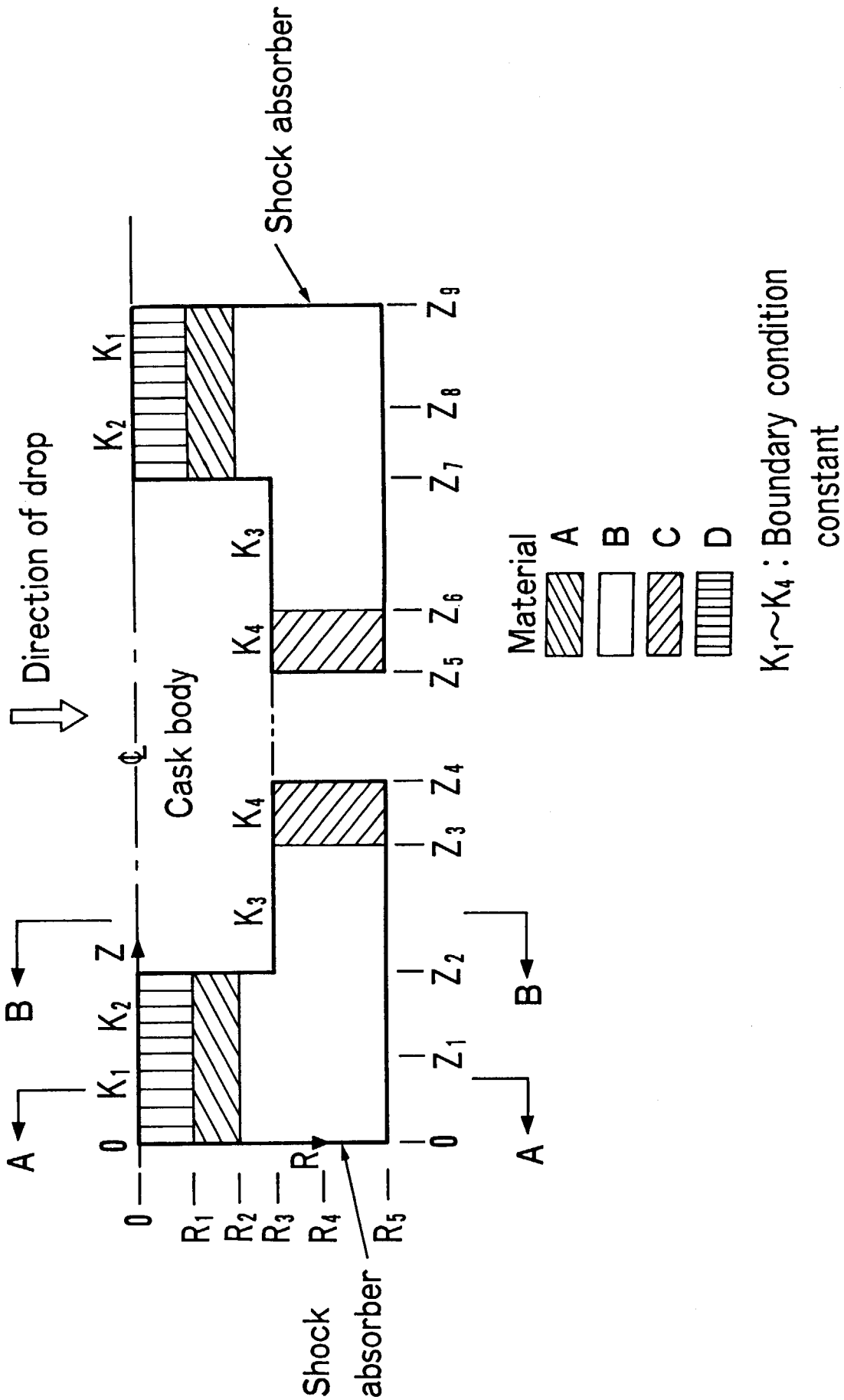

Fig. 3.6 Geometry and material in the case of horizontal drop model

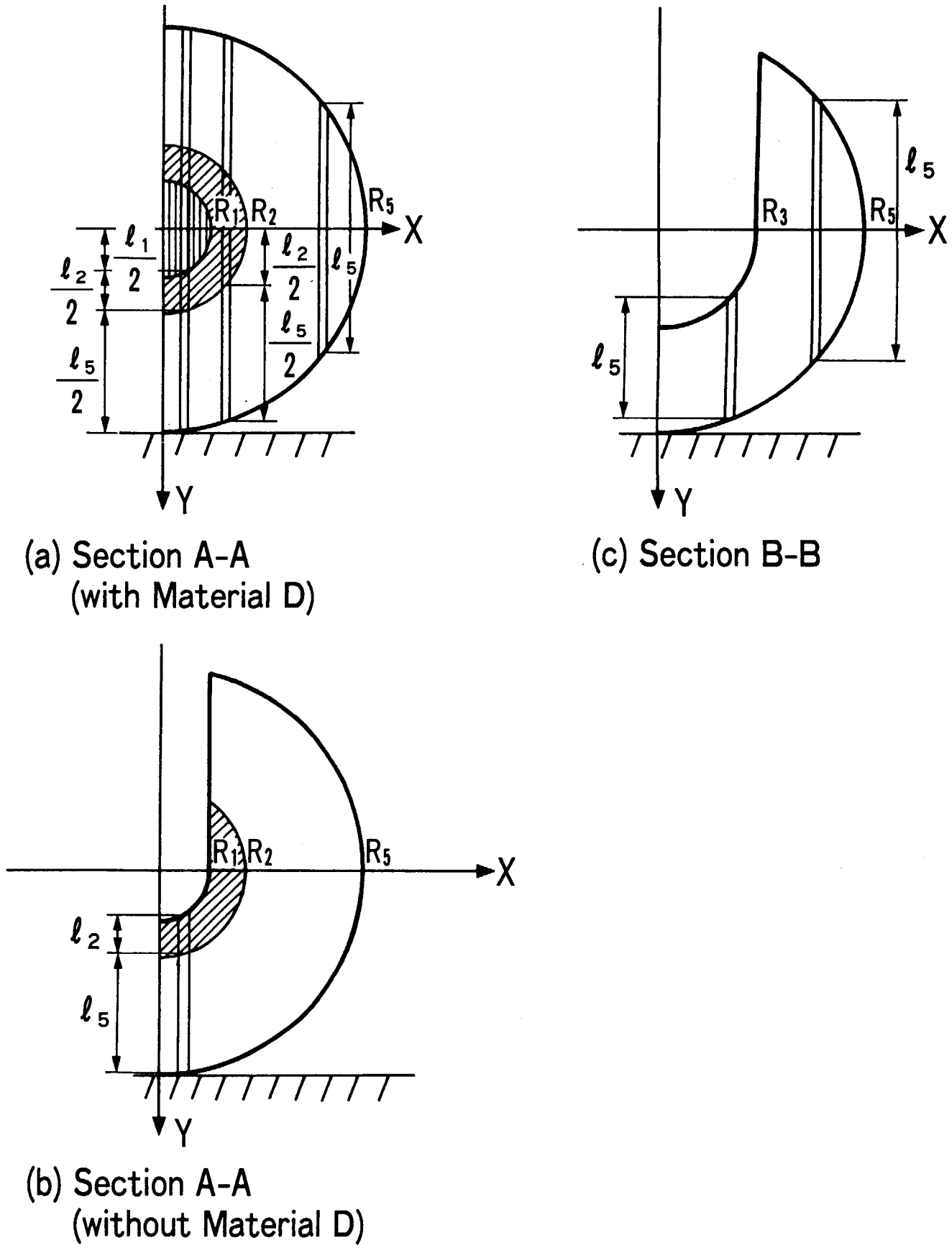

Fig. 3.7 Sectional view of horizontal drop model

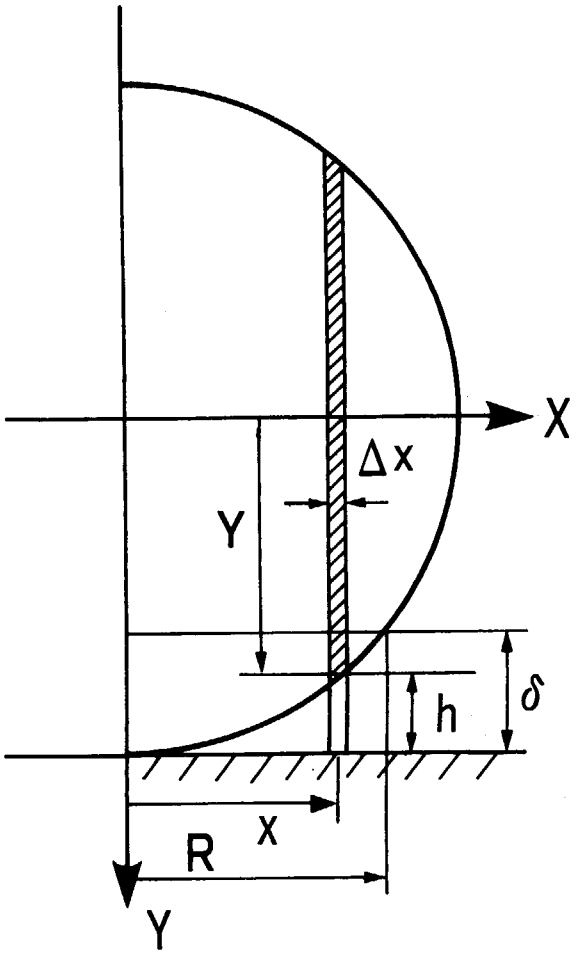

Fig. 3.8 Sectional area of shock absorber

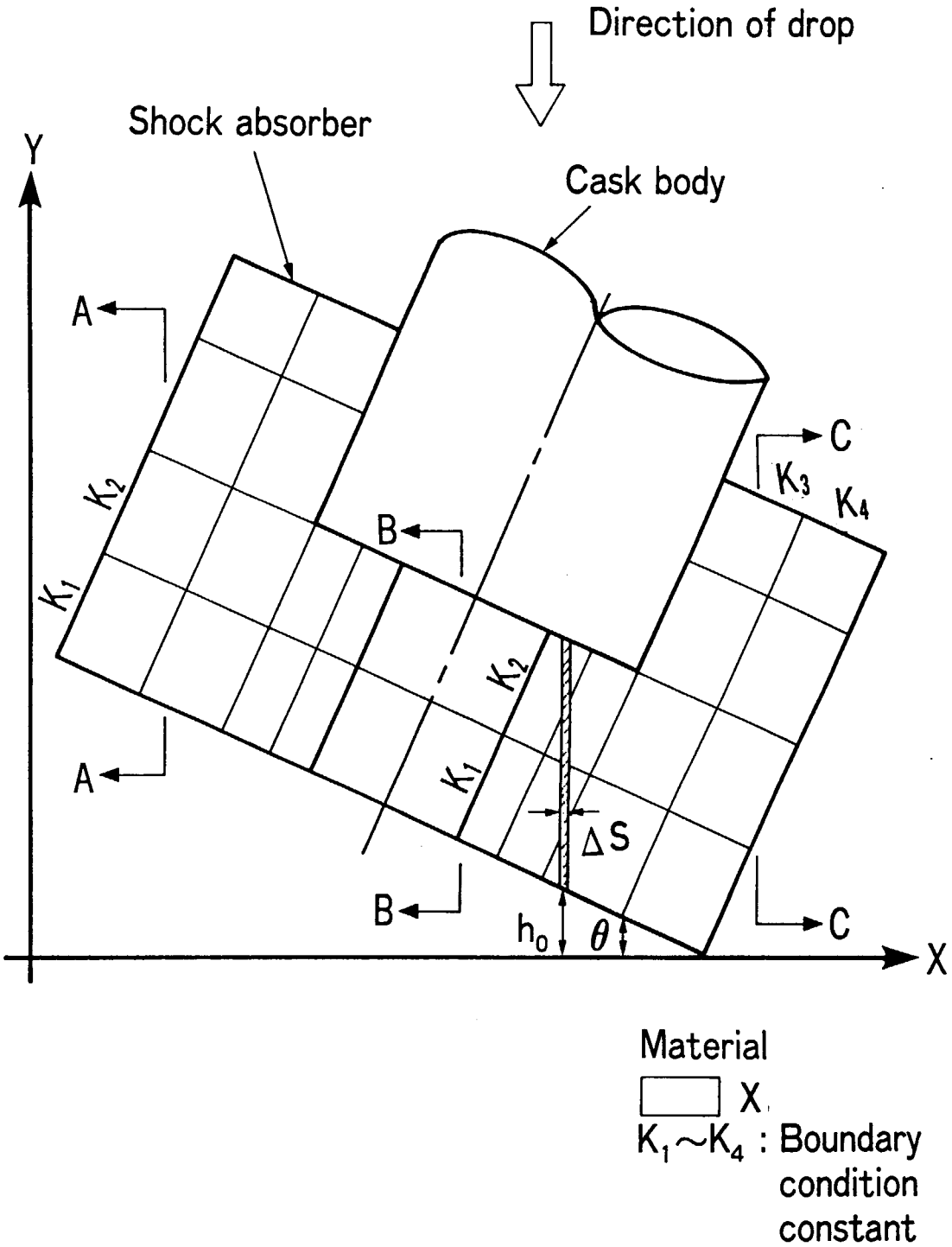

Fig. 3.9 Geometry and material in the case of oblique drop model

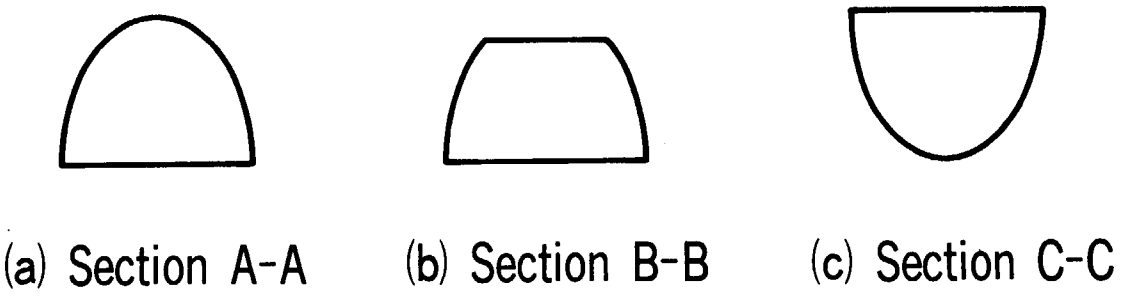

Fig. 3.10 Sectional figure of shock absorber in the case of oblique drop (I)

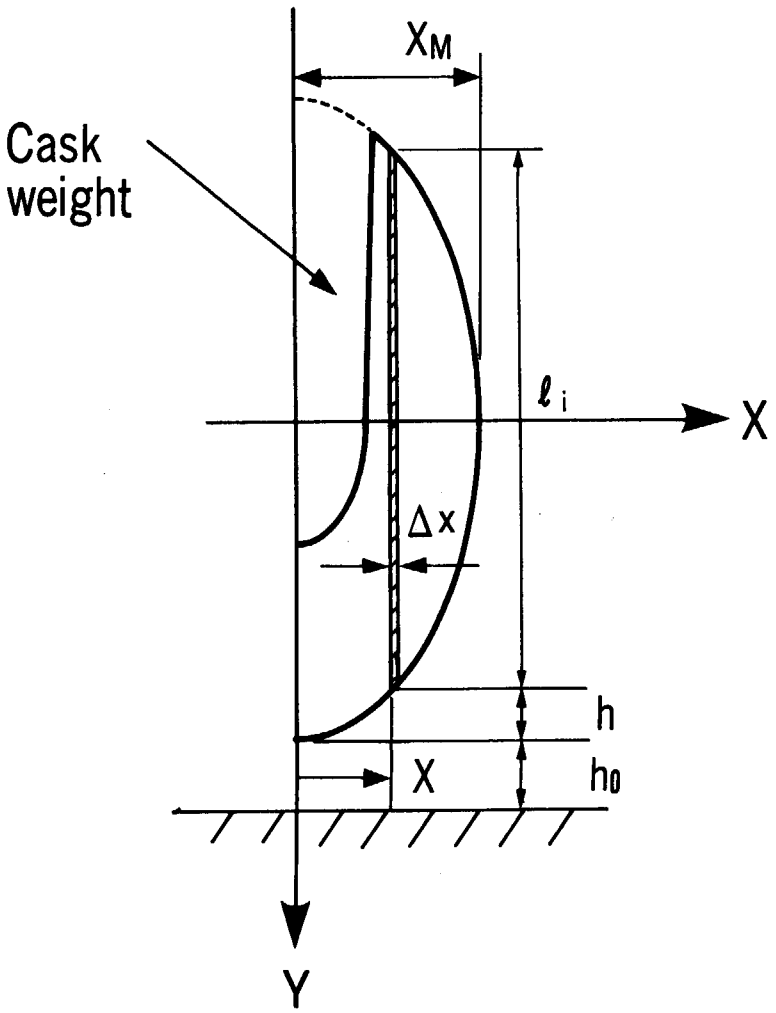

Fig. 3.11 Sectional figure of shock absorber in the case of oblique drop (II)

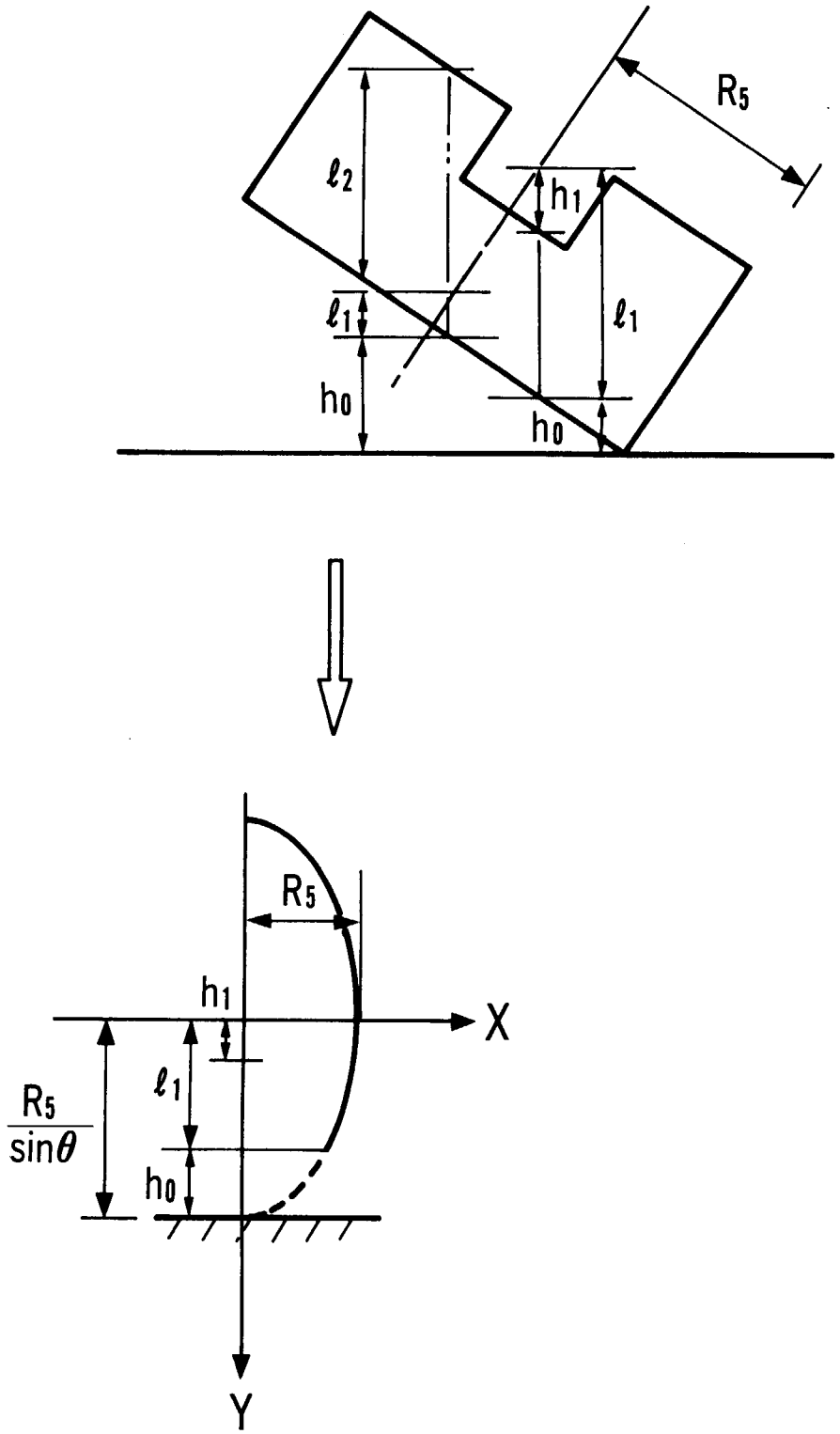

Fig. 3.12 Sectional figure of shock absorber in the case of oblique drop (Ⅲ)

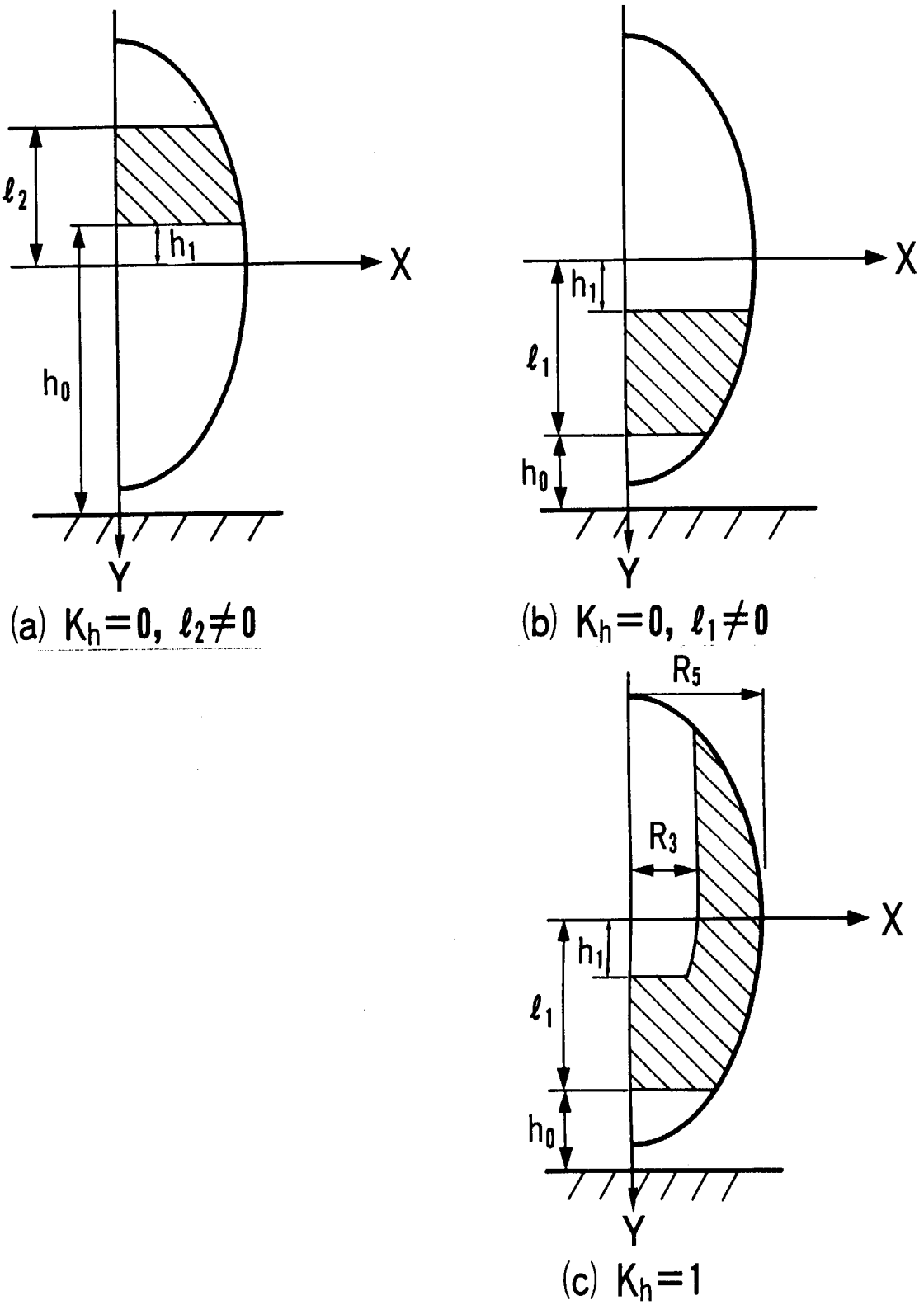

Fig. 3.13 Sectional figure of shock absorber in the case of oblique drop (Ⅳ)

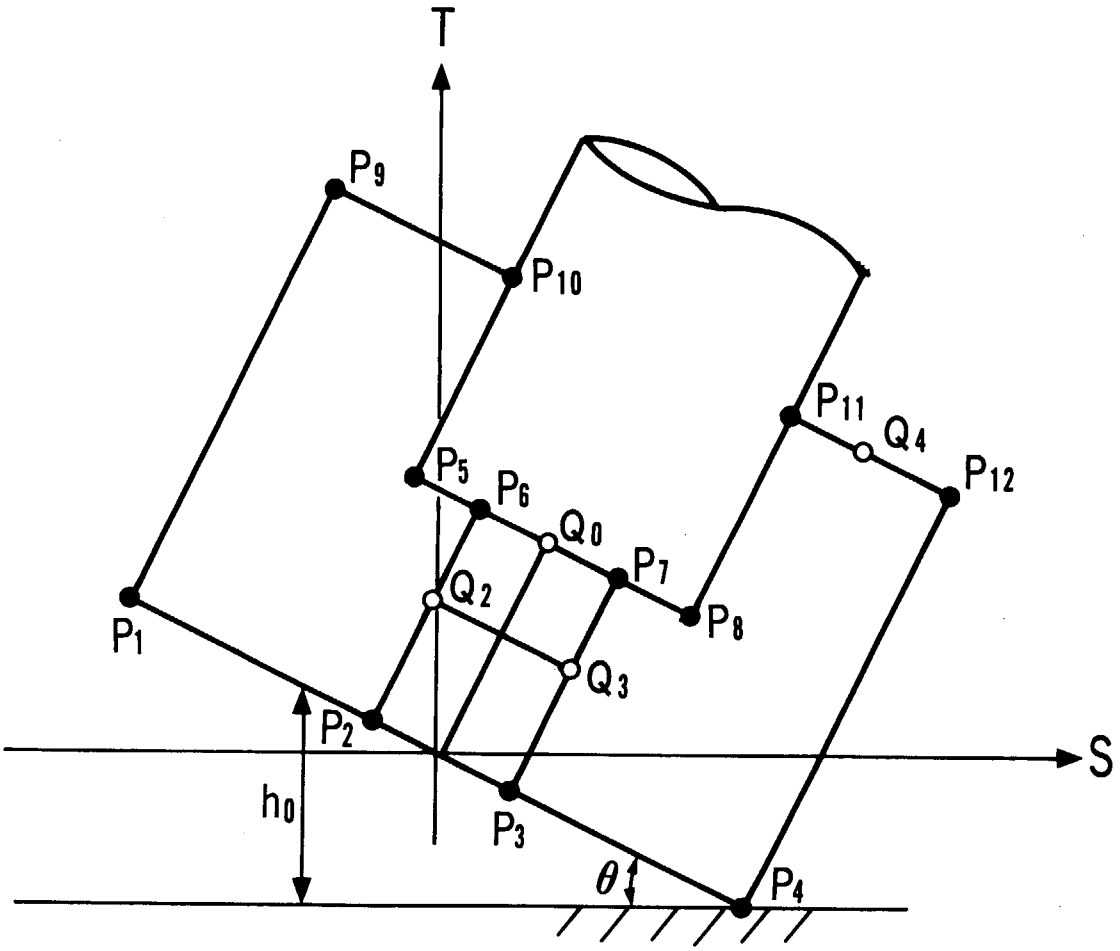

Fig. 3.14 Geometry of shock absorber in the case of oblique drop and S-T coordinate

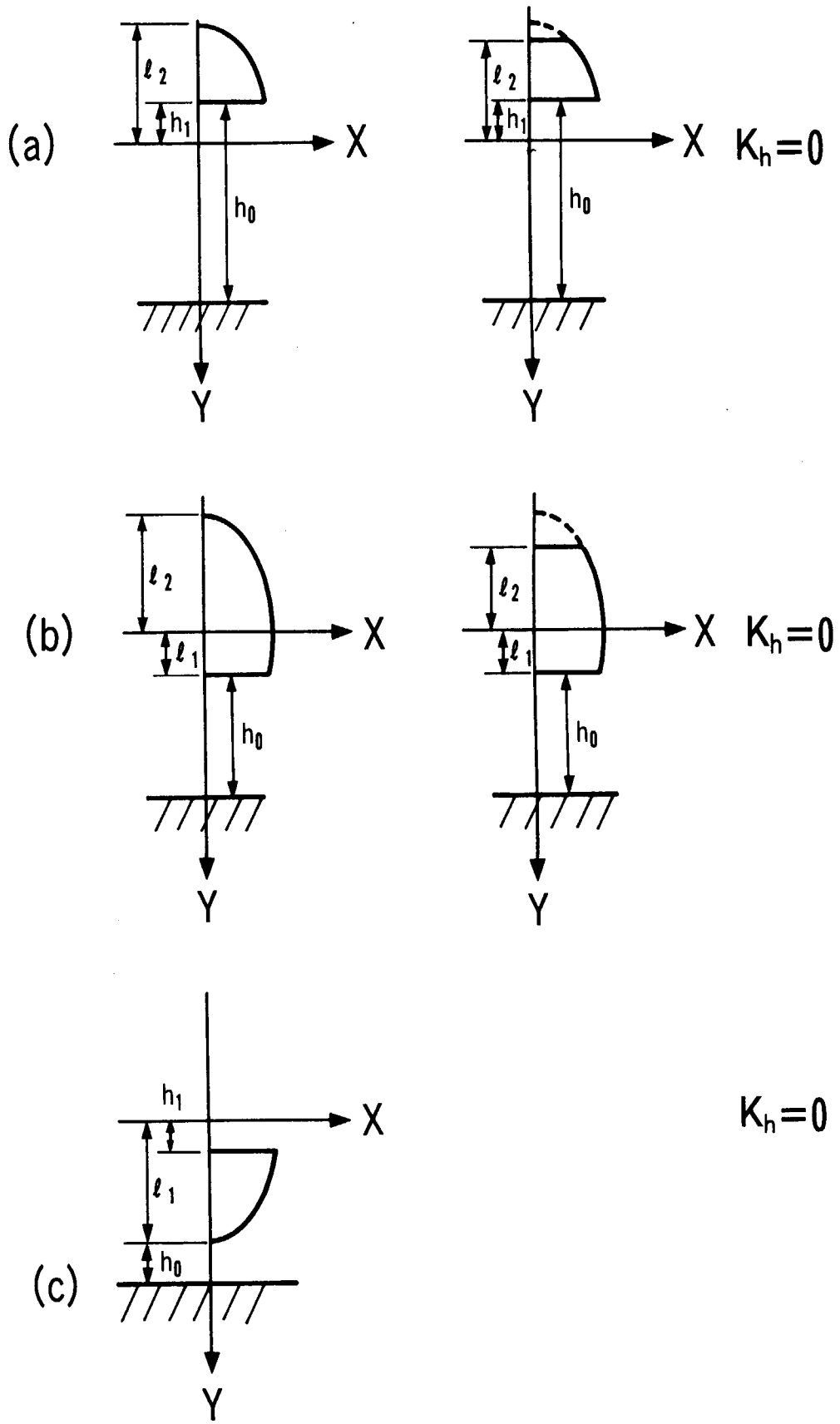

Fig. 3.15 Various sectional figure of shock absorber in the case of oblique drop (I)

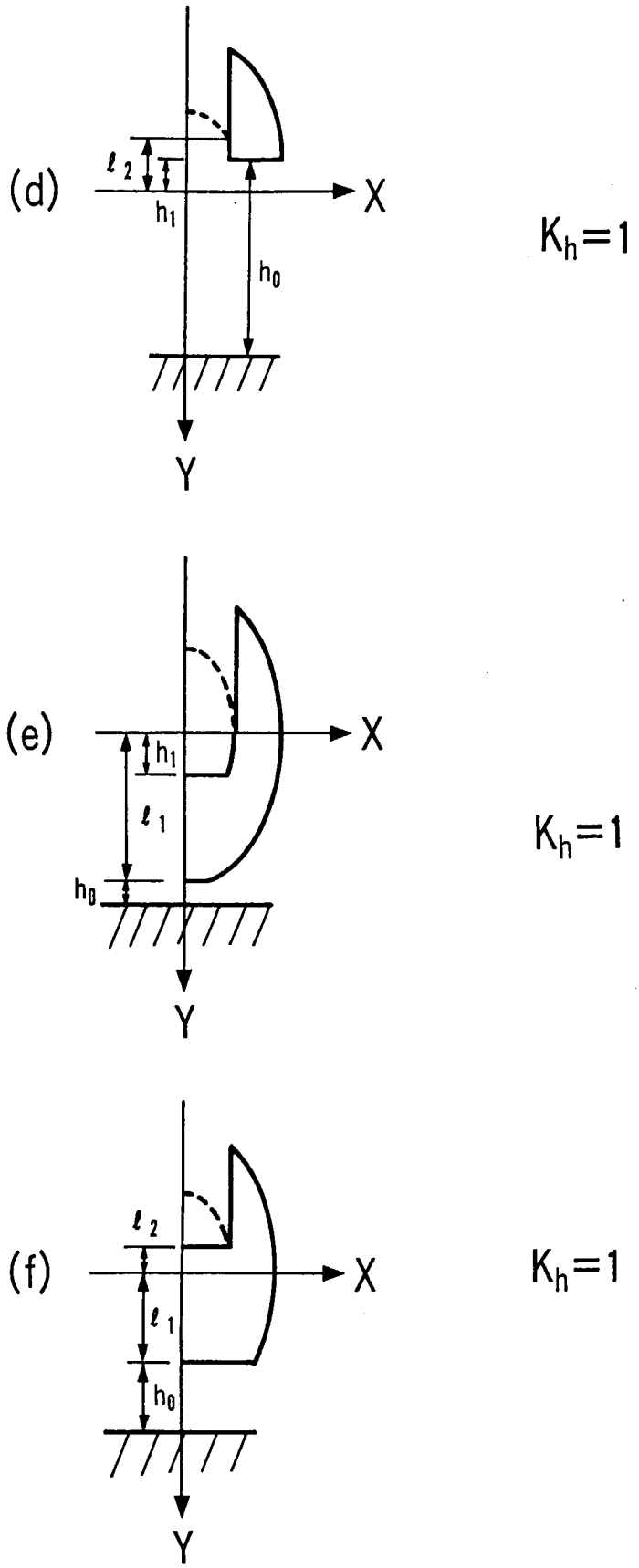

Fig. 3.16 Various sectional figure of shock absorber in the case of oblique drop (Ⅱ)

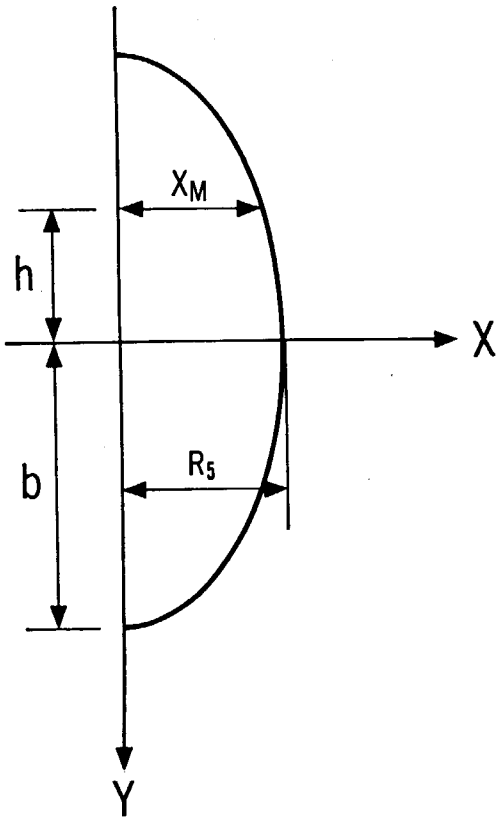

Fig. 3.17 Ellipsoid

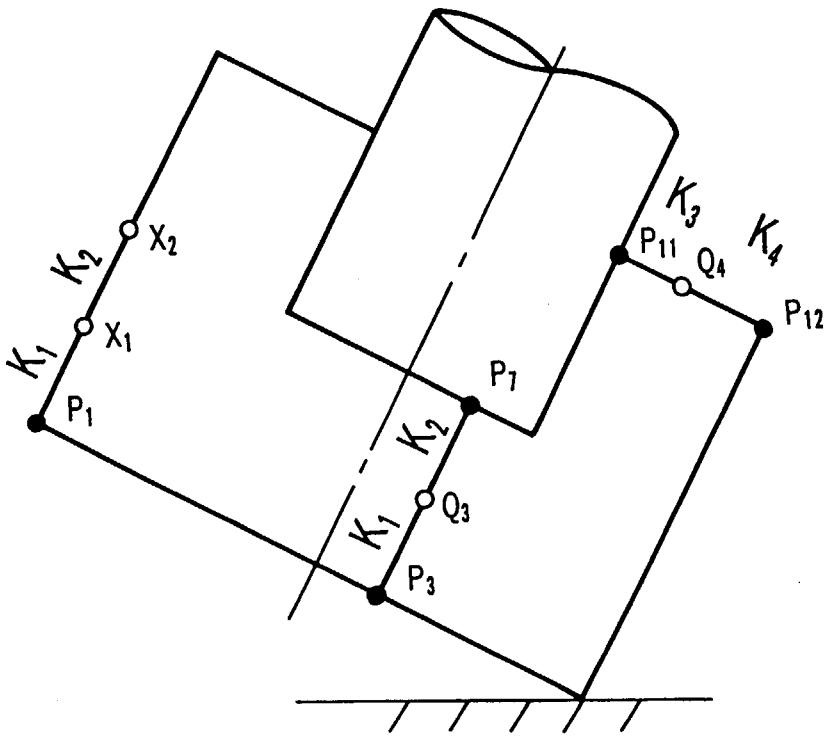

Fig. 3.18 Boundary condition constant in the case of oblique drop

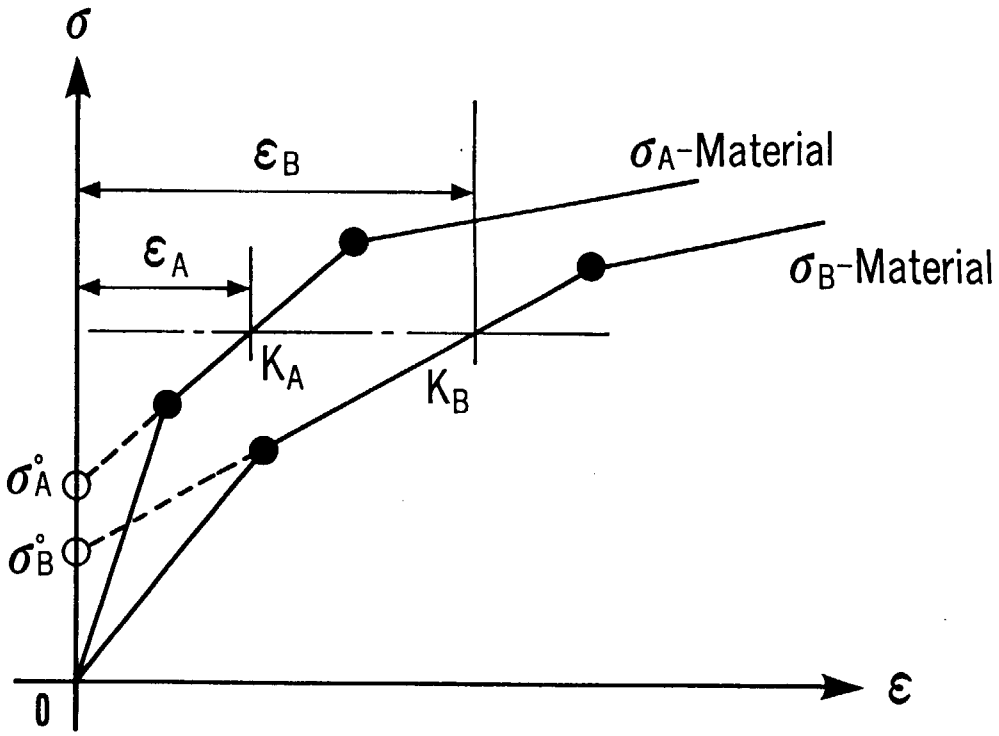

Fig. 3.19 Stress-strain curves of shock absorber materials

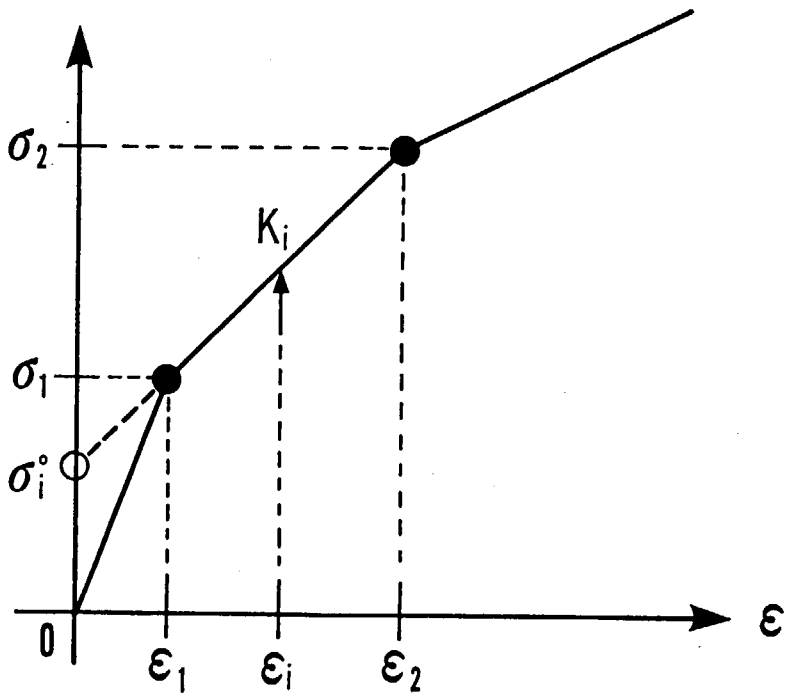

Fig. 3.20 Stress-strain curve of shock absorber material

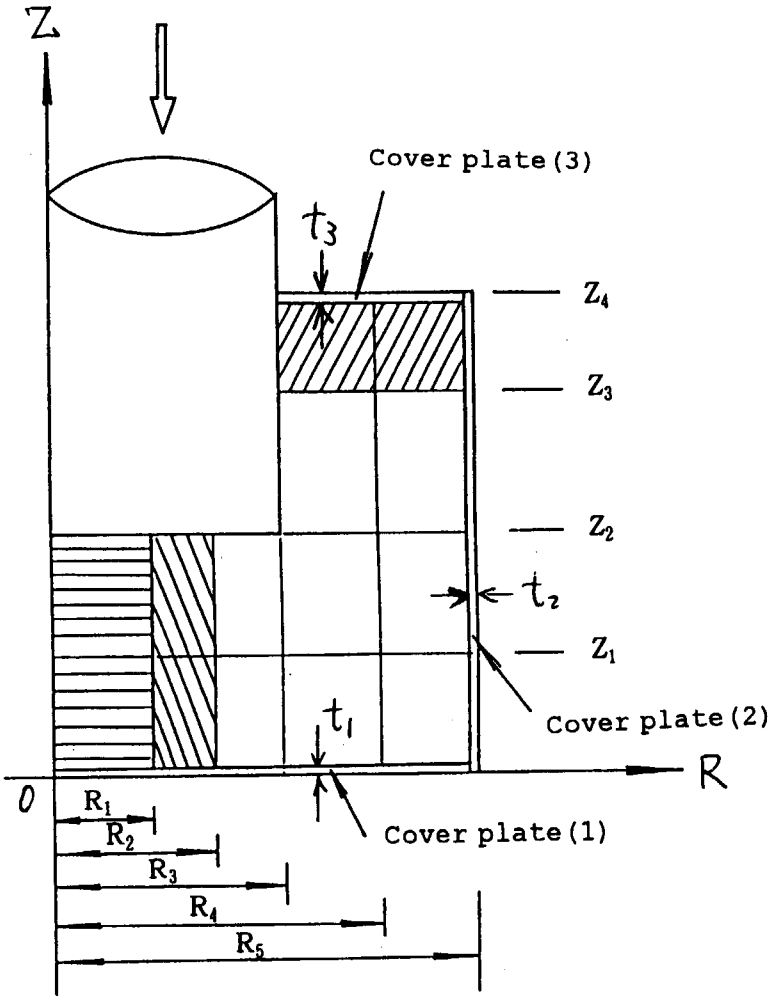

Fig. 3.21 Cover plate in the case of vertical impact model

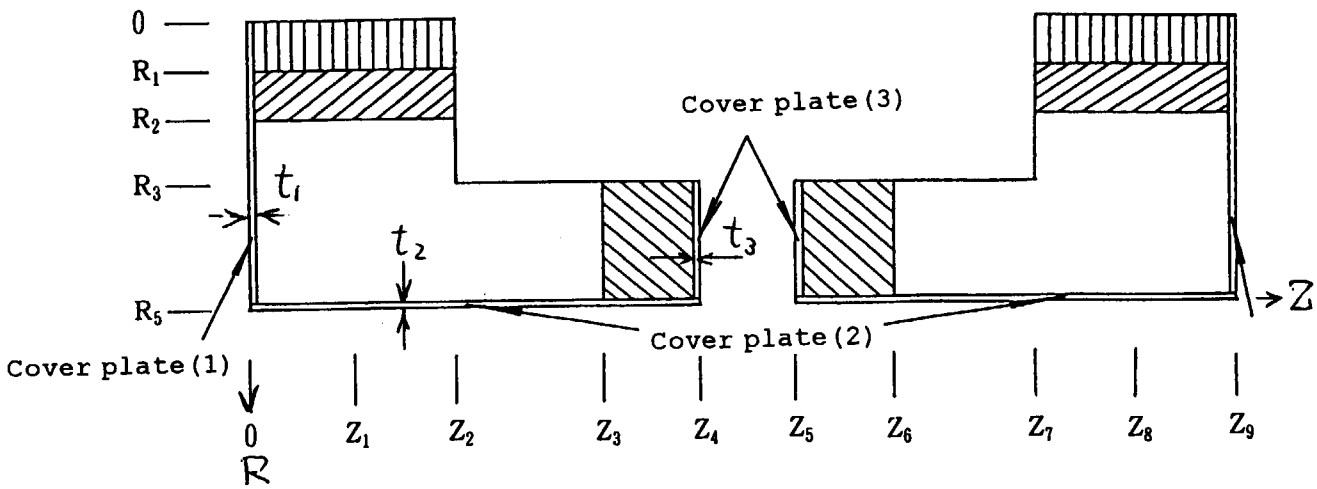

Fig. 3.22 Cover plate in the case of horizontal impact model

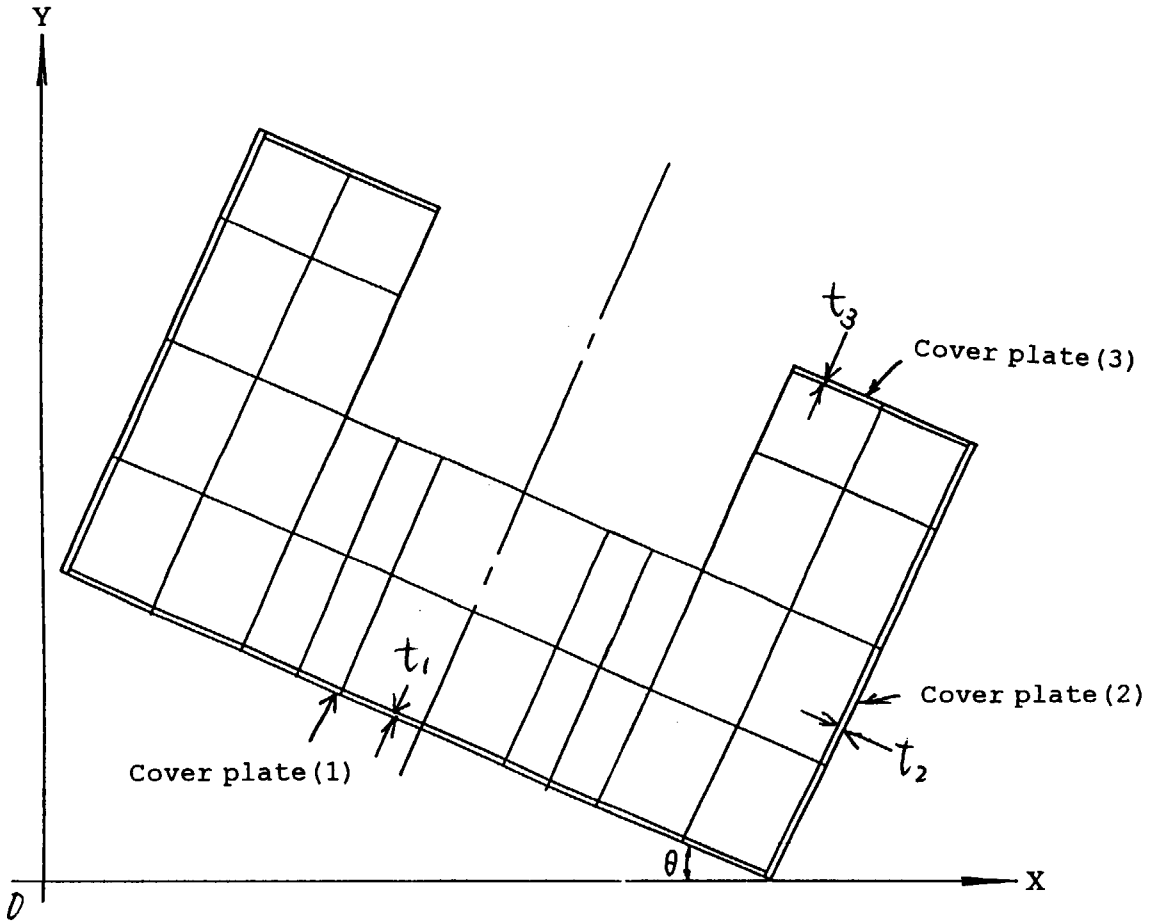

Fig. 3.23 Cover plate in the case of oblique impact model

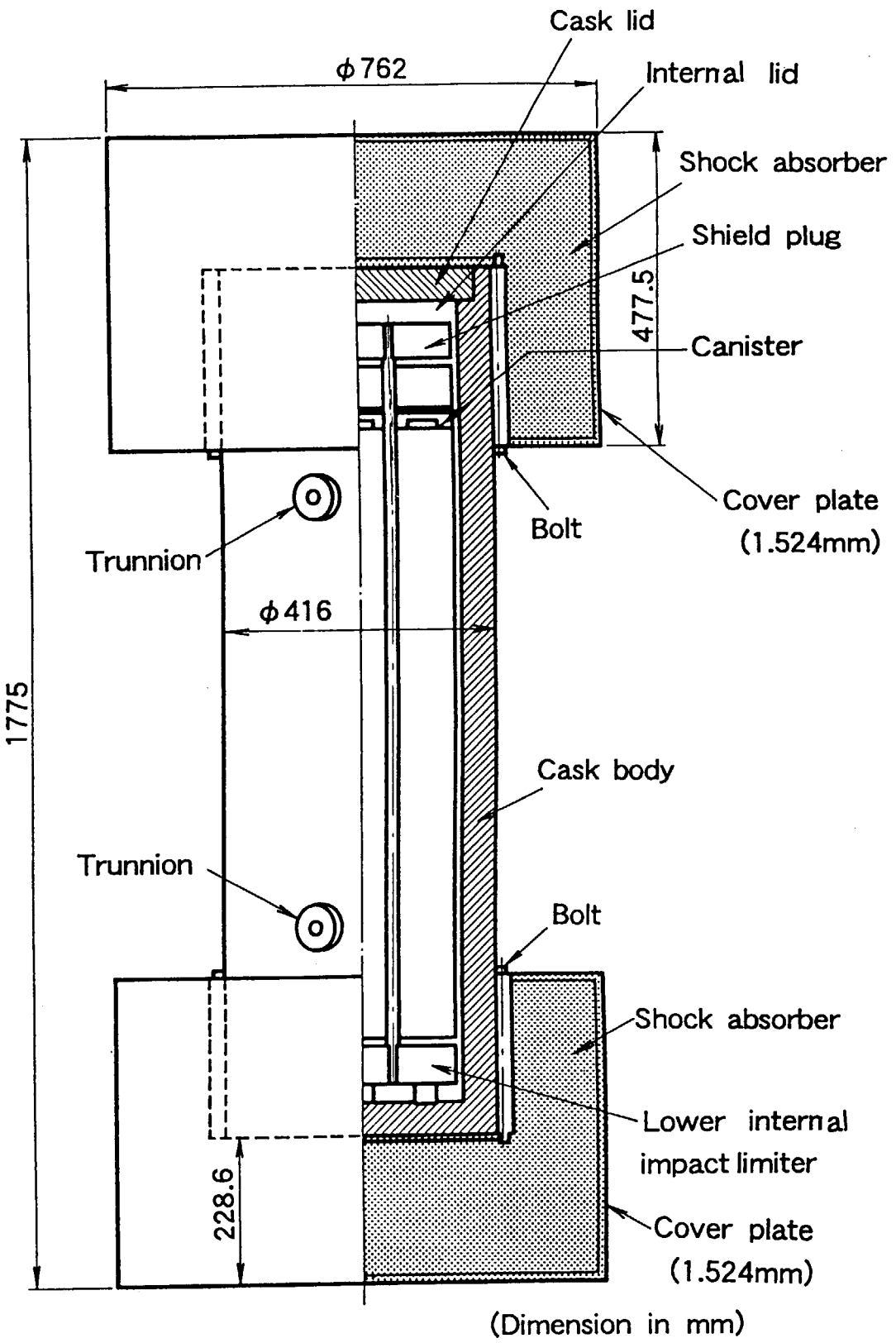

Fig. 3.24 Shipping cask NUPAC 125B (1/4 scale model)

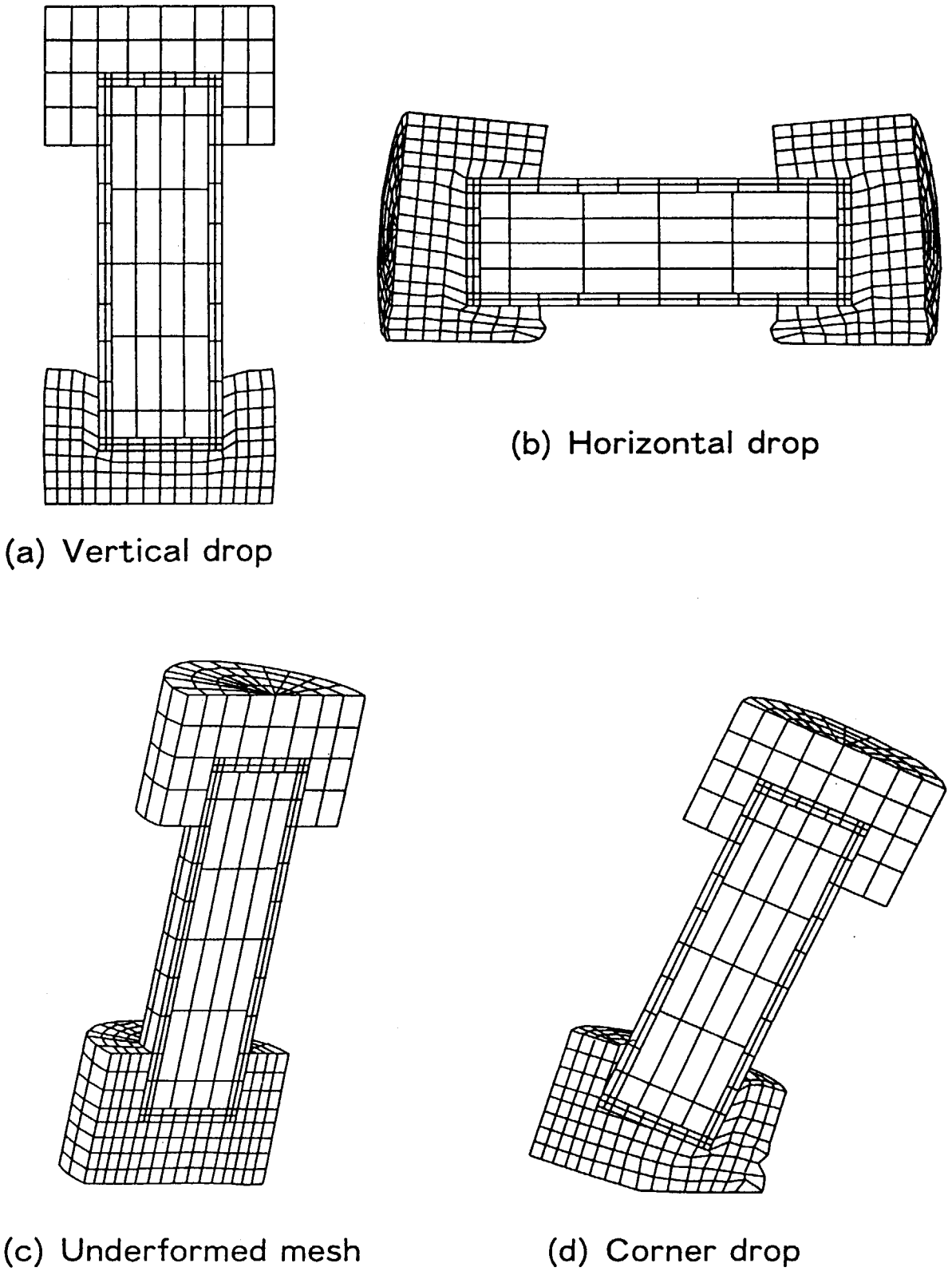

Fig. 3.25 Deformed shape after 9m drop impact (NUPAC 125B cask 1/4 scale model)

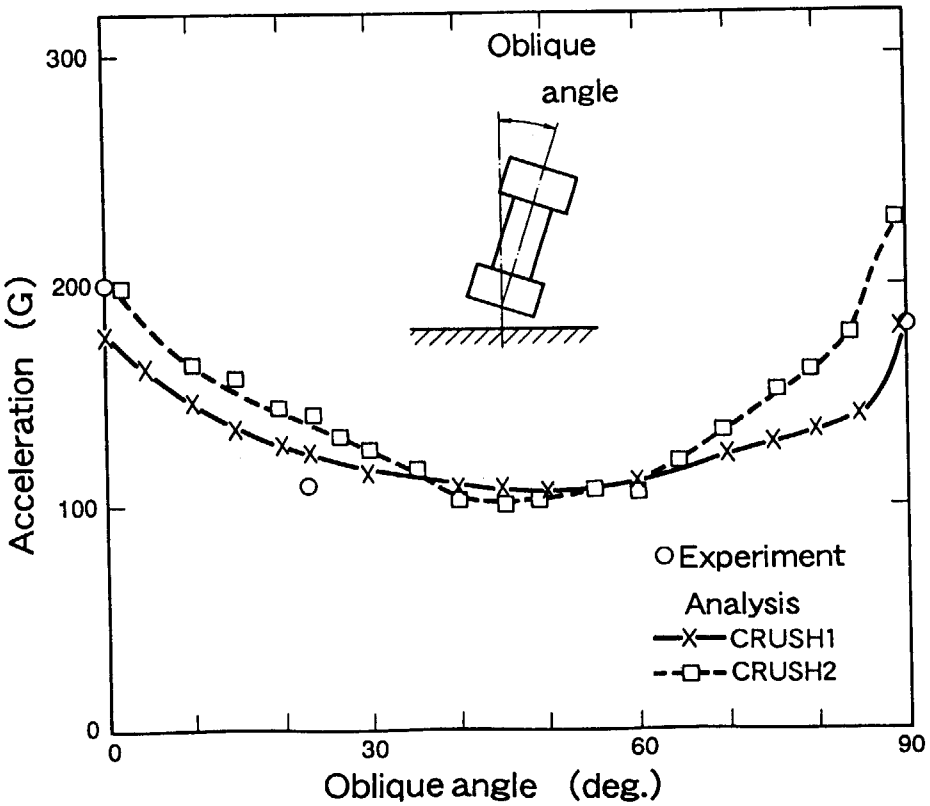

Fig. 3.26 Comparison between simplified analysis and experiment on impact acceleration

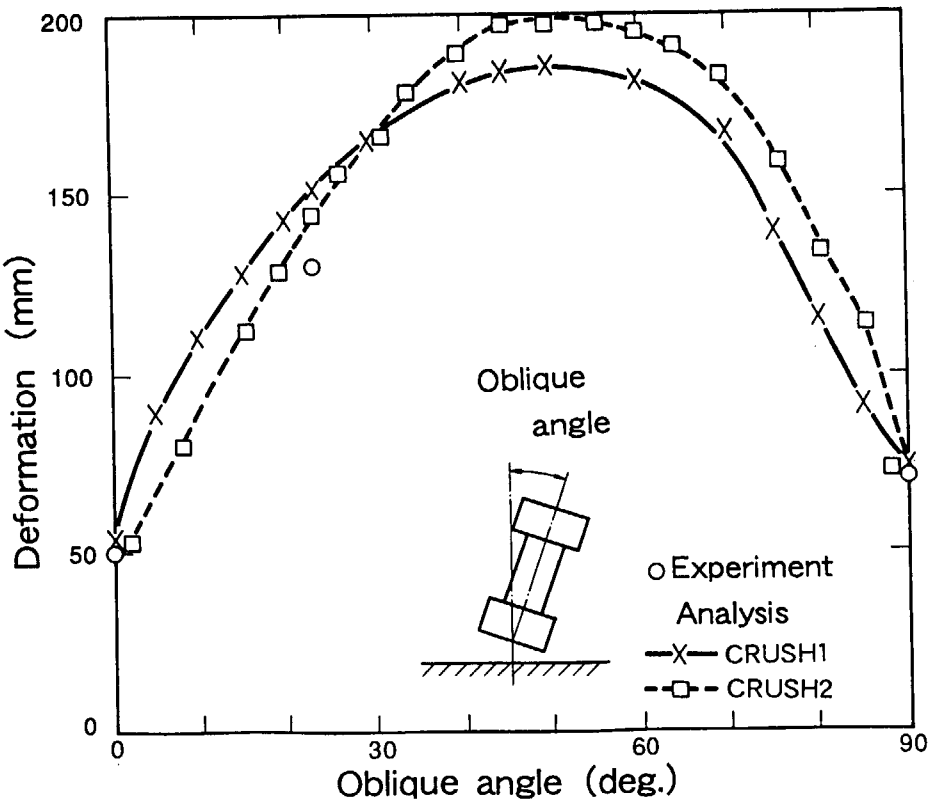

Fig. 3.27 Comparison between simplified analysis and experiment on shock absorber deformation

4. FINCRUSH

4.1 Description of FINCRUSH program

In the drop impact analyses for radioactive transport cask with cooling fins, it has become possible to perform them in detail by using interaction evaluation, computer programs, such as DYNA2D, DYNA3D, PISCES and HONDO. However, the considerable cost and computer time are necessitated to perform analyses by these programs. To meet the above requirements, a simplified computer program FINCRUSH[16] has been developed. The FINCRUSH is a static calculation computer program capable of evaluating the maximum acceleration of cask bodies and the maximum fin deformation using a relationship between the fin plastic deformation and the fin absorption energy. This relationship, the fin absorption energy vs. the fin deformation data, is obtained by Davis[17] of ORNL and Torr[18],[19] of MONSERCO in Canada from experiments. Using these data, the maximum acceleration of cask bodies and the maximum fin deformation are easily obtained.

4.2 Calculation equation

In the modeling of a fin impact analysis program FINCRUSH, it is assumed that the static plastic moment of fins is balanced with impact energy. That is

$$E_V = W H_0 , \tag{4.1}$$

where

E_V : impact energy,

W : weight of cask,

H_0 : height of cask drop.

On the other hand, the absorption energy of fins is

$$E_\Phi = F \delta , \tag{4.2}$$

where

E_Φ : impact energy,

F : impact force,

δ : fin deformation.

The cask drop energy is equal to the fin absorption energy. Therfore

$$E_V = E_\Phi \ . \tag{4.3}$$

The impact energy is absorbed by bending deformation of fins as shown in Fig. 4.1. The expression of the impact energy is derived from the Davis assumption. The static plastic moment may be expressed by the following equation:

$$M_p' = \sigma_y \left(\frac{b\ T^2}{4} \right) , \tag{4.4}$$

where

σ_y : yield stress,

b : length of fin,

T : thickness of fin,

M_p' : static plastic moment.

The static plastic moment per unit length of each of these fins is determined from the expression

$$M_p = \sigma_y \left(\frac{T^2}{4} \right) , \tag{4.5}$$

where M_p is static plastic moment per unit length. The fin absorption energy is given by

$$E_\Phi = \beta\ (\ \gamma\ )\ M_p\ b\ , \tag{4.6}$$

where β is the absorbed energy divided by the plastic moment and is written as follows:

$$\beta(\ \gamma\ ) = E_\Phi\ /\ (\ M_p\ b\ )\ . \tag{4.7}$$

In the other words, β is a constant and depends on the fin absorption energy versus the fin plastic moment obtained by Davis and Torr. In the data curve, β is shown on the ordinate and γ on the abcissa. The fin deformation ratio is defined by

$$\gamma = \delta_{\Phi} / H , \tag{4.8}$$

where

γ : fin deformation ratio,

δ_{Φ} : fin deformation,

H : fin height.

In the case of the inclined fin, the deformation of the fin is the following equation as shown in Fig. 4.2,

$$\delta_{\Phi} = R_0 - \frac{R_0 - \delta_0}{\cos\Phi} , \tag{4.9}$$

where

δ_{Φ} : fin deformation,

R_0 : outer radius of fin,

ϕ : attached angle of fin.

The fin deformation of the inclined fin is given by

$$\delta_0 = R_0 \cos\theta . \tag{4.10}$$

Davis and Torr present the fin absorption energy data as a function of the fin deformation ratio as shown in Figs 4.3 through 4.22. Therefore, the absorption energy in the case of fin impact is given by the following equation:

$$E_{\Phi} = \beta (\gamma) M_p b . \tag{4.11}$$

The force of the cask body may be expressed by the following equation:

$$F = dE_{\Phi} / d\delta_{\Phi} . \tag{4.12}$$

The acceleration of the cask body is determined by the following equation:

$$\alpha = F / (W / g) , \tag{4.13}$$

where

α : acceleration of cask body,

g : gravity constant.

4.3 Benchmark Calculation

In order to demonstrate the adequacy of the simplified computer program FINCRUSH, the benchmark calculations using experimental results of the JMS-18T-89Y (Japan Material Testing Reactor Spent Fuel Transport Cask) cask as shown in Fig. 4.23 have been performed.

Figure 4.24 and Table 4.1 show the comparison between experiment and analysis. According to Fig. 4.24 and Table 4.1, results by the computer program FINCRUSH agree with the experimental results.

Table 4.1 Comparison between experiment and analysis

Item	Experiment	Analysis	
		Fin data library	
		ORNL	MONSERCO
Acceleration(G)	−	50.3	42.2
Displacement(mm)	25	20.0	24.8

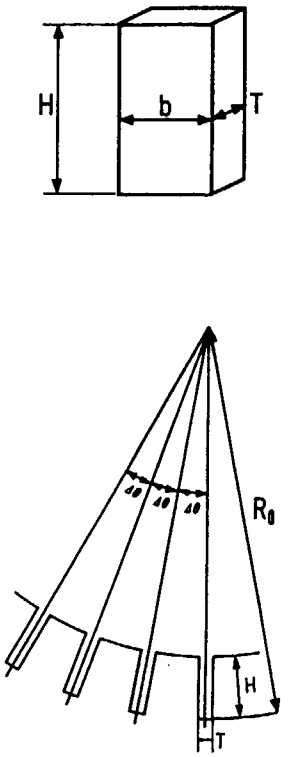

Fig. 4.1 Fin geometry

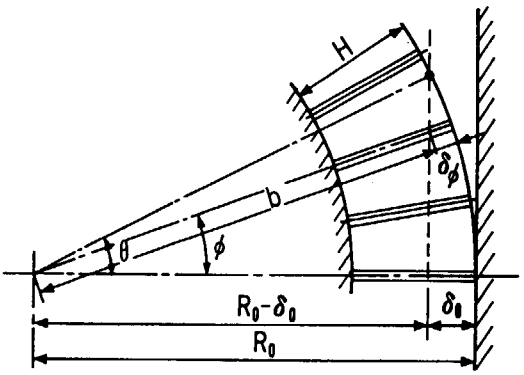

Fig. 4.2 Relationship between fin displacement and angle

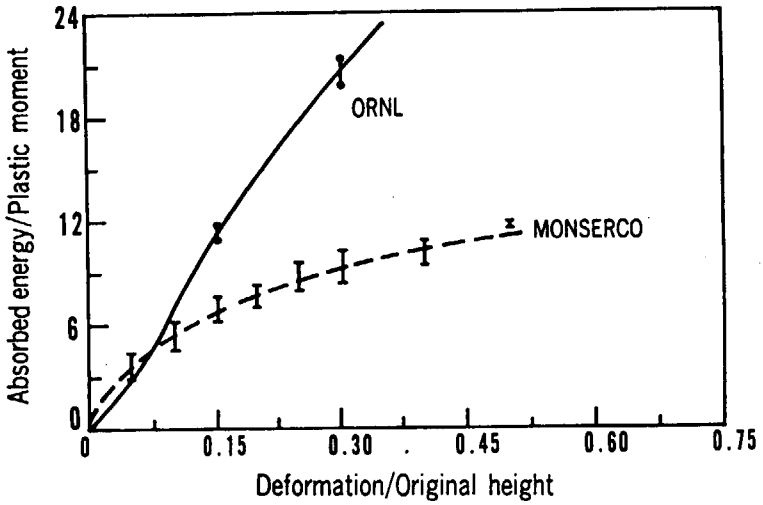

Fig. 4.3 Absorbed energy vs. deformation ratio of fin

[Fin height : 3.5 in.(89mm)
Inclination angle : 0 degree]

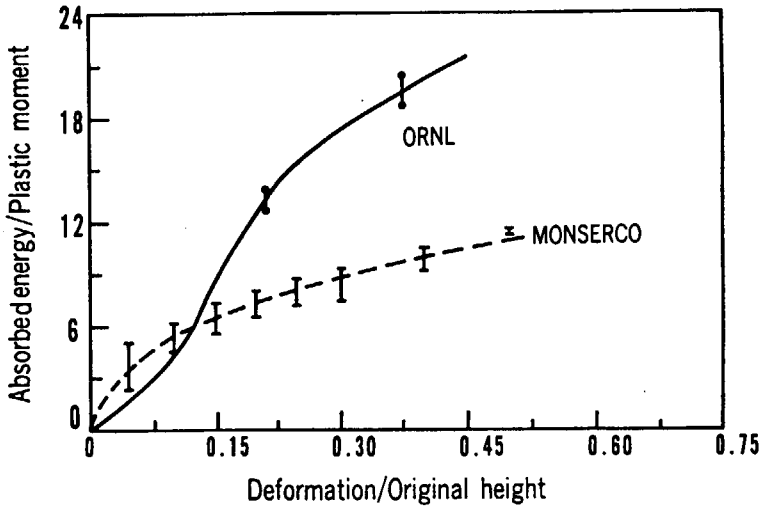

Fig. 4.4 Absorbed energy vs. deformation ratio of fin

[Fin height : 4.0 in.(102mm)
Inclination angle : 0 degree]

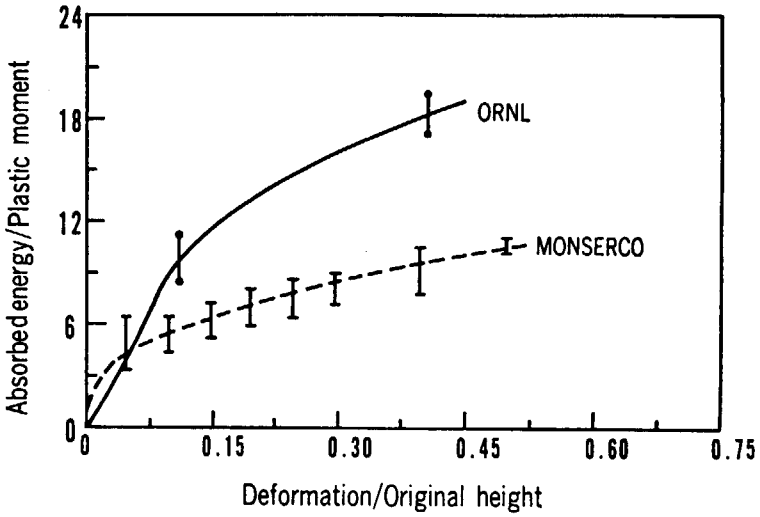

Fig. 4.5 Absorbed energy vs. deformation ratio of fin

[Fin height : 6.0 in.(152mm)
Inclination angle : 0 degree]

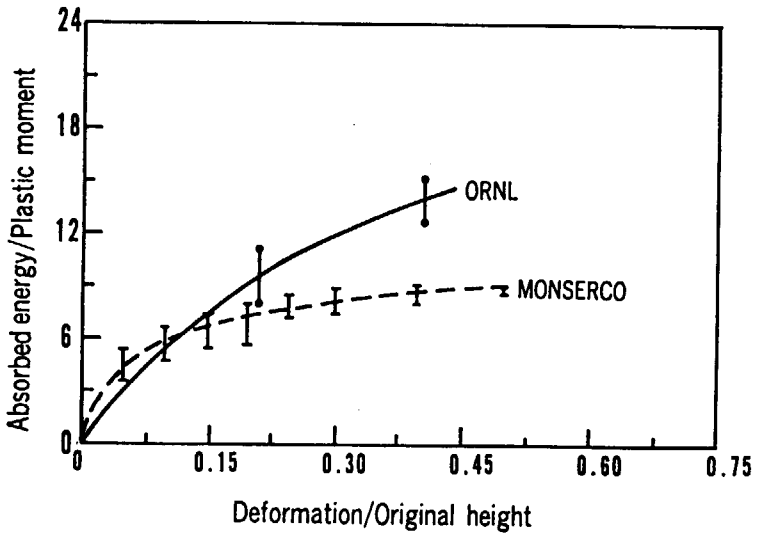

Fig. 4.6 Absorbed energy vs. deformation ratio of fin

[Fin height : 8.0 in.(203mm)
Inclination angle : 0 degree]

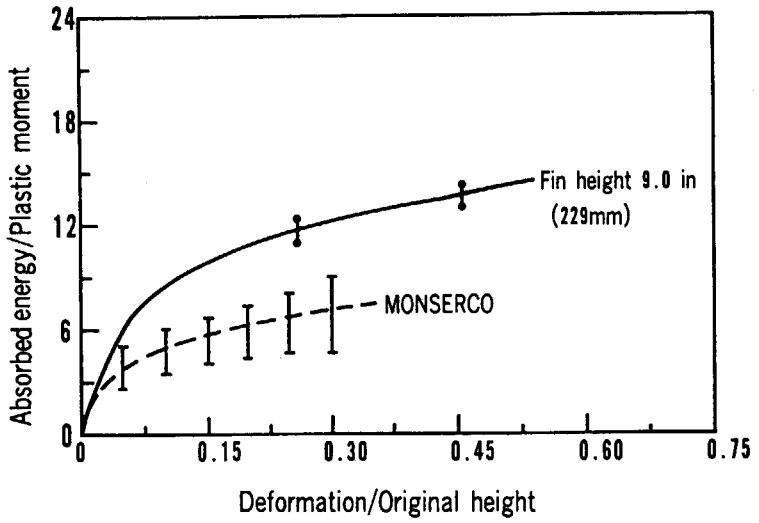

Fig. 4.7 Absorbed energy vs. deformation ratio of fin

[Fin height : 10.0 in.(254mm)
Inclination angle : 0 degree]

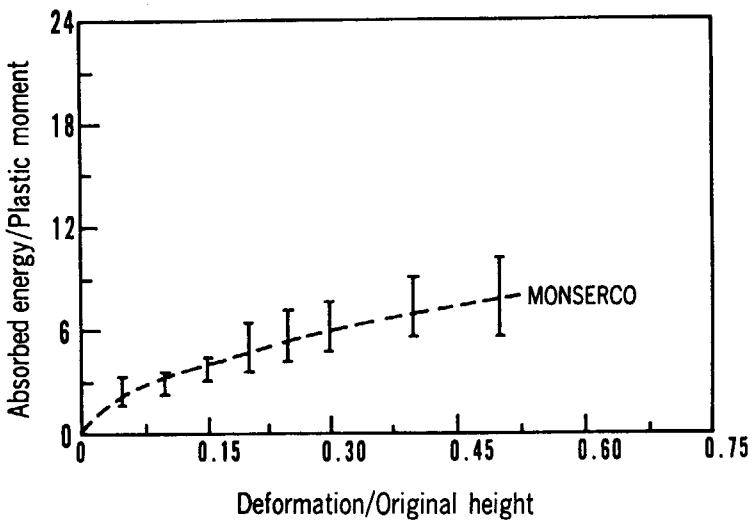

Fig. 4.8 Absorbed energy vs. deformation ratio of fin

[Fin height : 3.5 in.(89mm)
Inclination angle : 10 degree]

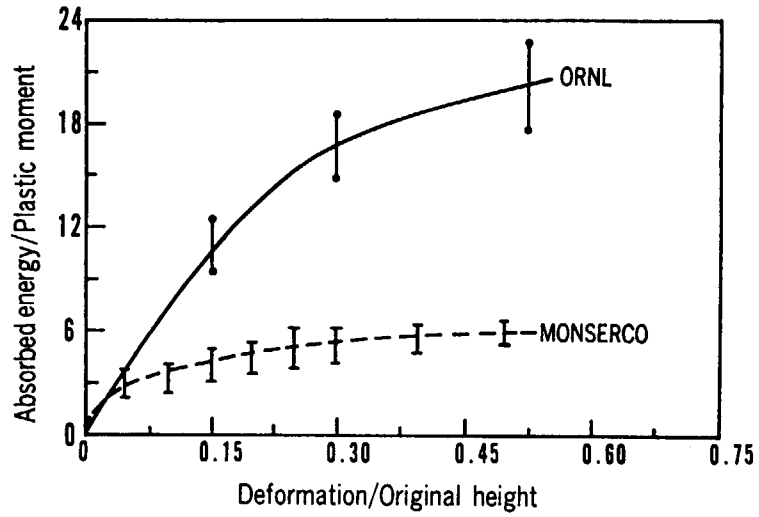

Fig. 4.9 Absorbed energy vs. deformation ratio of fin

[Fin height : 4.0 in.(102mm)
Inclination angle : 10 degree]

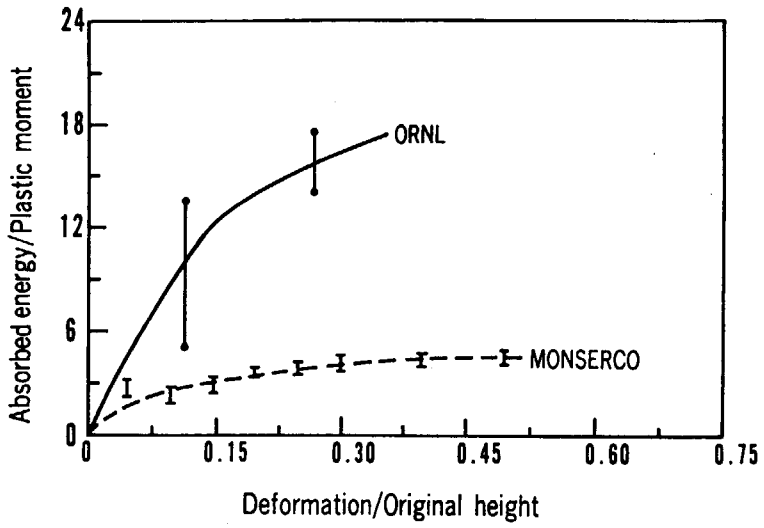

Fig. 4.10 Absorbed energy vs. deformation ratio of fin

[Fin height : 6.0 in.(152mm)
Inclination angle : 10 degree]

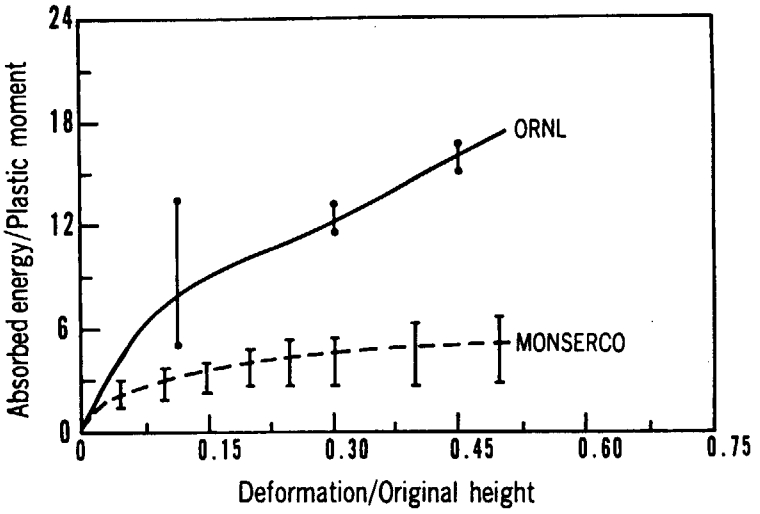

Fig. 4.11 Absorbed energy vs. deformation ratio of fin

[Fin height : 8.0 in.(203mm)
Inclination angle : 10 degree]

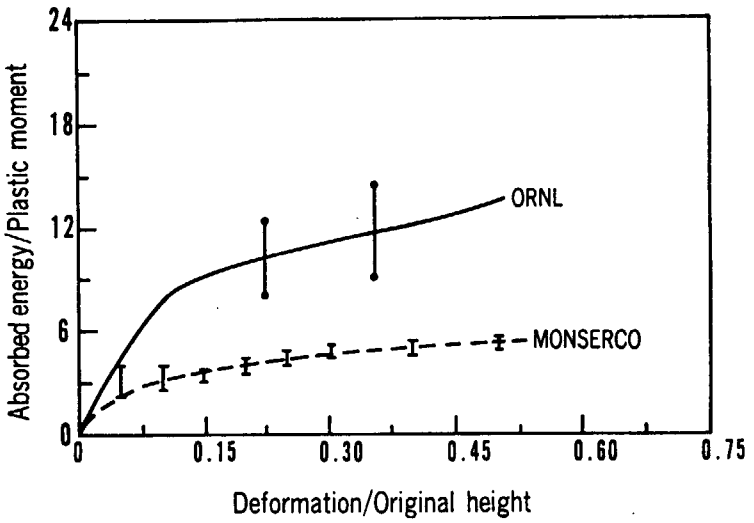

Fig. 4.12 Absorbed energy vs. deformation ratio of fin

[Fin height : 10.0 in.(254mm)
Inclination angle : 10 degree]

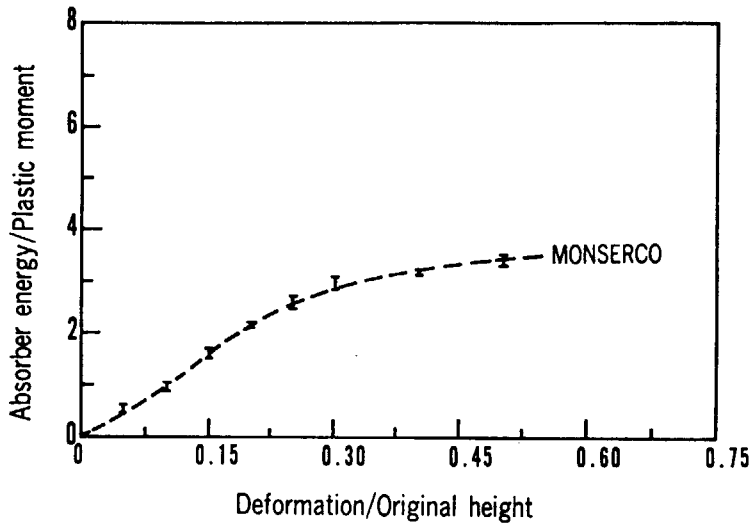

Fig. 4.13 Absorbed energy vs. deformation ratio of fin

[Fin height : 3.5 in.(89mm)
Inclination angle : 20 degree]

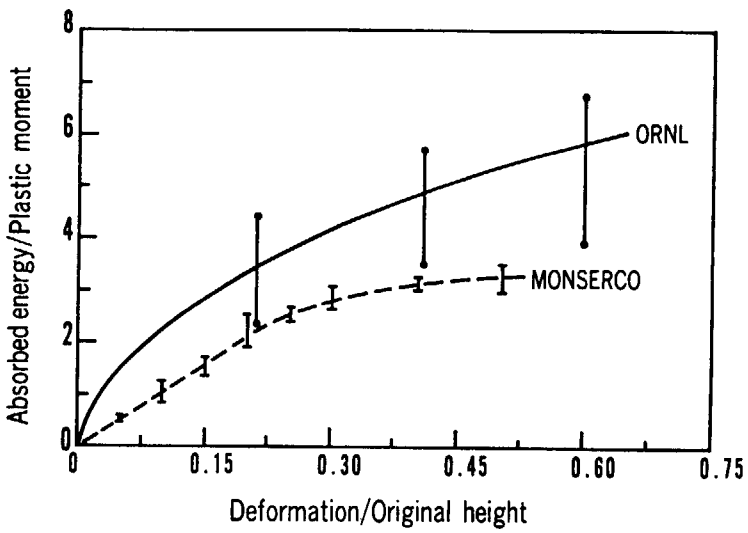

Fig. 4.14 Absorbed energy vs. deformation ratio of fin

[Fin height : 4.0 in.(102mm)
Inclination angle : 20 degree]

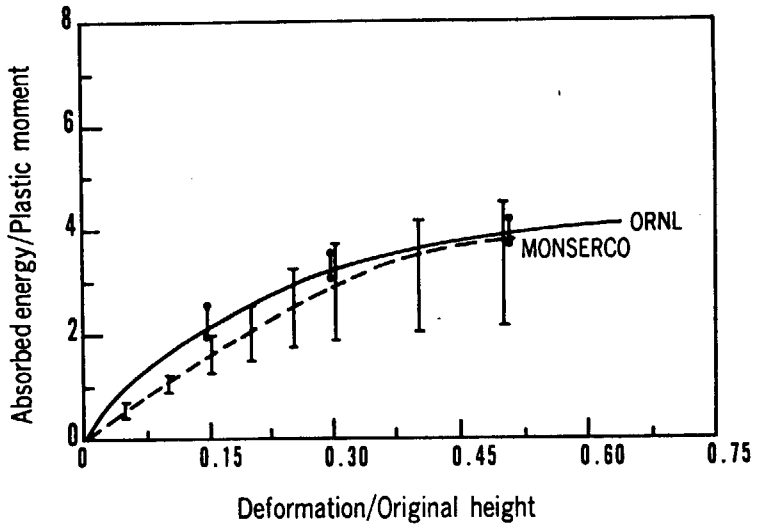

Fig. 4.15 Absorbed energy vs. deformation ratio of fin

[Fin height : 6.0 in.(152mm)
Inclination angle : 20 degree]

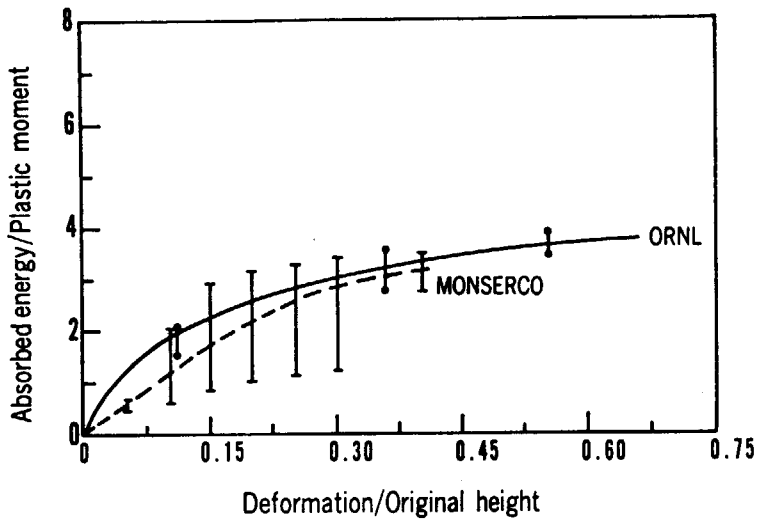

Fig. 4.16 Absorbed energy vs. deformation ratio of fin

[Fin height : 8.0 in.(203mm)
Inclination angle : 20 degree]

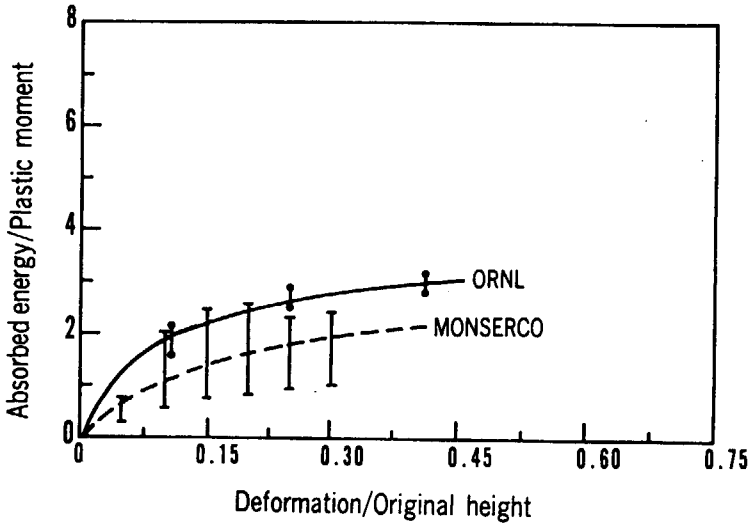

Fig. 4.17 Absorbed energy vs. deformation ratio of fin

[Fin height : 10 in.(254mm)
Inclination angle : 20 degree]

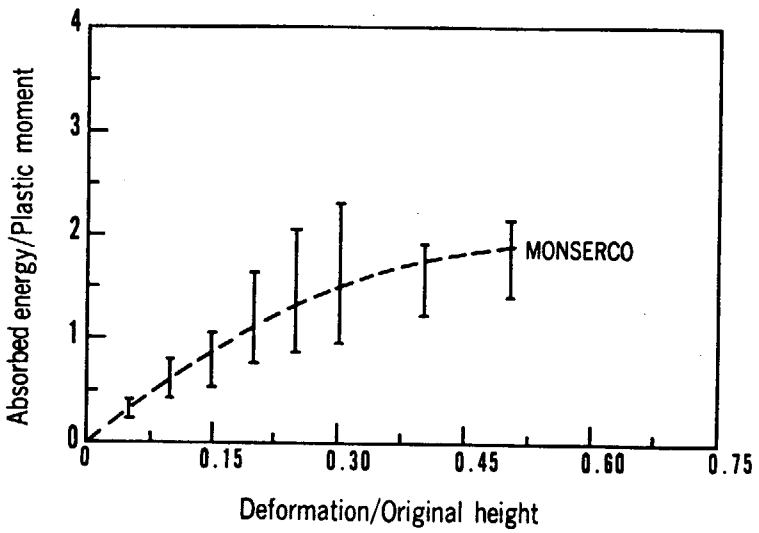

Fig. 4.18 Absorbed energy vs. deformation ratio of fin

[Fin height : 3.5 in.(89mm)
Inclination angle : 30 degree]

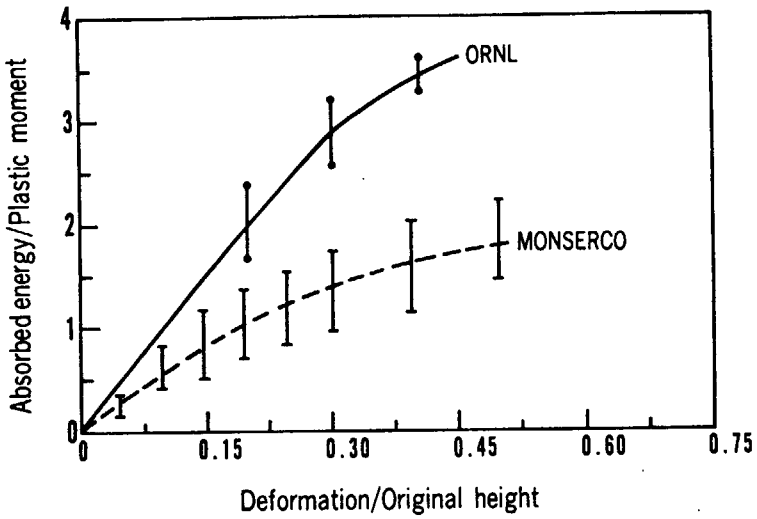

Fig. 4.19 Absorbed energy vs. deformation ratio of fin

[Fin height : 4.0 in.(102mm)
Inclination angle : 30 degree]

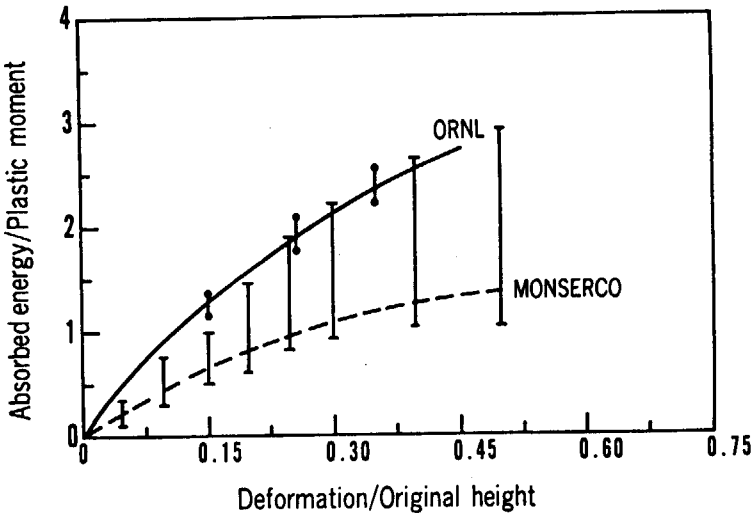

Fig. 4.20 Absorbed energy vs. deformation ratio of fin

[Fin height : 6.0 in.(152mm)
Inclination angle : 30 degree]

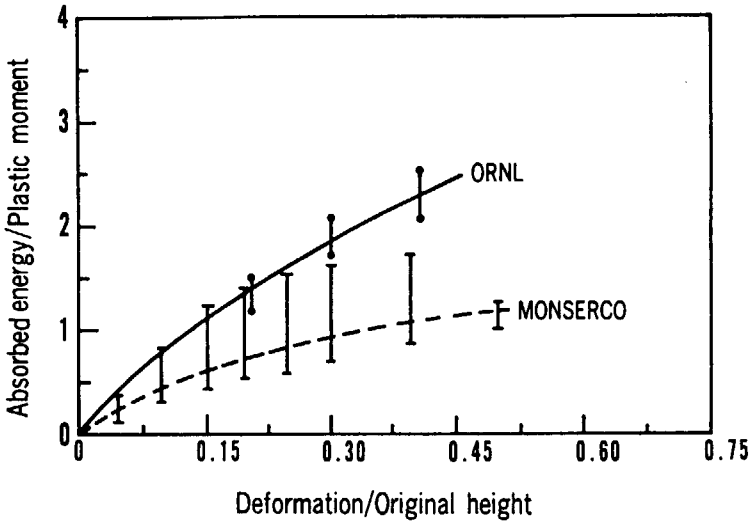

Fig. 4.21 Absorbed energy vs. deformation ratio of fin

[Fin height : 8.0 in.(203mm)
Inclination angle : 30 degree]

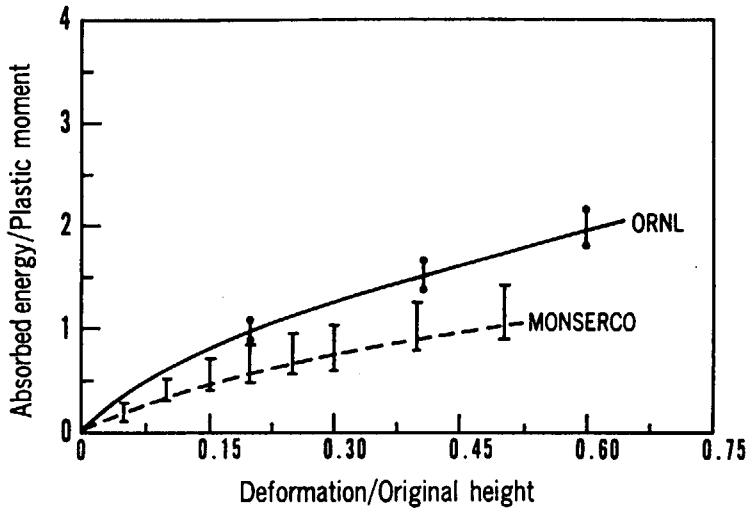

Fig. 4.22 Absorbed energy vs. deformation ratio of fin

[Fin height : 10.0 in.(254mm)
Inclination angle : 30 degree]

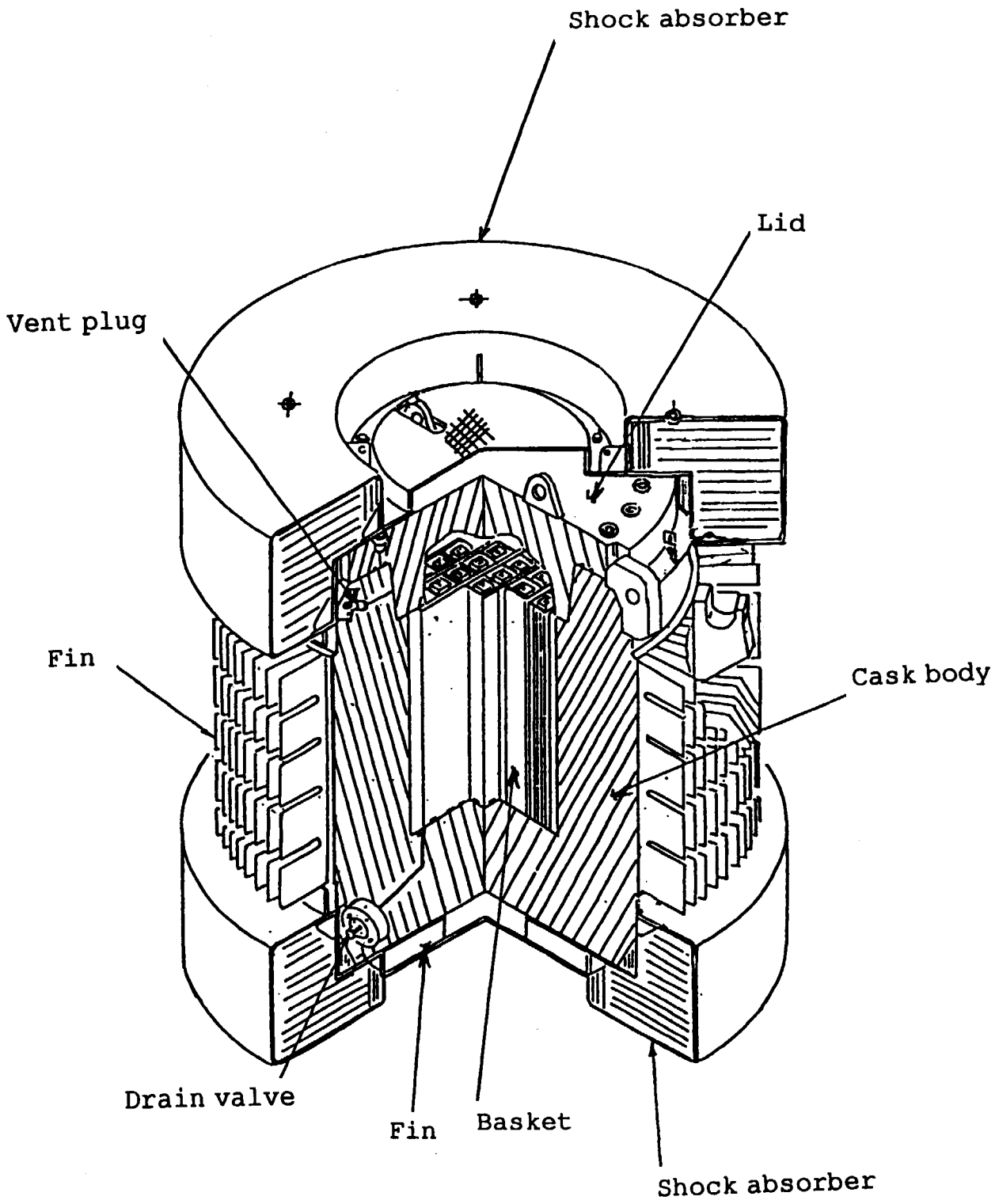

Fig. 4.23 JMS-18T-89Y cask (JMTR spent fuel cask)

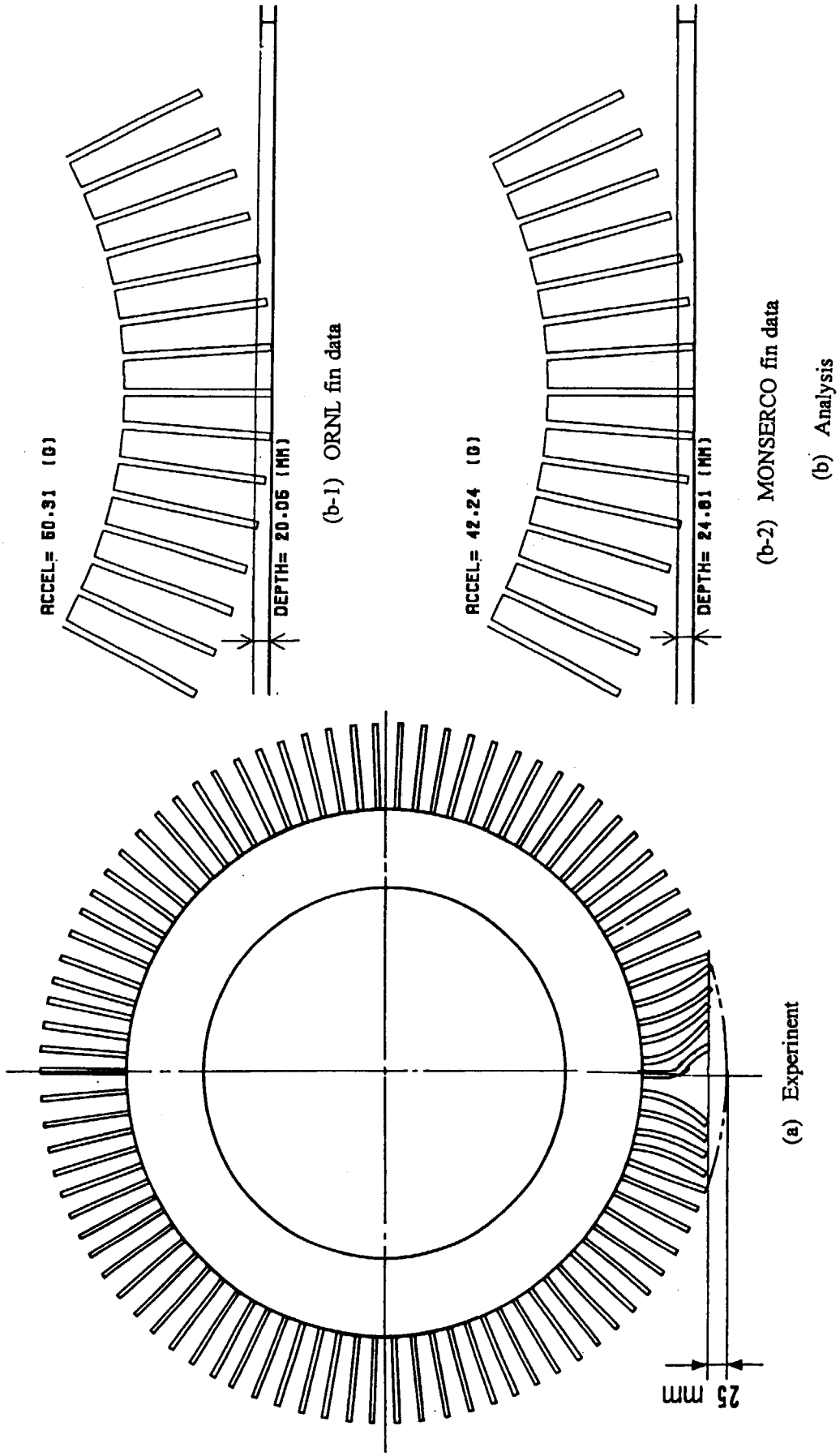

Fig. 4.24 Comparison between experiment and analysis

5. PUNCTURE

5.1 Description of PUNCTURE Program

Radioactive material transport casks (IAEA regulatory standard type B packages, type A fissile packages and so on) are required to maintain integrity against the puncture test where it is dropped onto a 150 mm diameter mild steel bar from a height of one meter.

In the drop puncture analyses for radioactive transport casks, it has become possible to perform them in detail calculation by using interaction evaluation computer programs, DYNA2D, DYNA3D, NIKE2D, NIKE3D, PISCES and HONDO. However, the considerable cost and the computer time are necessitated to perform analyses by these programs. To decrease the cost and the time, a simplified computer program PUNCTURE[20] shown in Fig.5.1 has been developed. The PUNCTURE is a static calculation computer program based on the Onat's theory[21] and Asada's research[15]. The PUNCTURE is capable of evaluating the acceleration of cask bodies, the deformation of puncture plates and the stress and the deformation of puncture bars.

5.2 Calculation Equation

5.2.1 Calculation Model

In the calculation model, the puncture does not occur when a cask is dropped onto a mild steel bar as shown in Fig.5.1. It is assumed that the kinetic energy of the cask is absorbed into deformations of both the cask body and the mild steel bar. The deformation generated on the cask body can be evaluated based on the fact that loads generated on the cask and the mild steel bar are equal to each other. In this evaluation, the plastic theory of bending of a circular plate having a multi-layer construction (e.g. steel-lead-steel three layers) is used, which has been developed by extending Onat's theory and Asada's research.

5.2.2 Energy Balance

In the modeling of the puncture analysis program PUNCTURE, it is assumed that plastic energy of a cask and a puncture bar is balanced with impact energy. That is

$$E_V = WH_o \ , \tag{5.1}$$

where

E_v: impact energy,

W : weight of impacting body,

H_0 : drop height of impacting body.

In the theory, elasticity of the material is usually neglected and the load-carrying capacity is estimated as the load at which a model composed of an ideal rigid-plastic material would begin to deform. It can be shown that, if the material is perfectly plastic (i.e., nonstrain hardening) and if the accompanying change in geometry is disregarded, plastic flow continues under constant load.

The load-deflection relationship of the mild steel bar is shown in the following equation.

$$P_p=f(\delta_p) \ , \tag{5.2}$$

where

P_p : load act on steel bar,

δ_P : plastic deformation of steel bar.

On the other hand, the load-deflection relationship of the cask body is shown in the following equation:

$$P_c=h\ (\delta_c) \ , \tag{5.3}$$

where

P_c : load act on cask body,

δ_c : plastic deformation of cask body.

In the case of the cask whose weight is W is dropped from a height H onto the mild steel bar, the following equations are given from the conservation law of energy:

$$WH_0=\int_0^{\delta_P} f(\delta_p)d\delta_p+\int_0^{\delta_c} h(\delta_c)d\delta_c \ , \tag{5.4}$$

$$f(\delta_P)=h(\delta_C) \ . \tag{5.5}$$

The acceleration of the cask body is determined by the following equation:

$$\alpha=h(\delta_C)\ /\ (W/g) \ , \tag{5.6}$$

where

α : acceleration of cask body,

g : gravity constant.

5.2.3 Load Deflection Relationship

(1) Fixed supported bending plate model

When a distributed load is applied to a three-layer circular rigidly clamped at its edges as shown in Fig.5.2, the relationship between the displacement and the load can be given by

$$P^*=1+\alpha_1 U+\alpha_2 U^2 \ ; \ (U \leqq U^*) \tag{5.7}$$

$$P^*=\beta_1+\beta_2 U+\beta_3/U \ ; \ (U \geqq U^*) \ , \tag{5.8}$$

where

$P^* = P/P_L$,

P^* : nondimensional load,

P : load,

P_L : limit load,

$U = \delta / t^*$,

U : nondimensional deflection,

δ : center deflection

t^* : equivalent plate thickness,

$$U^*=(1+\ln (R/\rho))/2 \ , \tag{5.9}$$

R : radius of plate,

ρ : discontinuity radius of velocity curvature,

a : radius of loaded area,

and the factors α_1, α_2, β_1, β_2 and β_3 are given by

$$\alpha_1=\frac{\left(1+2\ \ln\frac{R}{\rho}\right)}{\left(2+\ln\frac{R}{\rho}\right)\left(1+\ln\frac{R}{\rho}\right)} \ , \tag{5.10a}$$

$$\alpha_2=\frac{2\left(1+3\ \ln\frac{R}{\rho}\right)}{3\left(2+\ln\frac{R}{\rho}\right)\left(1+\ln\frac{R}{\rho}\right)^2} \ , \tag{5.10b}$$

$$\beta_1=\frac{\left(3+\ln\frac{R}{\rho}\right)}{2\left(2+\ln\frac{R}{\rho}\right)} , \tag{5.10c}$$

$$\beta_2=\frac{2\left(1+2\ \ln\frac{R}{\rho}\right)}{\left(2+\ln\frac{R}{\rho}\right)\left(1+\ln\frac{R}{\rho}\right)} , \tag{5.10d}$$

$$\beta_3=\frac{\left(1+\ln\frac{R}{\rho}\right)}{12\left(2+\ln\frac{R}{\rho}\right)} . \tag{5.10e}$$

The discontinuity radius of the velocity ρ curveture is determined by the following equations.

$$1-\frac{2a}{3\rho}\left(1+1n\frac{R}{\rho}\right)=0 \ ; \ (a/R\leqq 0.606) , \tag{5.11a}$$

$$1-\left(\frac{2}{\rho}\right)^2\left(1+2\ \ln\frac{R}{\rho}\right)+\frac{2}{3}\left(1+\ln\frac{R}{\rho}\right)=0 \ ; \ (a/R\geqq 0.606) , \tag{5.11b}$$

The limit load P_L is given by

$$P_L=2\pi M_p\frac{A}{B} , \tag{5.12}$$

where

$$A=2+\ln\frac{R}{\rho} , \tag{5.13a}$$

$$B=1+\ln\frac{R}{\rho}-\frac{2a}{3\rho} \ ; \ (\rho\geqq a) , \tag{5.13b}$$

$$B=\frac{1}{2}+\ln\frac{R}{a}-\frac{\rho^2}{6a^2}\ ;\ (\rho\leqq a)\ , \tag{5.13c}$$

$$M_p=\frac{(t^*)^2}{\rho}\sigma^*\ , \tag{5.13d}$$

where

M_p : sectional yield moment,

σ^* : equivalent stress.

(2) Simply supported plate bending model

In the case of the simply supported plate bending model as shown in Fig.5.3, the equivalent loads are given by

$$P^*=1+\frac{4}{3}U^2\ ;\ (U\leqq 0.5)\ , \tag{5.14a}$$

$$P^*=2U+\frac{1}{6U}\ ;\ (U\geqq 0.5)\ . \tag{5.14b}$$

The limit load P_L is given by

$$P_L=\frac{2\pi M_p}{\left(1-\frac{2a}{3}\right)}\ . \tag{5.15}$$

(3) Fixed supported membrane plate model

In the case of the fixed supported membrane plate model as shown in Fig.5.4, the load acting on the plate is given by the following:

$$P=\frac{2\pi N_p\delta}{\frac{1}{2}+\ln\frac{R}{a}}\ , \tag{5.16}$$

where N_p is the sectional yielding load of the plate,

$$N_P=\sigma^* t^* \ , \tag{5.17}$$

and t^* is an equivalent thickness of the plate.

5.2.4 Equivalent Thickness and Equivalent Stress

In converting a three-layer plate into an equivalent single plate, the equivalent plate thickness t^* and the equivalent stress σ^* are related by the following equations:

$$t^*=\frac{4M_p}{N_p} \ , \tag{5.18}$$

$$\sigma^*=\frac{N_p}{t^*} \ , \tag{5.19}$$

where the sectional yield load N_p is given by the following equations:

$$N_p=(\sigma_1)_T t_1+(\sigma_2)_T t_2+(\sigma_3)_T t_3 \ , \tag{5.20}$$

where

t_1 : thickness of outer plate,
t_2 : thickness of intermediate plate,
t_3 : thickness of inner plate,
σ_1 : stress of outer plate,
σ_2 : stress of intermediate plate,
σ_3 : stress of inner plate,
$(\ )_C$: denotes compression,
$(\ )_T$: denotes tension.

According to the position of the neutral axis of stress, there are three kinds of stress states as shown in Fig.5.5. Those are named stress states A, B and C. In the case of the stress state A, the neutral axis exists in the outer layer, the stress state B in the intermediate and the stress state C in the inner.

(1) Stress state A

The equilibirum of stress in the three layer plates leads the following equations (see Fig.5.5a):

$$(\sigma_1)_C t=(\sigma_1)_T(t_1-t)+(\sigma_2)_T t_2+(\sigma_3)_T t_3 \ , \tag{5.21}$$

where t is a distance from outer surface to neutral axis.

$$t=\frac{(\sigma_1)_T t_1+(\sigma_2)_T t_2+(\sigma_3)_T t_3}{(\sigma_1)_C+(\sigma_1)_T} \quad . \tag{5.22}$$

The sectional yield moment is given by the following equation:

$$M_p=\frac{(t)^2}{2}(\sigma_1)_C+\frac{1}{2}(t_1-t)^2(\sigma_1)_T+\left(t_2\left(t_1-t+\frac{t_2}{2}\right)\right)(\sigma_2)_T$$
$$+\left(t_3\left(t_1-t+t_2+\frac{t_3}{2}\right)\right)(t_3)_T \quad . \tag{5.23}$$

The stress state A is established by the following condition:

$$(\sigma_1)_C t_1 \geqq (\sigma_2)_T t_2+(\sigma_3)_T t_3 \quad . \tag{5.24}$$

(2) Stress state B

The equilibrium of stress in the three layer plates leads the following equations (see Fig.5.5b):

$$(\sigma_1)_C t_1+(\sigma_2)_C(t-t_1)=(\sigma_2)_T(t_1+t_2-t)+(\sigma_3)t_3 \quad , \tag{5.25}$$

$$t=\frac{-(\sigma_1)_C t_1+(\sigma_2)_C t_1+(\sigma_2)_T(t_1-t_2)+(\sigma_3)_T t_3}{(\sigma_2)_C+(\sigma_2)_T} \quad , \tag{5.26}$$

$$M_p=t_1\left(t-\frac{t_1}{2}\right)(\sigma_1)_C+\frac{1}{2}(t-t_1)^2(\sigma_2)_C$$
$$+\frac{1}{2}(t_1+t_2-t)^2(\sigma_2)_T+t_3\left(t_1+t_2-t+\frac{t_3}{2}\right)(\sigma_3)_T \quad , \tag{5.27}$$

$$(\sigma_1)_C t_1+(\sigma_2)_C t_2 \geqq (\sigma_3)_T t_3 \quad . \tag{5.28}$$

(3) Stress state C

The equilibrium of stress in the three layer plates leads the following equations (see Fig.5.5c):

$$(\sigma_1)_C t_1+(\sigma_2)_C t_2+(\sigma_3)_C(t-t_1-t_2)=(\sigma_3)_T(t_1+t_2+t_3-t) \ , \tag{5.29}$$

$$t=\frac{-(\sigma_1)_C t_1-(\sigma_2)_C t_2+(\sigma_3)_C(t_1+t_2)+(\sigma_3)_T(t_1+t_2+t_3)}{(\sigma_3)_C+(\sigma_3)_T} \ , \tag{5.30}$$

$$M_p=t_1\left(t-\frac{t_1}{2}\right)(\sigma_1)_C+t_2\left(t-t_1-\frac{t_2}{2}\right)(\sigma_2)_C$$
$$+\frac{1}{2}(t-t_1-t_2)^2(\sigma_3)_C+\frac{1}{2}(t_1+t_2+t_3-t)^2(\sigma_3)_C \ , \tag{5.31}$$

$$(\sigma_1)_C t_1+(\sigma_2)_C t_2 \leqq (\sigma_3)_T t_3 \ . \tag{5.32}$$

5.2.5 Condition of Plate Puncture

The condition of the three layer plate puncture is given by the following equation:

$$P \geqq \pi d(\tau_1 t_1+\tau_2 t_2+\tau_3 t_3) \ , \tag{5.33}$$

where

P : load,

τ_1 : failure shear stress of outer plate,

τ_2 : failure shear stress of intermediate plate,

τ_3 : failure shear stress of inner plate,

$$\tau_1=0.6(\sigma_1)_u \ , \tag{5.34a}$$

$$\tau_2=0.6(\sigma_2)_u \ , \tag{5.34b}$$

$$\tau_3=0.6(\sigma_3)_u \ , \tag{5.34c}$$

$(\sigma_1)u$: ultimate tensile strength of outer plate,

$(\sigma_2)u$: ultimate tensile strength of intermediate plate,

$(\sigma_3)u$: ultimate tensile strength of inner plate.

5.3 Benchmark Calculation

In order to demonstrate the adequacy of the simplified computer program PUNCTURE, the benchmark calculation using experimental results of the LLNL has been performed. Table 5.1 shows the LLNL experimental data.

Table 5.2 and Fig.5.6 show comparisons between the LLNL[22] experiments and the PUNCTURE results. According to Fig.5.6, results by the computer program PUNCTURE agree with the experimental results performed on multilayer plates. The PUNCTURE program can practicably estimate the actual data to be obtained by the puncture test.

Table 5.1 LLNL experimental data

Item	Diameter (mm)	Thickness (mm)	Length (mm)	Material
Outer circular plate	203.2	5.08		SUS304
Inner circular plate		15.24		Lead
Puncture bar	15.24		20.32	Steel

Table 5.2 Comparison between LLNL experiments and PUNCTURE

Item		Limit load (10^4 kgf)
LLNL experiments	Static test	1.15
	Dynamic test	1.21
PUNCTURE		1.04

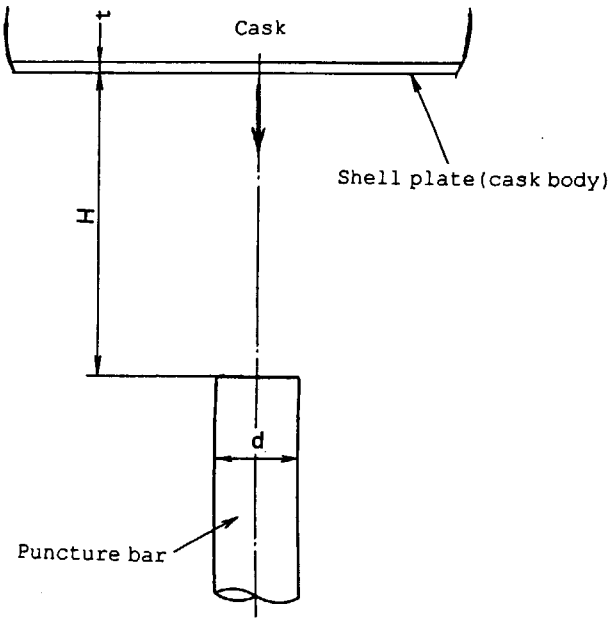

Fig. 5.1 Puncture analysis model

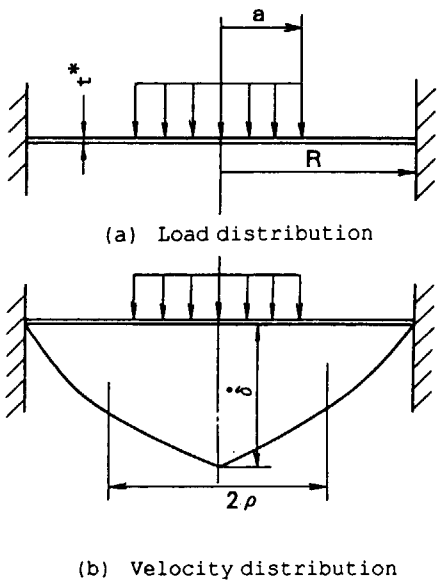

Fig. 5.2 Fixed supported bending plate with distributed load

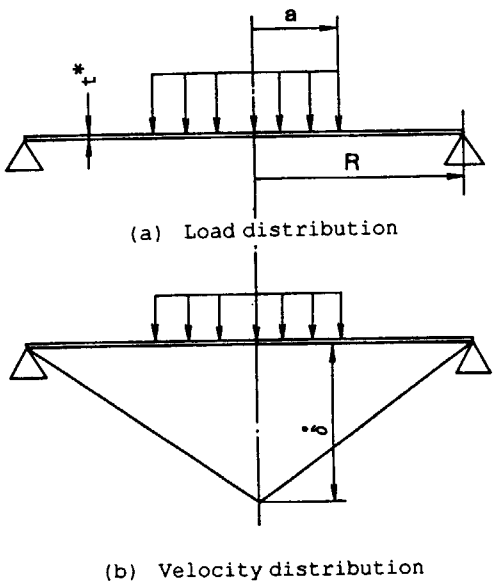

Fig. 5.3 Simply supported bending plate with distributed load

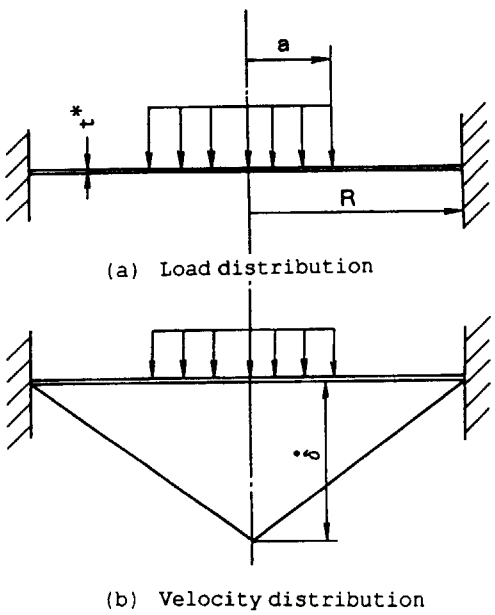

Fig. 5.4 Fixed supported membrane plate with distributed load

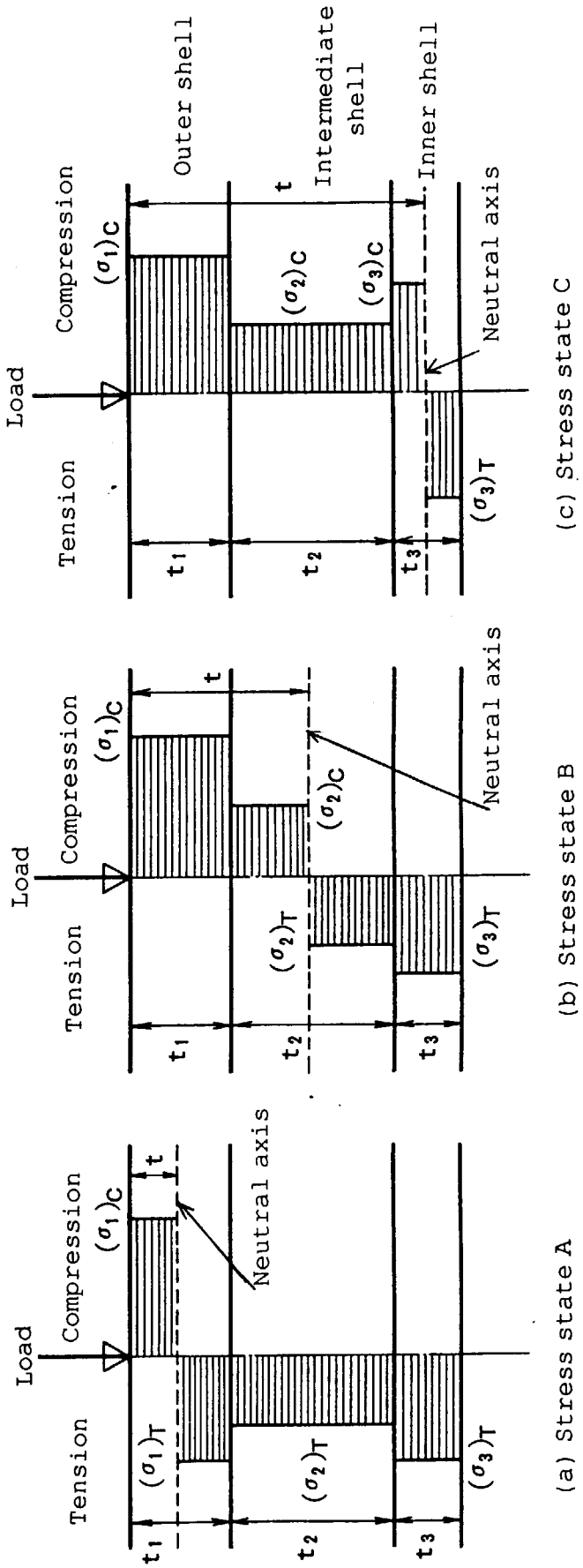

Fig. 5.5 Three kinds of stress states in three layer shells

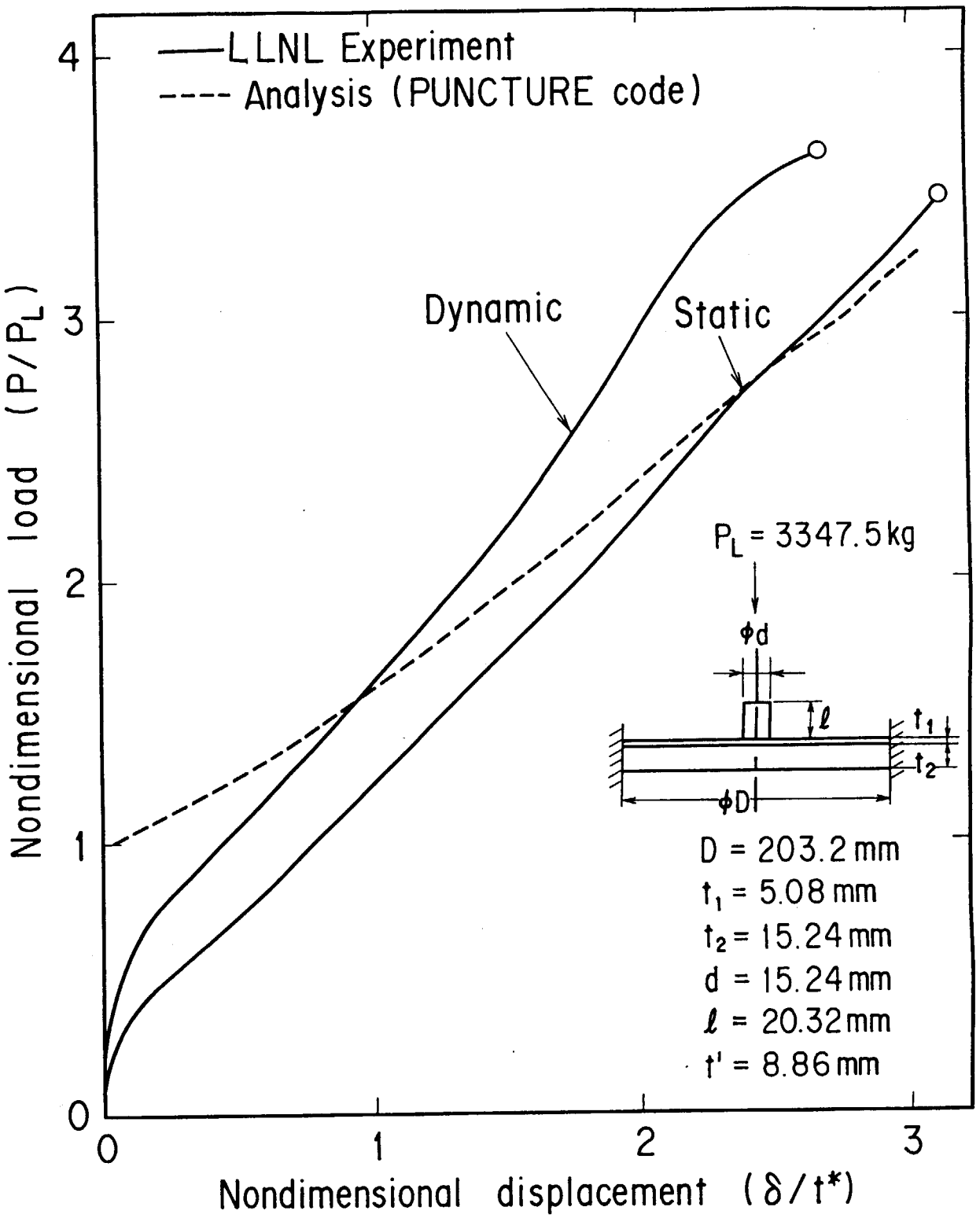

Fig. 5.6 Load vs. displacement

6. ROCKING

6.1 Description of ROCKING program

In the stand point of seismic safety of transport and/or storage casks for spent fuels, it is necessary to evaluate integrity of casks against seismic loads. Therefore, it is important to clarify the tip-over behavior of casks during seismic loads.

Central Research Institute of Electric Power Industry(CRIEPI)[23],[24] has studied seismic response behavior of casks experimentally and analytically. In this analysis, the Distinct Element Method(DEM) was used for tip-over behavior of casks. However, the considerable cost and calculation time are necessitated to perform such analysis by the DEM.

Therefore, simplified computer programs which are capable of reducing cost and calculation time are needed to perform parametric calculation in designing casks and conducting safety analysis. To meet the above requirements, the computer program ROCKING[25] has been developed.

In the program, a cask with (or without) tie-down wire ropes is modeled by a vertical cylindrical rigid body tied down with four non-linear springs having a certain tensile strength. An explicit or a semi-implicit numerical integration method is adopted to predict whether a cask will tip-over or not, and tie-down ropes will break or not. Moreover, in the ROCKING program, sliding between a cask and a floor and vertical seismic load are treated.

6.2 Calculation equation

6.2.1 Calculation model

In the computer program ROCKING, the following two-dimensional model is considered:

(1) a cask is modeled as a rigid body,

(2) the cask has three degrees-of-freedom, two translational displacements and one rotation around the cask center of gravity,

(3) impact forces are represented by a spring and dashpot model located at impact points,

(4) friction force due to surface sliding between the cask and a floor is represented by a nonlinear Coulomb element, and

(5) forces of wire ropes work against only as tensile loads.

6.2.2 Equation of governing motion

Let the coordinate system be chosen as shown in Fig.6.1. The cask has two translational coordinates, ξ and η, and one rotational coordinate θ. Figure 6.2 shows the forces and moments that act upon the cask. The equations of motion may be written as:

$$m\ddot{\xi} = -m\alpha_{\xi} + F_{\xi A} + F_{\xi B} + F_{\xi C} + F_{\xi D} + R_{\xi} + F_F \tag{6.1}$$

$$F_{\eta A} + F_{\eta B} + F_{\eta C} + F_{\eta D} = 0 \tag{6.2}$$

$$m\ddot{z} = -m(\alpha_z + g) + F_{zA} + F_{zB} + F_{zC} + F_{zD} + R_z \tag{6.3}$$

$$M_{\xi A} + M_{\xi B} + M_{\xi C} + M_{\xi D} = 0 \tag{6.4}$$

$$I\ddot{\theta} = M_{\eta A} + M_{\eta B} + M_{\eta C} + M_{\eta D} + M_{R\xi} + M_{RZ} + M_F \tag{6.5}$$

$$M_{ZA} + M_{ZB} + M_{ZC} + M_{ZD} = 0 \tag{6.6}$$

where

a : cask rocking spring half width,

b : radius of cask bottom,

d : cask outer radius,

F_F : friction force between cask and floor,

F_z : z-component of force,

F_{zA} : z-component of force generated by wire rope A,

F_{zB} : z-component of force generated by wire rope B,

F_{zC} : z-component of force generated by wire rope C,

F_{zD} : z-component of force generated by wire rope D,

F_{η} : η-component of force,

$F_{\eta A}$: η-component of force generated by wire rope A,

$F_{\eta B}$: η-component of force generated by wire rope B,

$F_{\eta C}$: η-component of force generated by wire rope C,

$F_{\eta D}$: η-component of force generated by wire rope D,

F_{ξ} : ξ-component of force,

$F_{\xi A}$: ξ-component of force generated by wire rope A,

$F_{\xi B}$: ξ-component of force generated by wire rope B,

$F_{\xi C}$: ξ-component of force generated by wire rope C,

$F_{\xi D}$: ξ-component of force generated by wire rope D,

g : garvity constant,

h : half height of cask,

I : mass moment of inertia,

m : mass of cask,

M_F : moment generated by force F_F,

M_{RZ} : moment generated by force R_z,

$M_{R\xi}$: moment generated by force R_{ξ},

M_z : moment generated by force F_z,

M_{ZA} : moment generated by force F_{zA},

M_{ZB} : moment generated by force F_{zB},

M_{ZC} : moment generated by force F_{ZC},
M_{ZD} : moment generated by force F_{ZD},
M_{η} : moment generated by force F_{η},
$M_{\eta A}$: moment generated by force $F_{\eta A}$,
$M_{\eta B}$: moment generated by force $F_{\eta B}$,
$M_{\eta C}$: moment generated by force $F_{\eta C}$,
$M_{\eta D}$: moment generated by force $F_{\eta D}$,
M_{ξ} : moment generated by force F_{ξ},
$M_{\xi A}$: moment generated by force $F_{\xi A}$,
$M_{\xi B}$: moment generated by force $F_{\xi B}$,
$M_{\xi C}$: moment generated by force $F_{\xi C}$,
$M_{\xi D}$: moment generated by force $F_{\xi D}$,
R_{Z} : impact force of z-direction,
R_{ξ} : impact force of ξ-direction,
z : z-coordinate or z-direction displacement,
$\dot{z}$: z-component of velocity,
$\ddot{z}$: z-component of acceleration,
α_{Z} : vertical floor acceleration,
α_{ξ} : horizontal floor acceleration,
η : η-coordinate or η-direction displacement,
θ : rotational angle,
$\dot{\theta}$: angular velocity,
$\ddot{\theta}$: angular acceleration,
ν : velocity,
ξ : ξ-coordinate or ξ-direction displacement,
$\dot{\xi}$: ξ-component of velocity,
$\ddot{\xi}$: ξ-component of acceleration,

6.2.3 Friction force between cask and floor and its associated moment

The friction force due to surface sliding is represented by a nonlinear Coulomb element. The equations for the friction force F_F and its associated moment M_F acting on the cask are as follows.

$$F_F = -\,\mathrm{sign}(\nu)F(\nu), \tag{6.7}$$

$$M_F = -F_F\,(-h\cdot\cos\theta - b\cdot\sin\theta), \tag{6.8}$$

where

$$\nu = \dot{\xi} - (h\cdot\cos\theta + b\cdot\sin\theta) - \dot{\theta} - \dot{\xi}_0. \tag{6.9}$$

where $\dot{\xi}$ and $\dot{\xi}_0$ are horizontal velocity of the center of gravity and support floor, respectively. $F(\nu)$ is a prescribed function for the friction characteristics which are related to the vertical contact force and the coefficients of both statical and dynamical friction.

$$F(\nu)=m \cdot g \ (\mu_d+\mu_s), \tag{6.10}$$

where μ_d and μ_s are the coefficients of dynamical and statical frictions, respectively.

6.2.4 Vertical impact force and its associated moment

The force acting on the interface between the cask and floor is derived in the term of deformation of a spring dashpot unit. When the gap is closing, the spring deformation γ and its time rate $\dot{\gamma}$ are

$$\gamma = 0.5[z_0-\{z+h(1-\cos\theta)-b\cdot\sin\theta\}] \tag{6.11}$$

$$\dot{\gamma} = 0.5[\dot{z}_0-\{\dot{z}+h\cdot\sin\theta-b\cdot\cos\theta\}\dot{\theta}] \tag{6.12}$$

where b is the cask rocking spring half width. z_0 and $\dot{z}_0$ are the vertical displacement and velocity of the floor, respectively. The vertical impact force R_z and its associated moment M_{RZ} acting on the cask are as follows. If $\gamma > 0$

$$R_z = -(K_z\cdot\gamma+C_z\cdot\dot{\gamma}), \tag{6.13}$$

$$M_{RZ} = -R_z(h\cdot\cos\theta-a\cdot\sin\theta), \tag{6.14}$$

where K_z and C_z are the vertical boundary spring and damping coefficients, respectively. If $\gamma \leqq 0$

$$R_z = 0, \tag{6.15}$$

$$M_{RZ} = 0. \tag{6.16}$$

6.2.5 Lowr corner impact force and its associated moment

The force acting on the cask lower corner as a result of the impact is derived by deformation of a spring dashpot unit which is located on the lower corner of the cask. During impact against the lower corner, spring deformation τ and its time rate $\dot{\tau}$ of the cask are follows.

$$\tau = \xi+h\cdot\sin\theta-b(1-\cos\theta)-\xi_0-\delta, \tag{6.17}$$

$$\dot{\tau} = \dot{\xi}+(h\cdot\cos\theta-b\cdot\sin\theta)\dot{\theta}-\dot{\xi}_0, \tag{6.18}$$

where δ is the gap between the cask and its lower boundary wall. The boundary wall impact force R_ξ and its associated moment $M_{R\xi}$ acting on the cask are as follows.

If $\tau > 0$

$$R_\xi = -(K_\xi\cdot\tau+C_\xi\cdot\dot{\tau}), \tag{6.19}$$

$$M_{R\xi} = R_\xi(h\cdot\cos\theta-b\cdot\sin\theta), \tag{6.20}$$

where K_ξ and C_ξ are the horizontal boundary spring and damping coefficients, respectively. If $\tau \leqq 0$

$$R_{\xi} = 0, \tag{6.21}$$

$$M_{R\xi} = 0. \tag{6.22}$$

6.2.6 Force due to wire rope

A tensile force due to a wire rope is as follows:

$$F = \sigma \cdot A, \tag{6.23}$$

where

F : tensile force of wire rope,

σ : tensile stress of wire rope,

$$\sigma = E \cdot \Delta L / L, \tag{6.24}$$

A : sectional area of wire rope,

E : Young's modulus,

ΔL : elongation of wire rope,

L : wire rope length.

6.3 Benchmark calculation

In order to demonstrate the adequacy of ROCKING, benchmark calculations using the CRIEPI experimental results of the 1/3 scale model of spent fuel cask as shown in Fig.6.3 have been performened.

The rocking analysis of the model cask was performed under constant sinusoidal excitations. Figure 6.4 shows the maximum rotational angles in comparison with the experimental results. According to Fig.6.4 analytical results of ROCKING agree with the experimental ones.

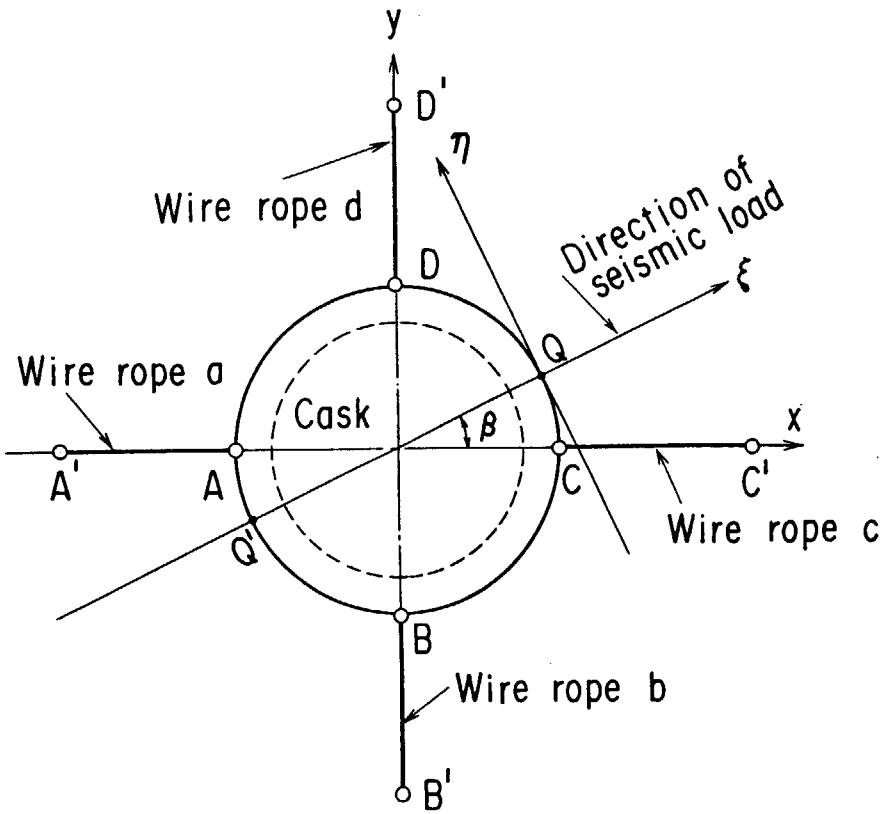

(b) Plane view

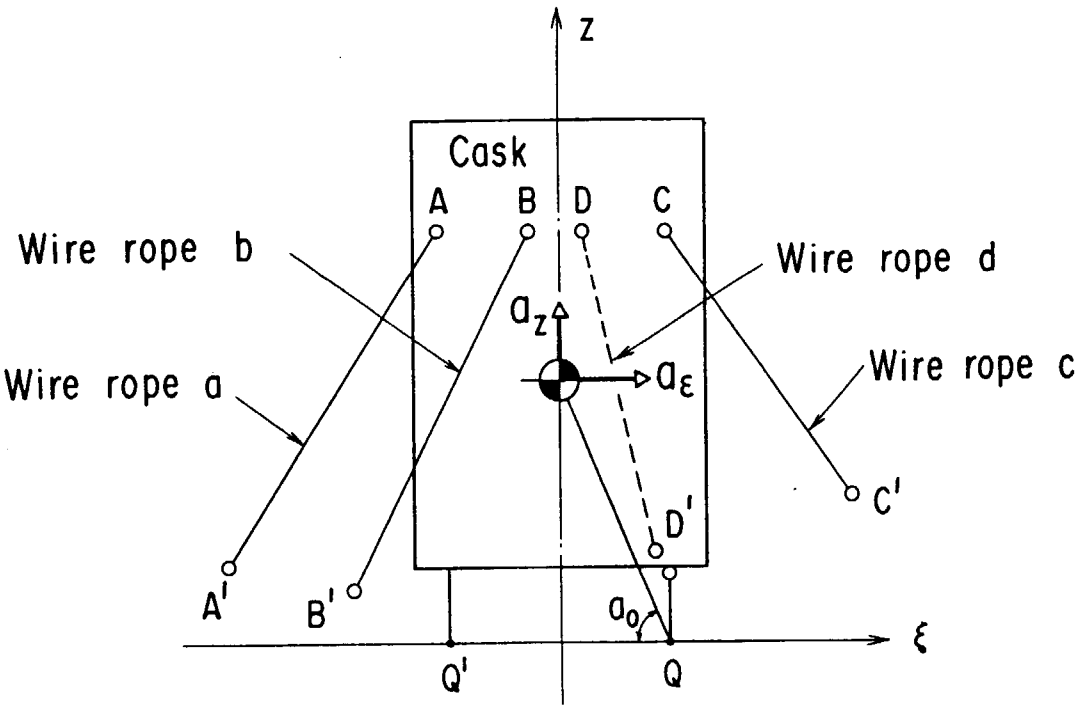

(a) Vertical view

Fig. 6.1 Coordinate system

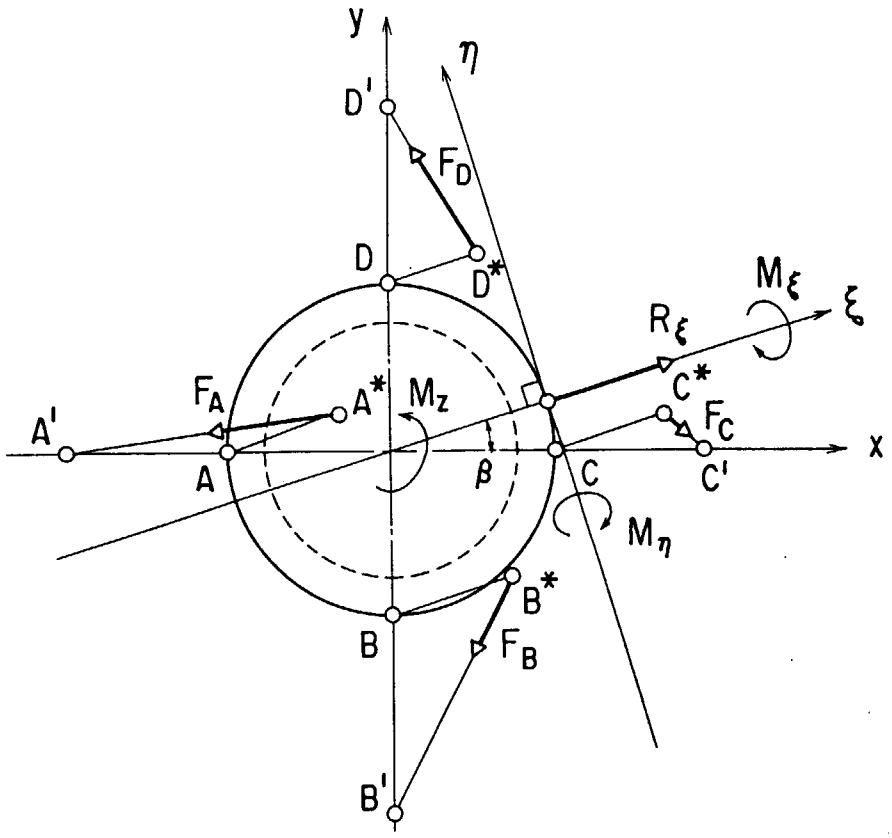

(b) Plane view

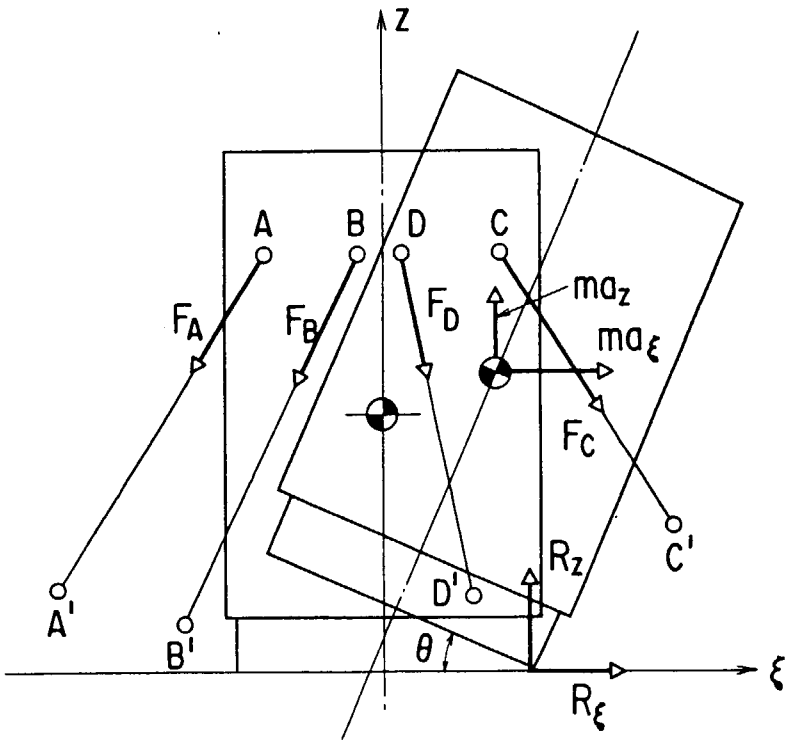

(a) Vertical view

Fig. 6.2 Forces and moments acting on cask

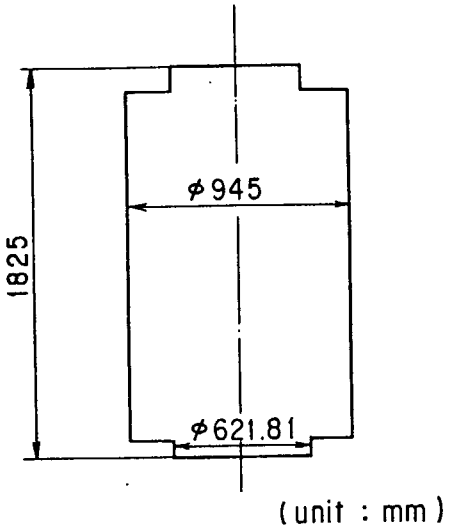

Fig. 6.3 Analysis model

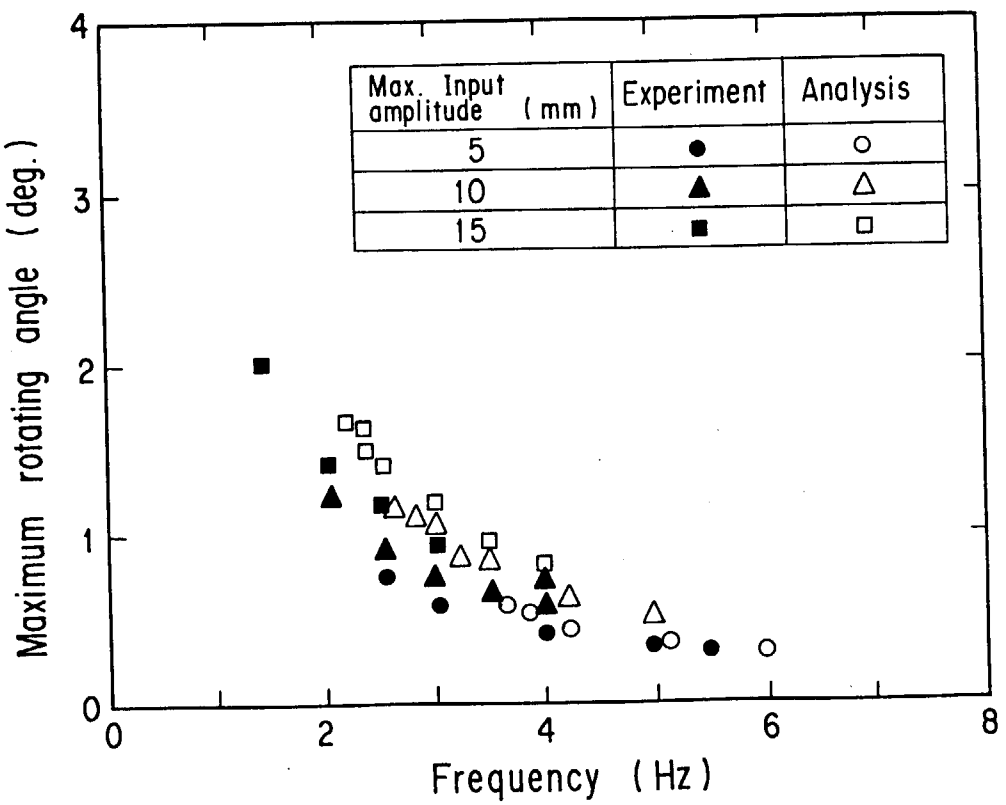

Fig. 6.4 Comparison between experiment and analysis

7. IMPACLIB

7.1 Description of IMPACLIB Program

In the drop impact and stress analyses for radioactive transport casks, it has become possible to perform them in detail by using interaction evaluation, computer programs, such as DYNA2D, DYNA3D, NIKE2D, NIKE3D, PISCES and HONDO. Simplified computer programs CRUSH1, CRUSH2, FINCRUSH and PUNCTURE are also used for parametric study and design of casks. Availability of these computer programs, makes it possible to accurately solve large numbers of problems involving a wide variety of material data provided that accurate input data are used. The structural properties of the materials, including coefficient of thermal expansion, modulus of longitudinal elasticity, modulus of transverse elasticity, Poisson's ratio and stress-strain relationship (temperature and/or strain rate dependent data) should be known as accurately as possible. Some of these properties are difficult to measure. In paticular, stress-strain relationships may vary from data to data depending on test methods. Therefore, when used in calculations, the possible inaccuracy of variability of structural data should be accounted for to properly interpret the results. For this reason, we have made an effort to collect stress-strain data and make it available in a form convenient for handling by a computer.

Four kinds of materials data, structure steels (mild steel or carbon steel), stainless steels, leads and woods have been compiled, and are summerized in this report. The structural data library and data processing program IMPACLIB(one computer program of CASKET code system as shown in Fig. 1.1)[26] for impact and stress analyses has been developed.

The structural property data including coefficient of thermal expansion, modulus of longitudinal elasticity, modulus of transverse elasticity, Poisson's ratio and stress-strain relationship have been tabulated against temperature and/or strain rate for more than 100 materials. These data have been collected from over 50 references. The data have been arranged in computer card image and stored in magnetic disks (hard or floppy disks) in a format suitable for computer processing, with the material identified numerically according to a general and flexible classification system. An accompanying numerical index, also in card image form, describes

each material, assigns it an identification number and references the sources of the data by code number. The SI unit system is used for all data, and if desired, data can be converted the MKS(meter-kilogram-second) unit system. In addition the data are obtained from a source list. The IMPACLIB has been written to search the material data list for specific material identification number.

7.2 Material Property Data Library

The computer program IMPACLIB has been developed. Four kinds of material data, structure steels (mild steel and carbon steel), stainless steels, leads and woods have been compiled and are summerized.

(1) structure steels	(14 materials)
① carbon steel (JIS SS41)	(8 materials)
② mild steel (JIS SS4100)	(1 material)
③ structure steel (JIS S35C)	(1 material)
④ structure steel (JIS S45C)	(2 materials)
⑤ structure steel (JIS S55C)	(1 material)
⑥ mild steel (AISC 1020)	(1 material)
(2) stainless steels	(35 materials)
① stainless steel (JIS SUS302)	(1 material)
② stainless steel (JIS SUS303)	(1 material)
③ stainless steel (JIS SUS304)	(24 materials)
④ stainless steel (JIS SUS304L)	(1 material)
⑤ stainless steel (JIS SUS316)	(3 materials)
⑥ stainless steel (JIS SUS316L)	(2 materials)
⑦ stainless steel (AISC 1316L)	(1 material)
⑧ stainless steel (JIS SUS316H)	(1 material)
⑨ stainless steel (JIS SUS316)	(1 material)
(3) leads	(20 materials)
① pure lead	(17 materials)
② hard lead	(3 materials)
(4) woods	(24 materials)
① oak tree	(19 materials)
② playwood	(3 materials)

③ balsa wood (2 materials)

The structural properties of materials, including coefficient of thermal expansion, modulus of longitudinal elasticity, modulus of transverse elasticity, Poisson's ratio and stress-strain relationship have been compiled and are summerized.

(a) coefficient of thermal expansion (temperature dependent)

(b) modulus of longitudinal elasticity (temperature dependent)

(c) modulus of transverse elasticity (temperature dependent)

(d) Poisson's ratio (temperature dependent)

(e) stress-strain relationship (temperature dependent or strain rate dependent)

Table 7.1 shows relationships the among material number, the identification number and property data in the IMPACLIB library.

7.3 Example

Figure 7.1 shows an example of stress-strain curves of structure steel data in the IMPACLIB library.

Table 7.1 Material name, identification number and data in library

Category	Material name	ID number	Data
Structure steel	AISC1020	1001	σ－ε
	S45C	1002	σ－ε
	STEEL	1003	σ－ε
	STEEL	1004	σ－ε
	STEEL	1005	σ－ε
	STEEL	1006	σ－ε
	STEEL	1007	σ－ε
	STEEL	1008	σ－ε
	STEEL	1009	σ－ε
	SS41	1010	σ－ε
	S35C	1011	σ－ε
	S45C	1012	σ－ε
	S55C	1013	σ－ε
	STEEL	1100	α，E，G，ν
Stainless steel	SUS302	2001	σ－ε
	SUS303	2002	σ－ε
	SUS304	2003	σ－ε
	SUS316H	2004	σ－ε
	SUS304	2005	σ－ε
	AISI316L	2006	σ－ε
	SUS304L	2007	σ－ε
	SUS304	2008	σ－ε
	SUS316	2009	σ－ε
	SUS304	2010	σ－ε
	SUS316	2011	σ－ε
	SUS316L	2012	σ－ε
	SUS316L	2013	σ－ε
	SUS304	2014	σ－ε
	SUS(18－8)	2015	σ－ε
	SUS304	2016	σ－ε
	SUS304	2017	σ－ε
	SUS304	2018	σ－ε
	SUS304	2019	σ－ε
	SUS304	2020	σ－ε
	SUS304	2021	σ－ε
	SUS304	2022	σ－ε
	SUS304	2023	σ－ε
	SUS304	2024	σ－ε
	SUS304	2025	σ－ε
	SUS304	2026	σ－ε
	SUS304	2027	σ－ε
	SUS304	2028	σ－ε
	SUS304	2029	σ－ε
	SUS304	2030	σ－ε
	SUS304	2031	σ－ε
	SUS304	2032	σ－ε
	SUS304	2033	σ－ε
	SUS304	2100	α，E，G，ν
	SUS316	2200	α，E，G，ν
Lead	PURE LEAD	3001	σ－ε
	PURE LEAD	3002	σ－ε
	PURE LEAD	3003	σ－ε
	LEAD	3004	σ－ε
	PURE LEAD	3005	σ－ε
	PURE LEAD	3006	σ－ε

Table 7.1 (Continued)

Category	Material name	ID number	Data
Lead	PURE LEAD	3007	$\sigma-\varepsilon$
	PURE LEAD	3008	$\sigma-\varepsilon$
	PURE LEAD	3009	$\sigma-\varepsilon$
	PURE LEAD	3010	$\sigma-\varepsilon$
	PURE LEAD	3011	$\sigma-\varepsilon$
	PURE LEAD	3012	$\sigma-\varepsilon$
	PURE LEAD	3013	$\sigma-\varepsilon$
	PURE LEAD	3014	$\sigma-\varepsilon$
	PURE LEAD	3015	$\sigma-\varepsilon$
	PB	3016	$\sigma-\varepsilon$
	PB2	3017	$\sigma-\varepsilon$
	PB4	3018	$\sigma-\varepsilon$
	PB6	3019	$\sigma-\varepsilon$
	LEAD	3100	α, E, G, ν
Wood	OAK	4001	$\sigma-\varepsilon$
	OAK	4002	$\sigma-\varepsilon$
	PLYWOOD	4003	$\sigma-\varepsilon$
	PLYWOOD	4004	$\sigma-\varepsilon$
	BALSA	4005	$\sigma-\varepsilon$
	BALSA	4006	$\sigma-\varepsilon$
	BALSA	4007	$\sigma-\varepsilon$
	BALSA	4008	$\sigma-\varepsilon$
	BALSA	4009	$\sigma-\varepsilon$
	BALSA	4010	$\sigma-\varepsilon$
	BALSA	4011	$\sigma-\varepsilon$
	BALSA	4012	$\sigma-\varepsilon$
	BALSA	4013	$\sigma-\varepsilon$
	BALSA	4014	$\sigma-\varepsilon$
	BALSA	4015	$\sigma-\varepsilon$
	BALSA	4016	$\sigma-\varepsilon$
	BALSA	4017	$\sigma-\varepsilon$
	BALSA	4018	$\sigma-\varepsilon$
	BALSA	4019	$\sigma-\varepsilon$
	BALSA	4020	$\sigma-\varepsilon$
	BALSA	4021	$\sigma-\varepsilon$
	BALSA	4022	$\sigma-\varepsilon$
	BALSA	4023	$\sigma-\varepsilon$
	PLYWOOD	4100	α, E, G, ν

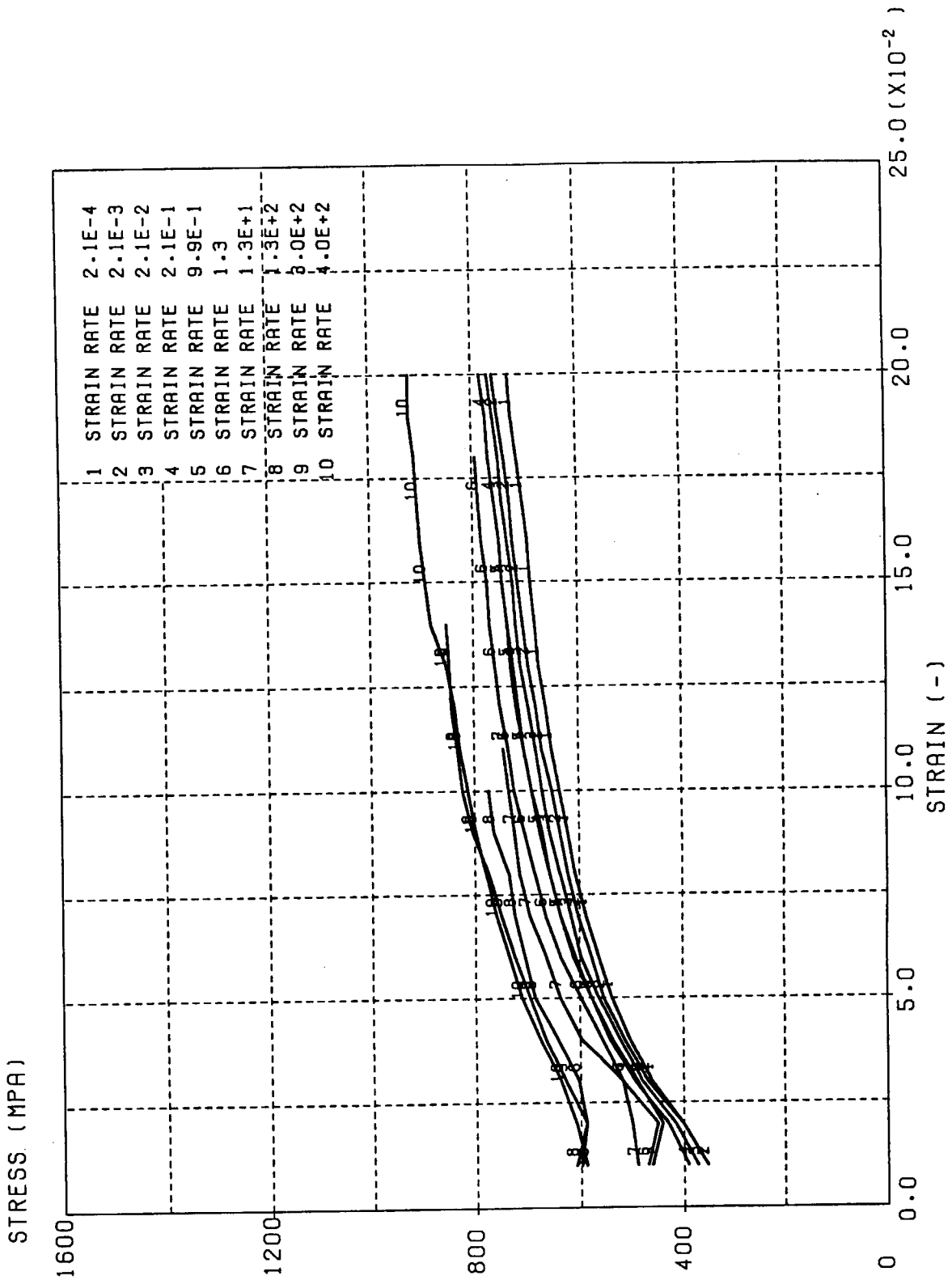

STRESS STRAIN CURVES OF STEEL TEMP.=293.0

Fig. 7.1 Graphical Output of IMPACLIB

8. THERMLIB

8.1. Description of THERMLIB Program

In the thermal analysis for radioactive transport casks, it has become possible to perform them in detail by computer programs, such as TRUMP3[27], HEATING5[28], HEATING6[29], NASTRAN[30], ABAQUS[30], TOPAZ2D and TOPAZ3D[31]. Availability of these computer programs, makes it possible to accurately solve large numbers of problems involving a wide variety of material data provided that accurate input data are used. The thermal properties of the materials, including density, thermal conductivity (temperature dependent data), specific heat (temperature dependent data), phase change or solid-state transition temperature and latent heat should be known as accurately as possible. Some of these properties are difficult to measure. In paticular, heat conduction may vary from data to data depending on test methods. Therefore, when used in calculations, the possible in accuracy of variability of thermal data should be accounted for to properly interpret the results. For this reason, Lawrence Livermore National Laboratory (LLNL) has made an effort to collect thermal data and make it available in a form convenient for handling by computer. More than 1000 material data[32] have been compiled.

Using this data library, a data library processing program THERMLIB[33] for thermal analysis has been developed. The THERMLIB is one computer program of CASKET code system for thermal and structural analysis of radioactive material transport and/or strage casks as shown in Fig. 1.1.

The thermal property data including density, specific heat (temperature depen-dent data), thermal concutivity (temperature dependent data), phase change or solid-state transition temperature and latent heat have been compiled. These data have been collected from over 50 references.

The data have been arranged in computer card image and stored in magnetic disks (hard orfloppy disks) in a format suitable for computer processing, with the material identified numerically according to a general and flexible classification system. An accompanying numerical index, also in card image form, describes each material, assigns it an identification number, references the sources of the data by code number. The CGS-cal-℃(centimeter, gram, second-calorie-degree C) unit system

is used for all data. In addition the data are obtained from source list. The THERMLIB has been written to search the material data list for a specific material identification number.

8.2. Material Property Data Library

The computer program THERMLIB has been developed for searching data and plotting data from the data library compiling by LLNL. Thermal property data for over 1000 materials shown as Table 8.1 have been compiled and are summerized in the data library. The compilation includes:

(a) a numbered list of data sources,

(b) a numerical classification system used as a guide in assigning an identification number,

(c) a system of quality indicators used to show the gerneral reliability or accuracy of data,

(d) thermal property data for each material collected and estimated by LLNL and converted to a standard system of units,

(e) an alphabetical index of materials that includes the identification number assigned to each material and

(f) a list of material property data arranged in order of the material identification numbers and in the format used for input data in the computer program TRUMP.

These material property data incude the material identification number and alphanumeric designator, density, specific heat, thermal conductivity, phase-change or transition temparature, the latent heat effect, and tables of specific heat and thermal conductivity versus temperature.

8.3 Example

Figures 8.1 and 8.2 show examples of heat capacity and heat cinductivity curves of steel in the THERMLIB library.

Table 8.1 Material classification system

Material ID No.	Material classifications
1000	ELEMENTS
1001-1499	SOLIDS, LIQUIDS
1501-1599	GASES
1601-1999	NOT USED
2000	ALLOYS
2001-2099	ALUMINUM ALLOYS
2101-2399	COPPER ALLOYS
2401-2499	MAGNESIUM ALLOYS
2501-2599	NICKEL ALLOYS
2601-2699	COBALT ALLOYS
2701-2799	TITANIUM ALLOYS
2801-2999	NOT USED
3000	ALLOYS (CONTINUED)
3001-3099	IRON ALLOYS
3101-3299	STEELS
3301-3499	SUPER ALLOYS (CR-NI-FE)
3501-3599	BERYLLIUM ALLOYS
3601-3649	LEAD, TIN, AND INDIUM ALLOYS
3651-3679	MOLYBDENUM ALLOYS
3681-3699	NIOBIUM (COLUMBIUM) ALLOYS
3701-3749	PLUTONIUM ALLOYS
3751-3779	SILVER ALLOYS
3781-3799	TANTALUM ALLOYS
3801-3829	TUNGSTEN ALLOYS
3831-3859	URANIUM ALLOYS
3861-3879	ZINC ALLOYS
3881-3899	ZIRCONIUM ALLOYS
3901-3999	MISCELLANEOUS ALLOYS
4000	INORGANIC COMPOUNDS
4001-4199	OXIDES (SINGLE)
4201-4299	OXIDES (MIXED)
4301-4399	SILICATES
4401-4499	NITRIDES
4501-4599	CARBIDES
4601-4699	BORIDES
4701-4739	BERYLLIDES

Table 8.1 (Continued)

Material ID No.	Materials
4741-4759	SULFIDES
4761-4769	PHOSPHIDES
4771-4799	SILICIDES
4801-4899	HALIDES
4901-4949	INTERMETALLICS, METALLOIDS
4951-4999	MISCELLANEOUS COMPOUNDS
5000	INORGANIC MIXTURES
5001-5199	GLASSES
5201-5299	CERAMICS, BRICKS
5301-5399	NOT USED
5401-5499	CERMETS
5501-5799	GAS MIXTURES
5801-5999	NOT USED
6000	INORGANIC COMPOSITES
6001-6099	ROCKS, MINERALS, SANDS, SOILS
6101-6999	NOT USED
7000	ORGANIC COMPOUNDS AND MIXTURES
7001-7499	POLYMERS (INCLUDING FOAMS)
7501-7599	HIGH EXPLOSIVES (INCLUDING MOCK H. E.)
7601-7699	NOT USED
8000	ORGANIC COMPOSITES AND NATURAL MATERIALS
8001-8499	MISCELLANEOUS
8501-8599	WOODS
8601-8999	NOT USED
9000	MISCELLANEOUS
9001-9099	IDEALIZED MATERIALS
9101-9999	NOT USED

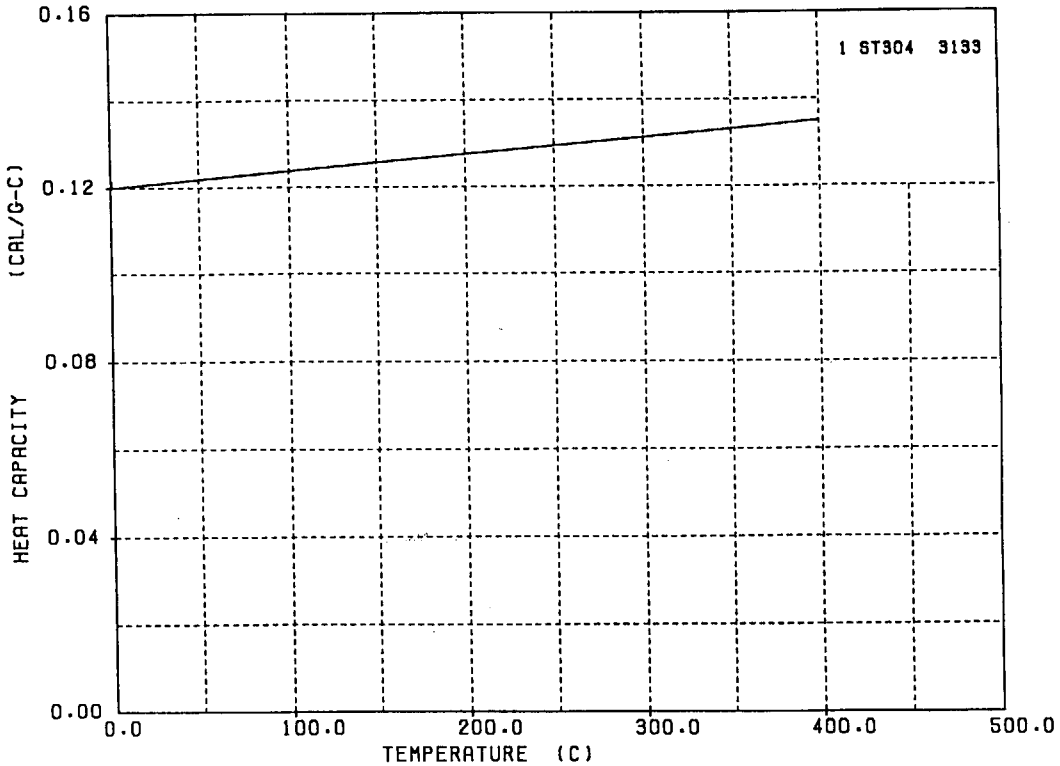

Fig. 8.1 Graphical Output of THERMLIB(1)

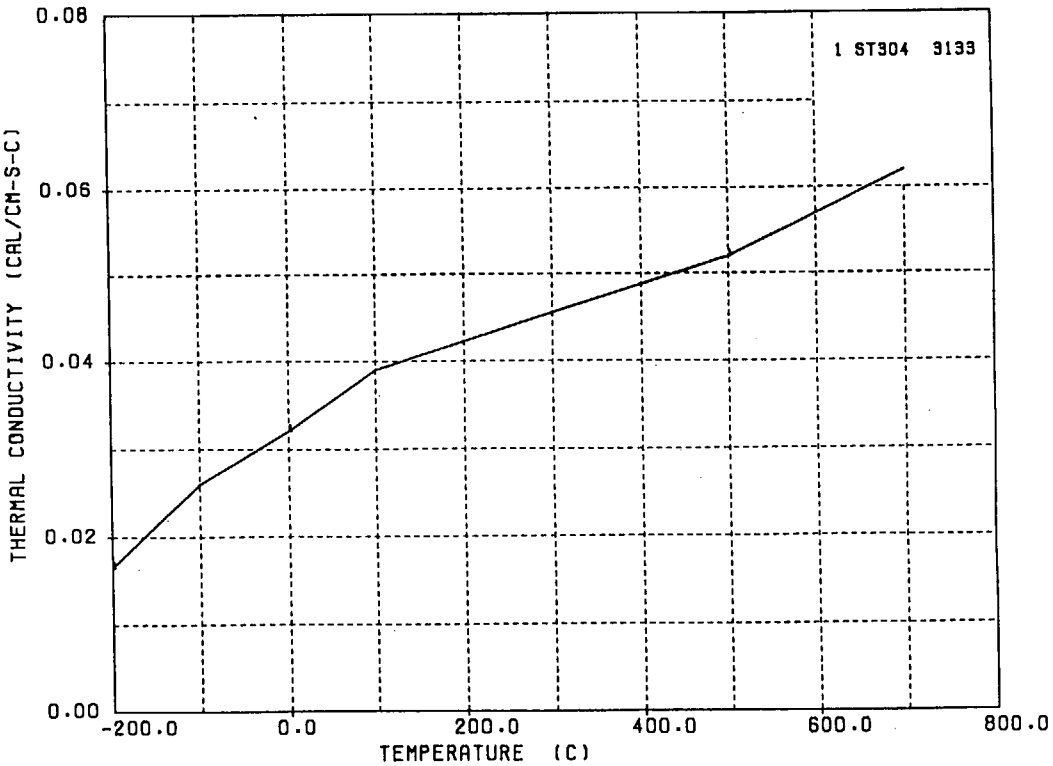

Fig. 8.2 Graphical Output of THERMLIB(2)

9. FINLIB

9. 1 Description of FINLIB program

Detail analyses of the drop impact for a radioactive transport cask with cooling fins, have become possible to perform by using interaction evaluation computer programs with a function of interaction step, such as DYNA2D, DYNA3D, PISCES and HONDO. However, considerable cost and computer time necessitate for performing analyses by these programs. To decrease the computer time and cost, a simplified computer program FINCRUSH as illustrated in Fig.1.1 has been developed. The FINCRUSH is a static calculation computer program capable of evaluating the maximum acceleration of cask bodies and the maximum fin deformation using a relationship between the fin plastic deformation and the fin absorption energy. This relationship, the fin absorption energy versus the fin deformation data, is obtained by Davis of ORNL and Torr of MONSERCO in Canada from experiments. The FINLIB[34] has been developed to make data library of the fin energy absorption for the FINCRUSH.

9.2 Data Library

One of the most widely used fin data sets of design curves comes from impact experiments done in 1971 by Davis of ORNL. His investigation measured the impact performance of single fins 2 inches (50.8 mm) wide varying in length from 3.5 to 10 inches (88.9 to 254 mm), in thickness from 1/4 to 3/4 inches (6.4 to 19.1 mm) and an angle of inclination to the impact direction from 0 to 40 degrees as shown in Fig. 9.1.

In the MONSERCO experiments six kinds of fins were used as shown in Table 9.1 and Fig. 9.2. Test fins were of two thickness, in thickness from 1/4 inches (6.4 mm) and 3/8 inches (9.5 mm), and of five different lengths between 3.5 to 10 inches (88.9 to 254 mm). The single fins had four different angles of inclination; 0, 10, 20 and 30 degrees from the vertical.

In this data library there are eleven data base as shown in Table 9.2. Those data are obtained by ORNL and MONSERCO.

Table 9.1 Dimensions of fin specimens tested at MONSERCO

FIN ANGLE OF INCLINATION (degrees)	FIN LENGTH (inches)	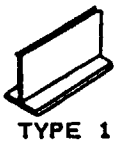 TYPE 1	 TYPE 2	 TYPE 3	 TYPE 4	 TYPE 5	 TYPE 6
0°	3.5	X	X	(X)	X	X	X
	4.0	X	X	(X)	X	X	X
	6.0	X	X	(X)	X	X	X
	8.0	X	X	(X)	X	X	X
	10.0	X	X	(X)	X	X	X
10°	3.5	X	X				
	4.0	X	X				
	6.0	X	X				
	8.0	X	X				
	10.0	X	X				
15°	3.5			(X)			
	4.0			(X)			
	6.0			(X)			
	8.0			(X)			
	10.0			(X)			
20°	3.5	X	X				
	4.0	X	X				
	6.0	X	X				
	8.0	X	X				
	10.0	X	X				
30°	3.5	X	X				X
	4.0	X	X				X
	6.0	X	X				X
	8.0	X	X				X
	10.0	X	X				X

Table 9.2 Data library of FINLIB

Research organization	Identification name	Descriptions
ORNL	ORNL	ORNL single fin(mean values)
	OHIG	ORNL single fin(higher values)
	OLOW	ORNL single fin(lower values)
MONSERCO	MEAN	MONSERCO single fin(mean values)
	MHIG	MONSERCO single fin(higher values)
	MLOW	MONSERCO single fin(lower values)
	MWID	MONSERCO wide single fin
	MPAR	MONSERCO double parallel fin
	MCON	MONSERCO double converging fin
	MBRA	MONSERCO double braced fin
	MOAK	MONSERCO Oak Ridge type single fin

9.3 Example

Figures 9.3 through 9.24 are examples of fin energy absorption curves in the FINLIB library.

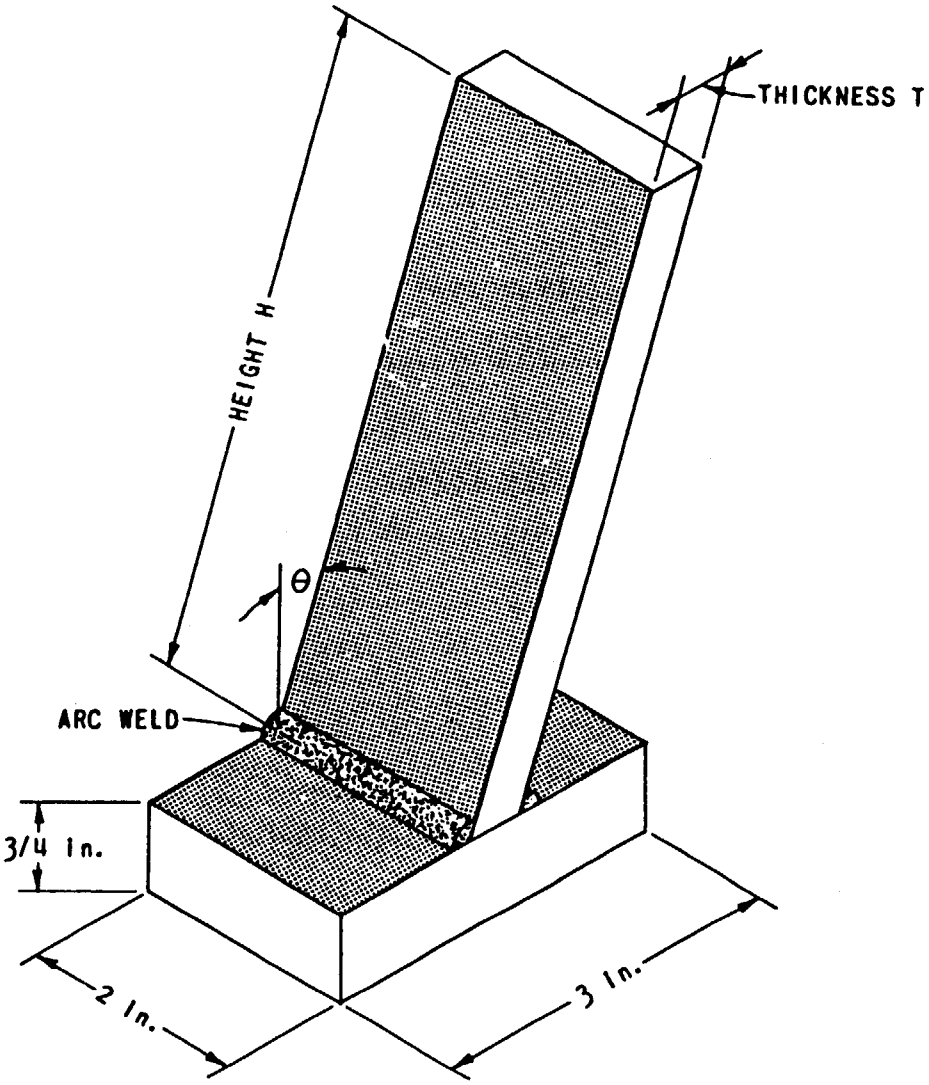

T (In.)	θ																				
	0°					10°				20°				30°				40°			
	H (In.)																				
	3½	4	6	8	9	4	6	8	10	4	6	8	10	4	6	8	10	4	6	8	10
1/4		X	X				X	X	X		X	X	X		X	X	X		X	X	X
3/8						X	X	X	X	X	X	X	X	X	X	X		X	X	X	X
1/2	X		X	X		X	X	X	X	X	X	X	X	X	X	X	X	X	X	X	X
5/8							X	X	X	X	X	X	X	X	X	X		X	X	X	X
3/4			X		X	X	X	X	X	X	X	X	X	X	X		X	X	X	X	X

Fig. 9.1 Dimensions of fin specimen tested at ORNL

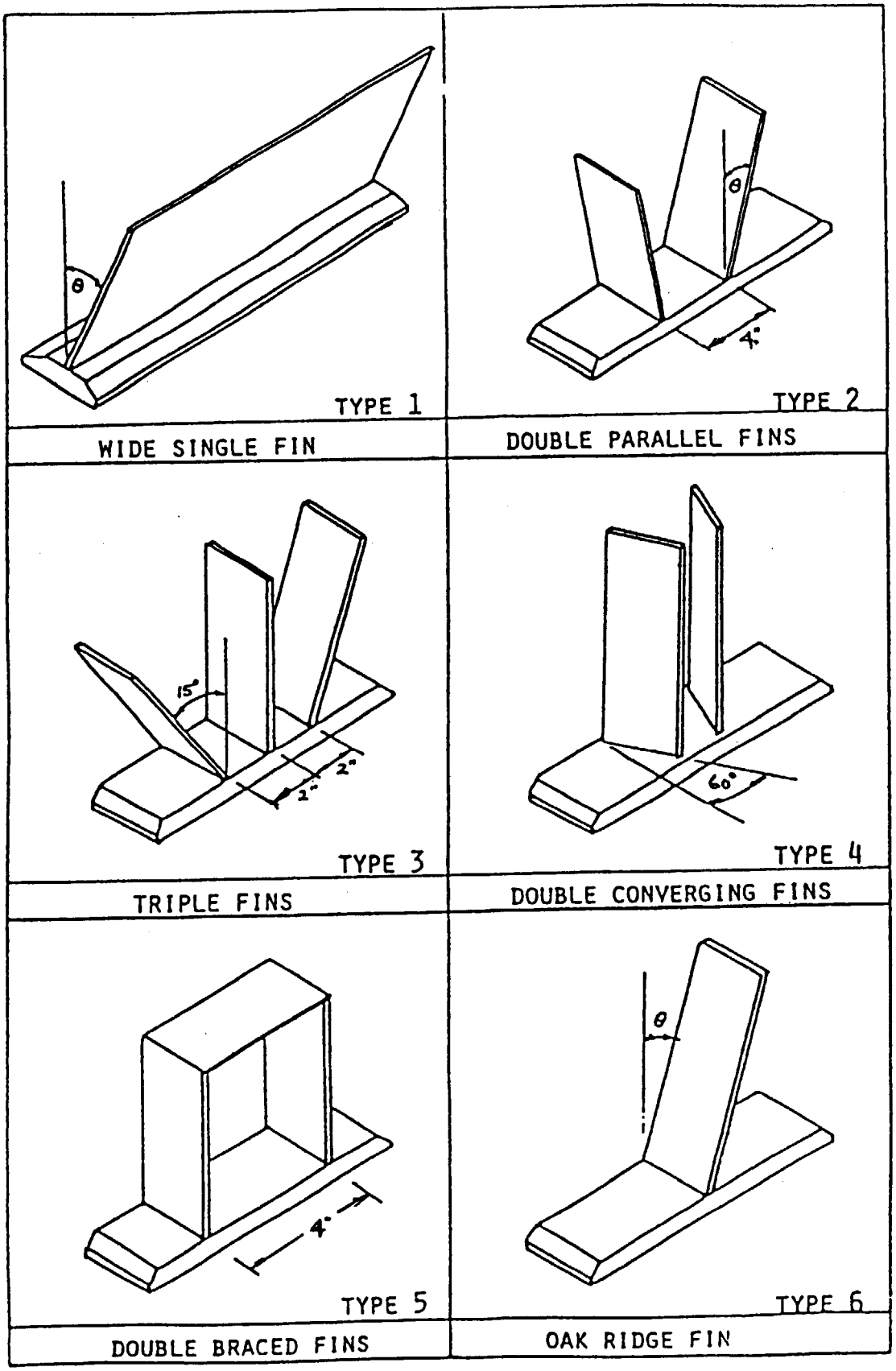

Fig. 9.2 Configuration of fins tested at MONSERCO

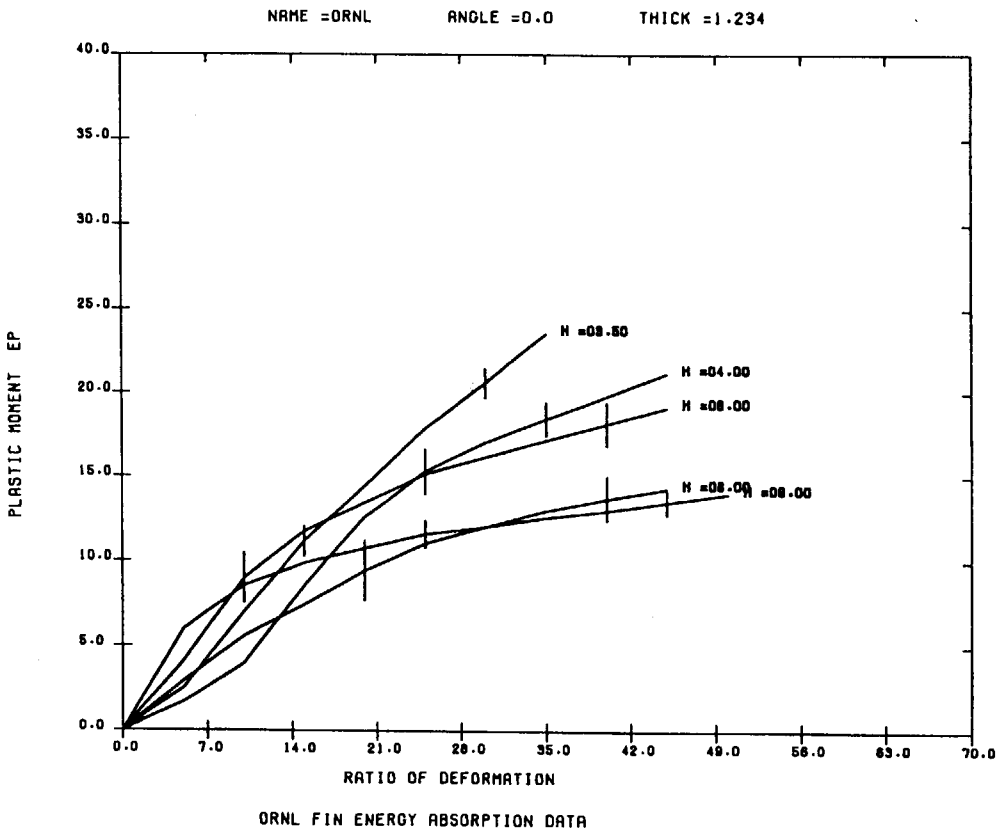

Fig. 9.3 Graphical Output of FINLIB(1)

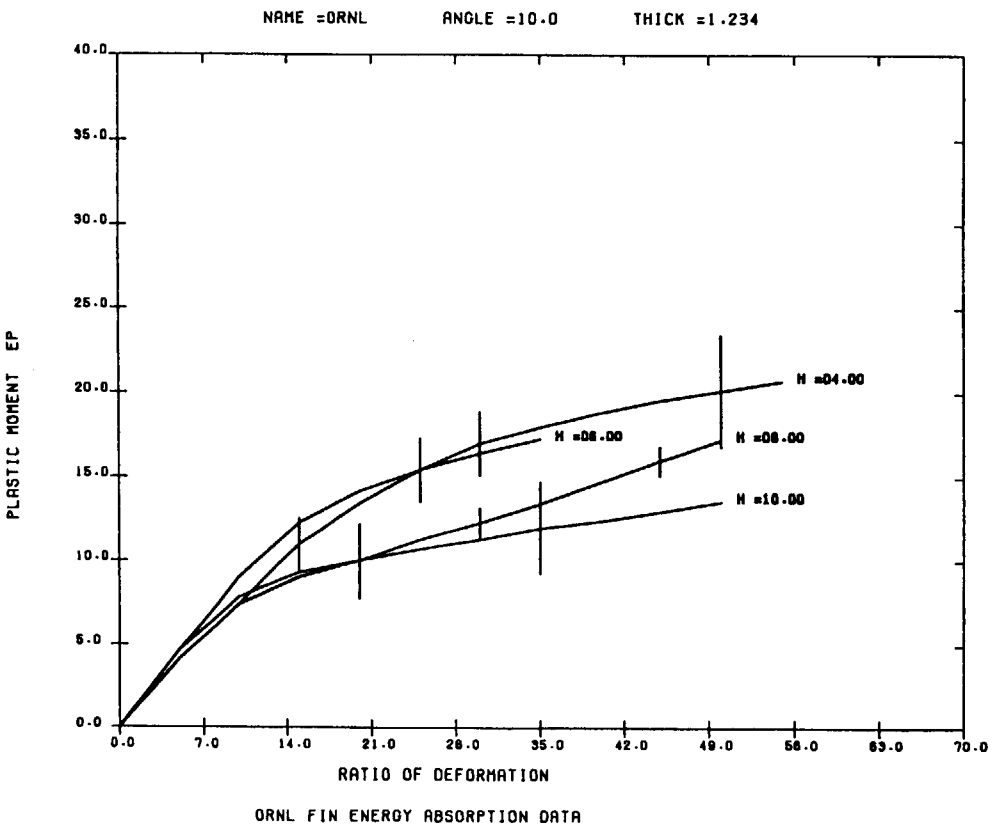

Fig. 9.4 Graphical Output of FINILB(2)

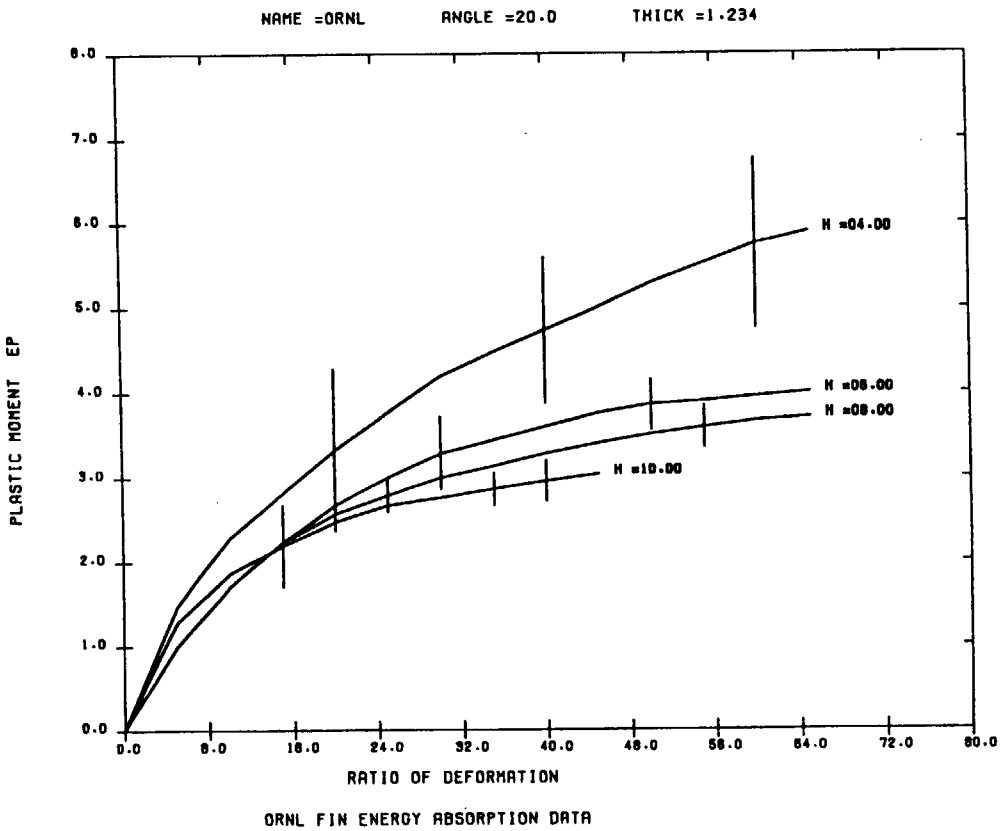

Fig. 9.5 Graphical Output of FINILB(3)

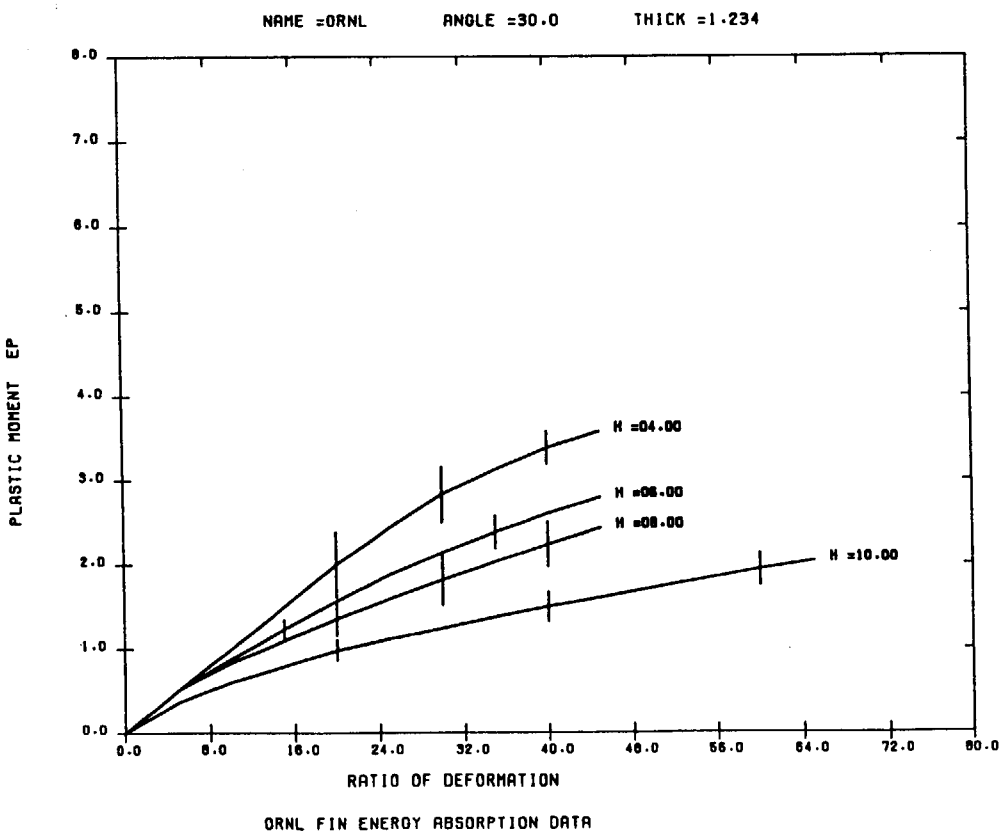

Fig. 9.6 Graphical Output of FINILB(4)

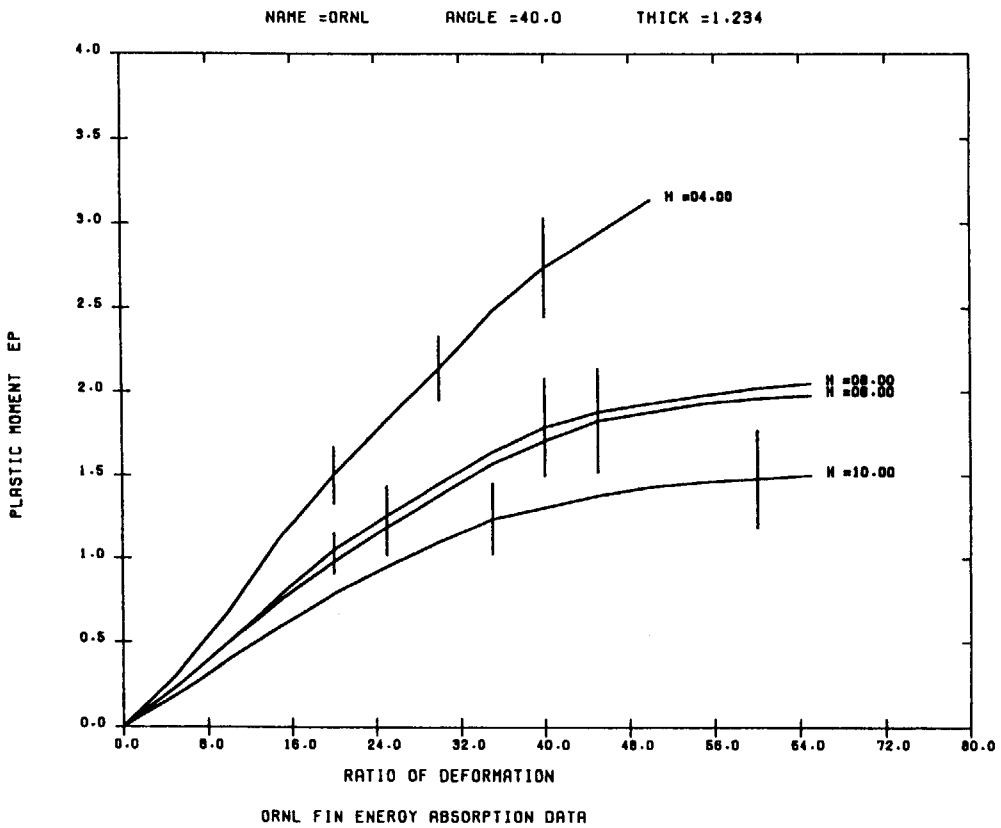

Fig. 9.7 Graphical Output of FINILB(5)

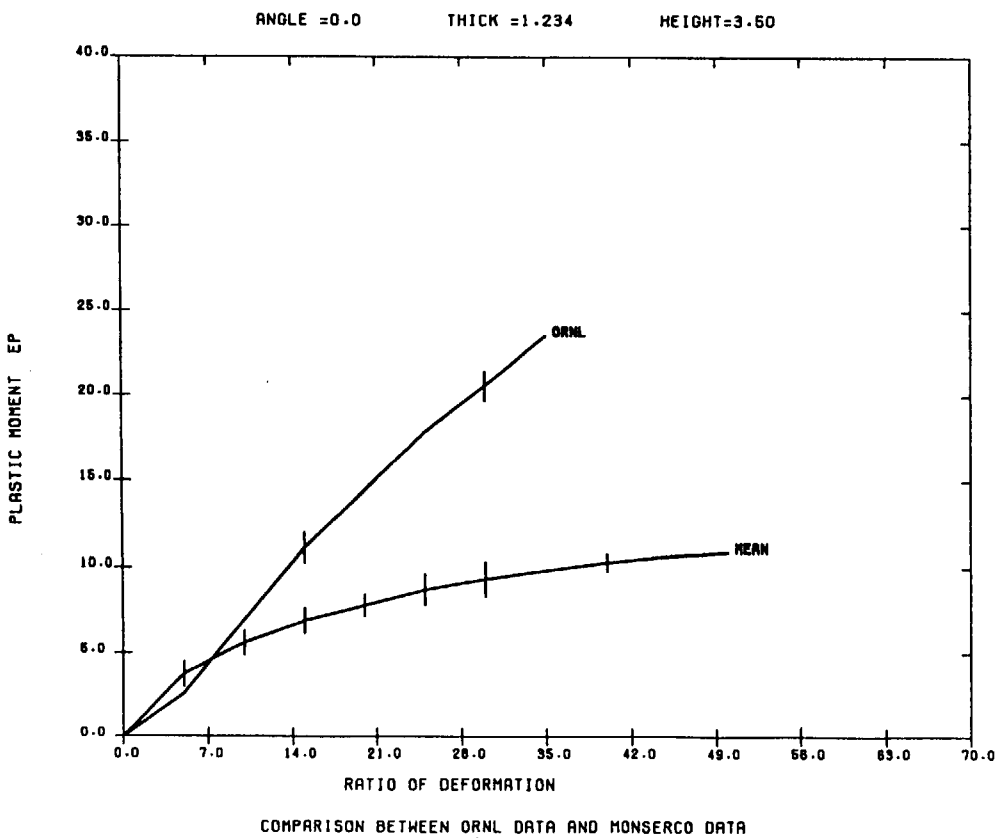

Fig. 9.8 Graphical Output of FINILB(6)

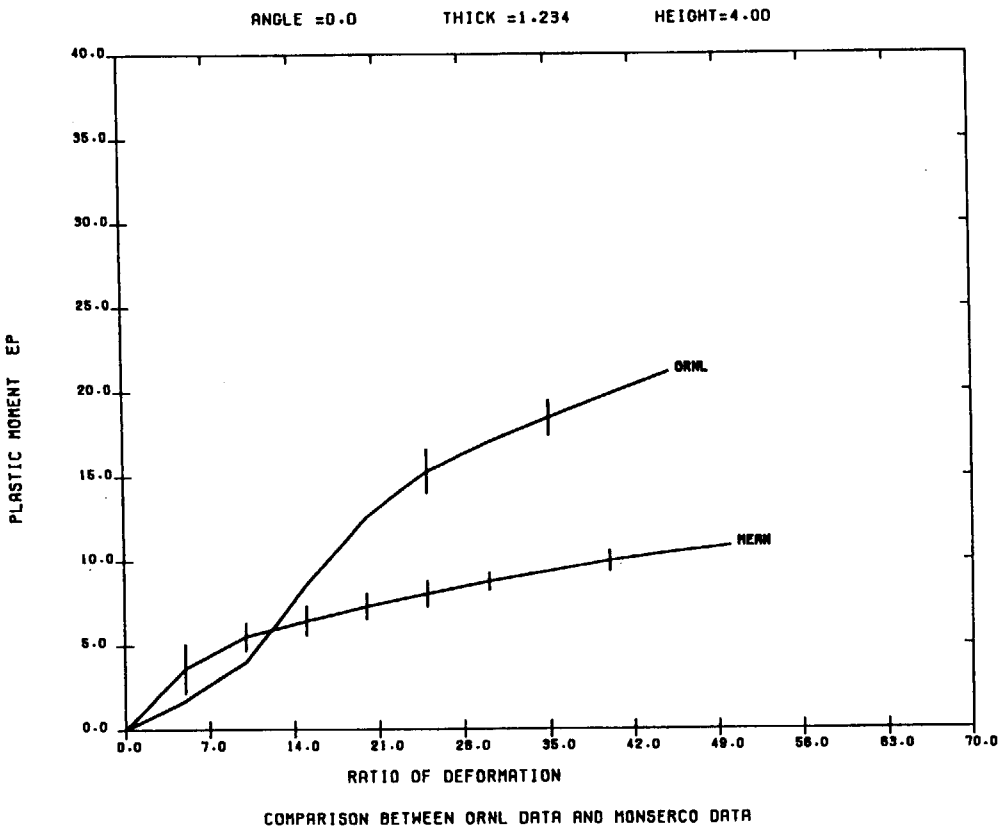

Fig. 9.9 Graphical Output of FINILB(7)

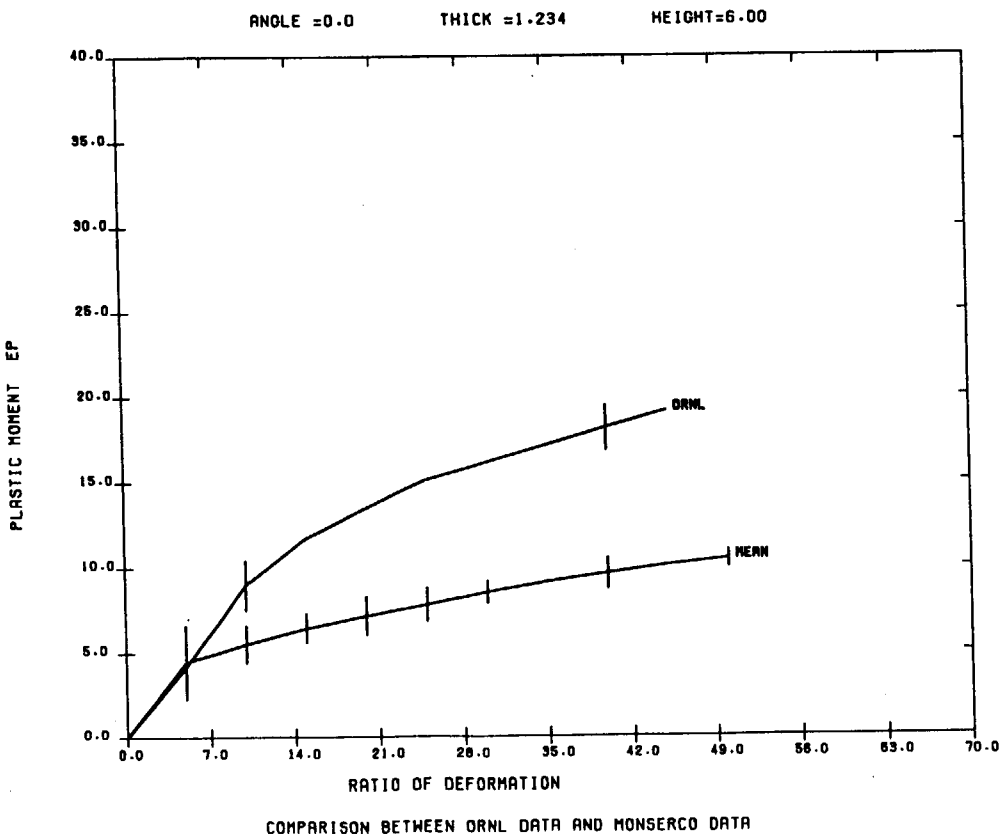

Fig. 9.10 Graphical Output of FINILB(8)

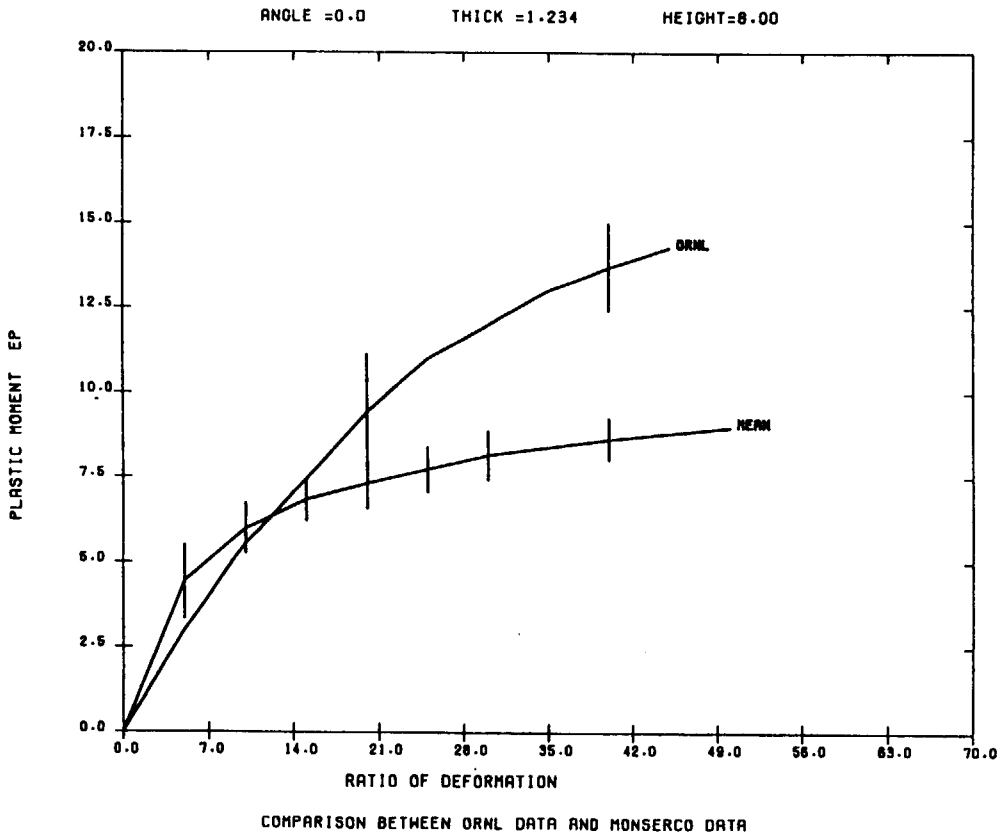

Fig. 9.11 Graphical Output of FINILB(9)

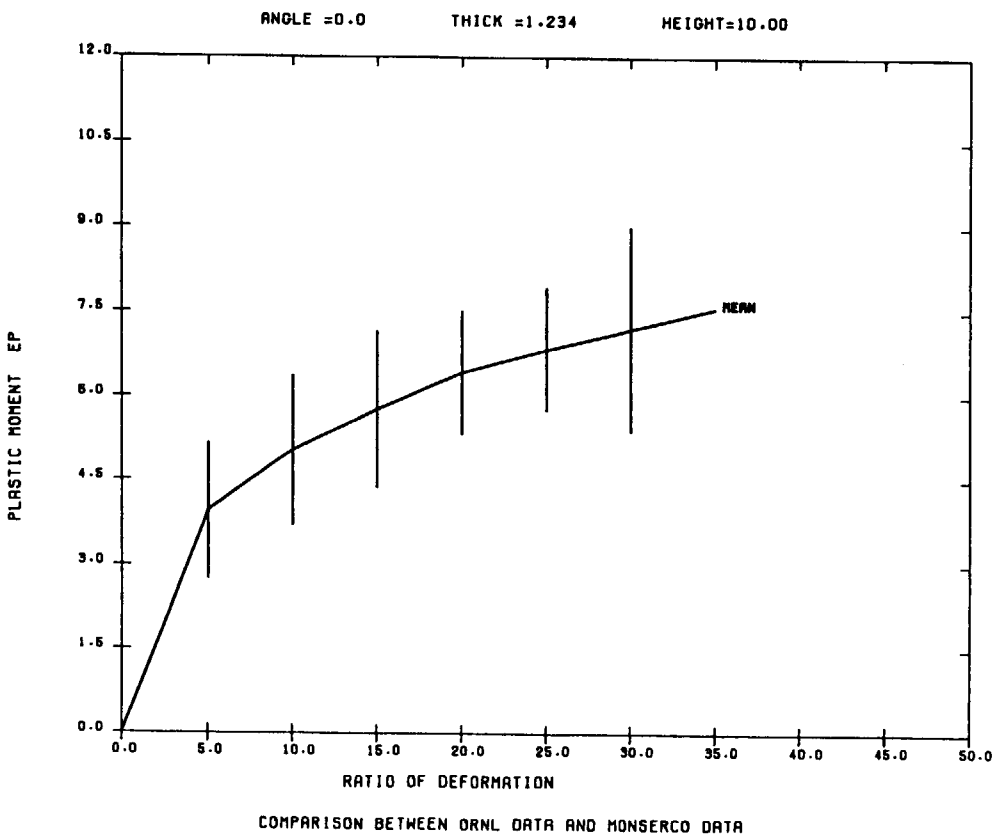

Fig. 9.12 Graphical Output of FINILB(10)

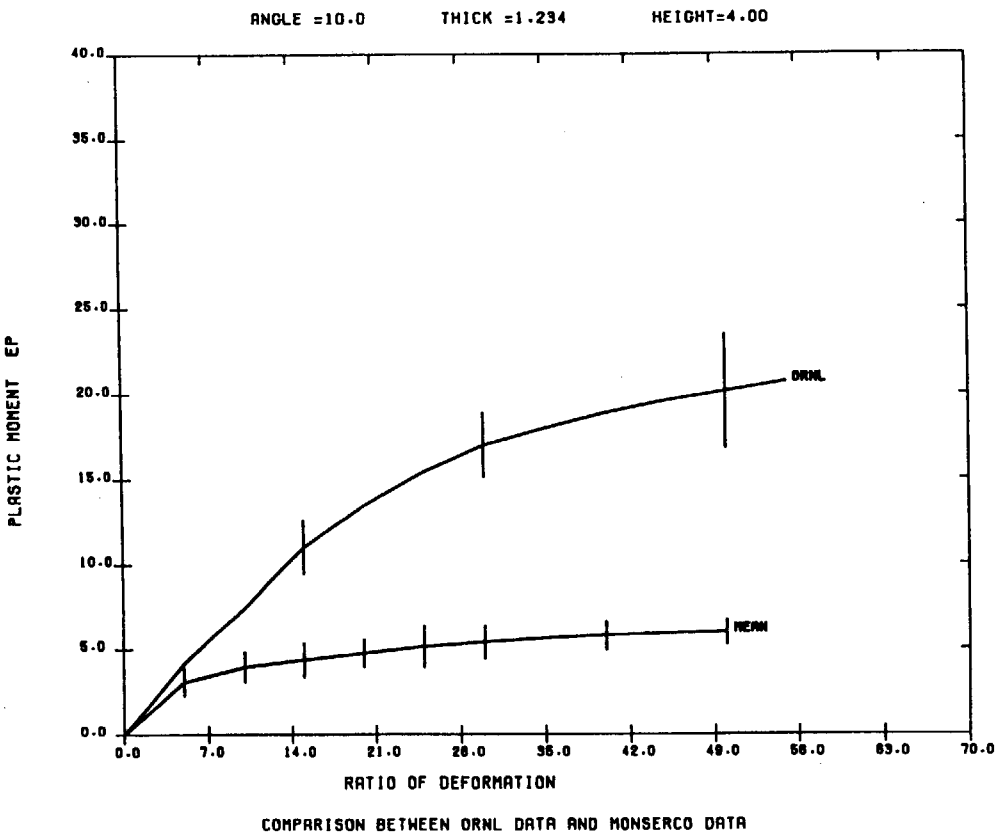

Fig. 9.13 Graphical Output of FINILB(11)

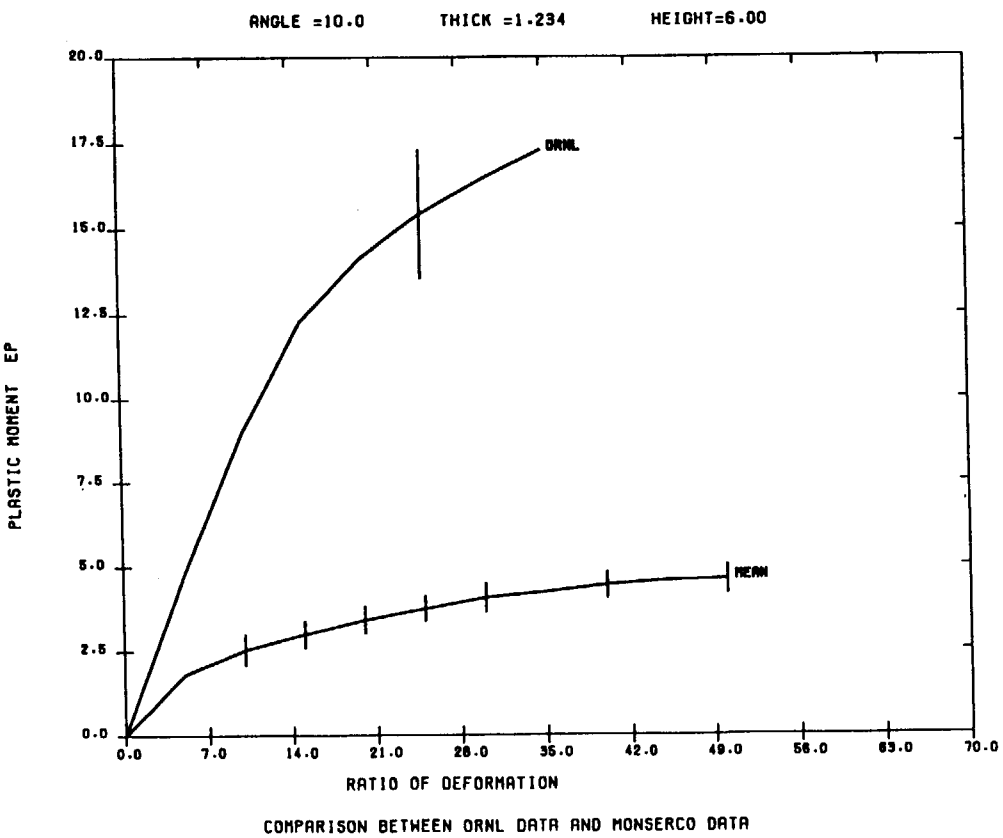

Fig. 9.14 Graphical Output of FINILB(12)

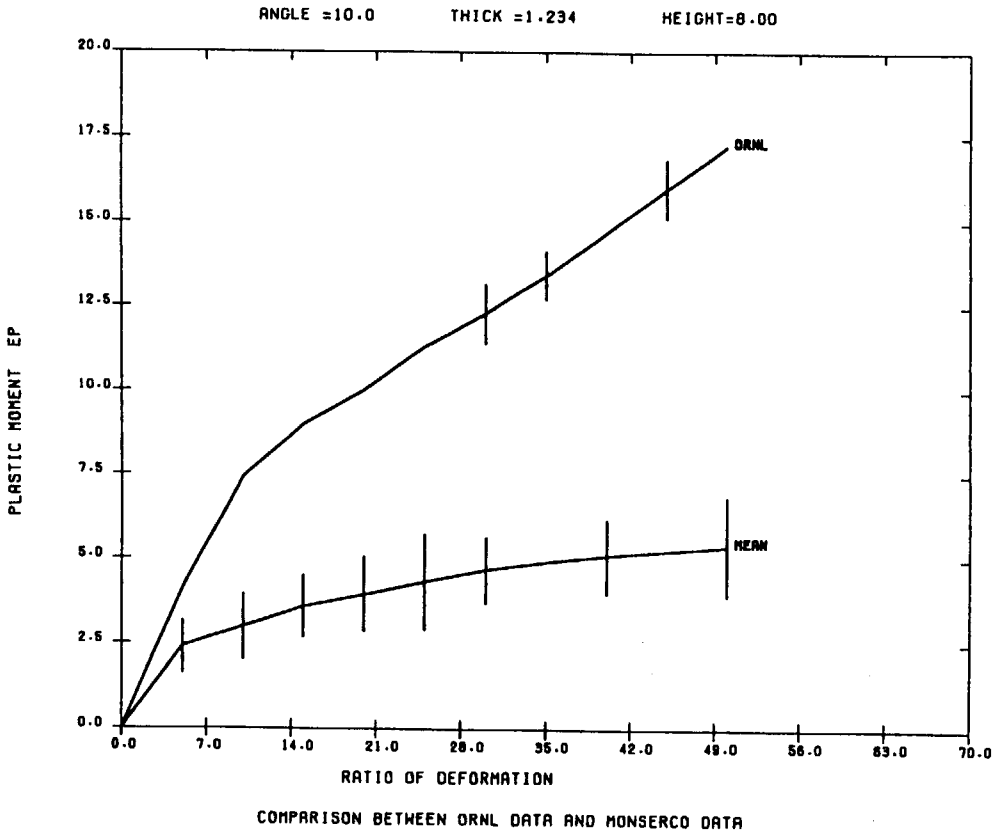

Fig. 9.15 Graphical Output of FINILB(13)

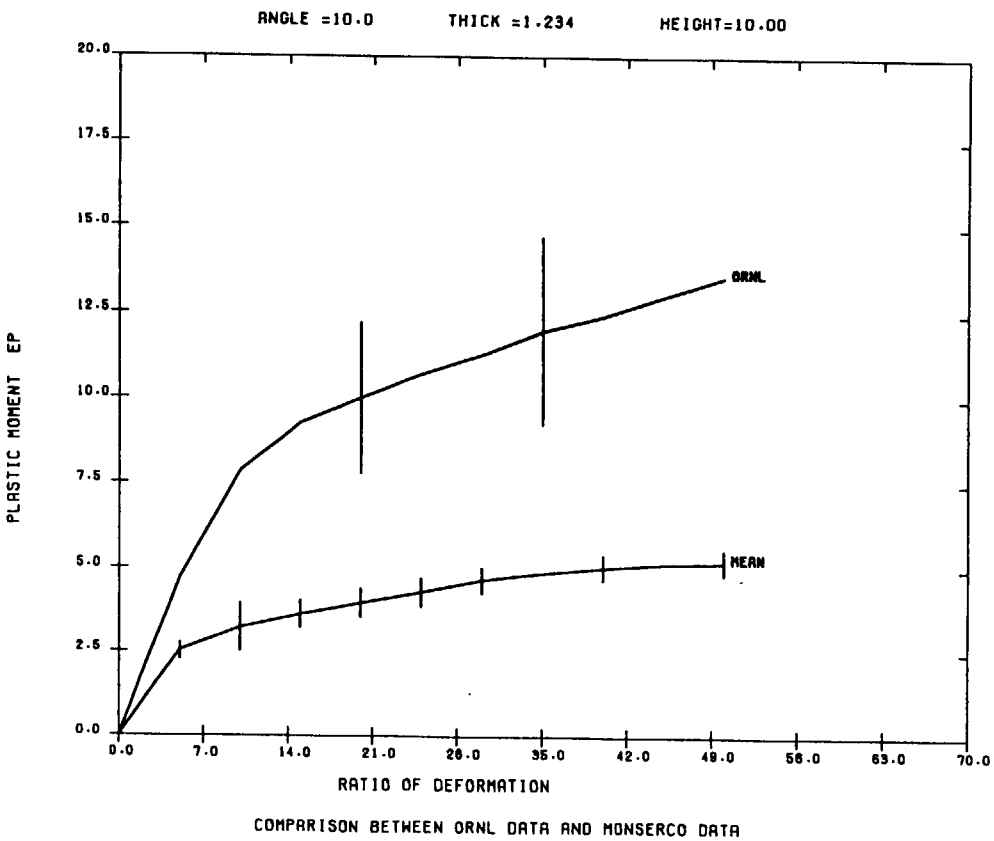

Fig. 9.16 Graphical Output of FINILB(14)

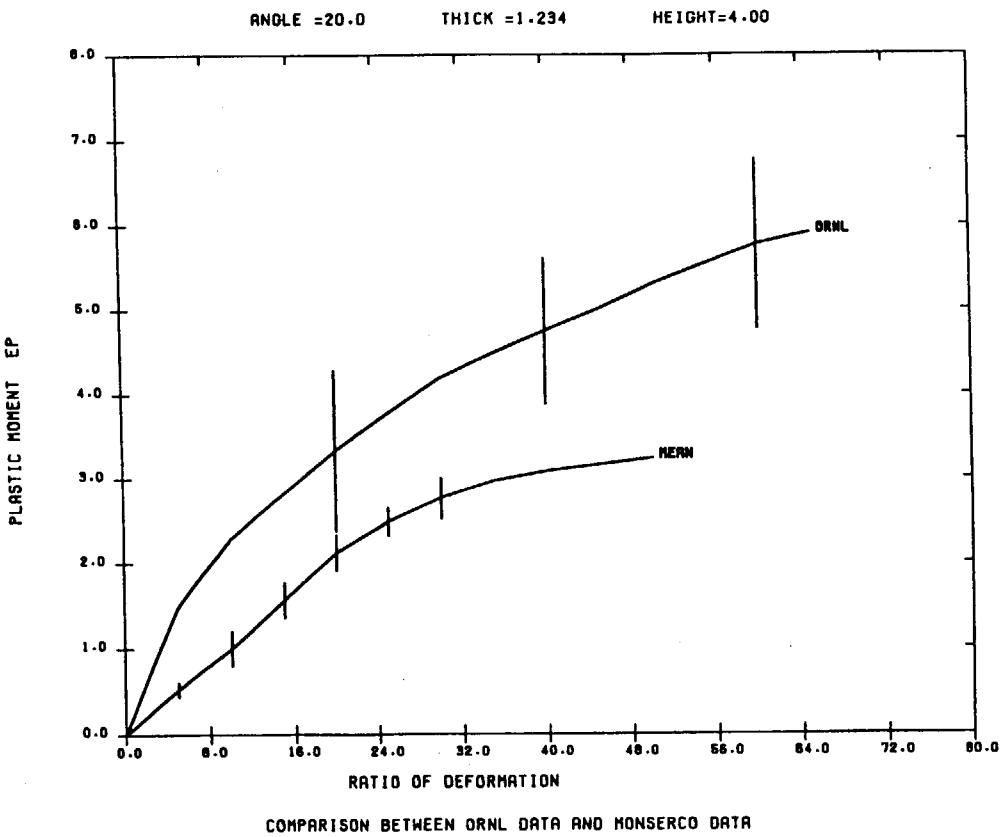

Fig. 9.17 Graphical Output of FINILB(15)

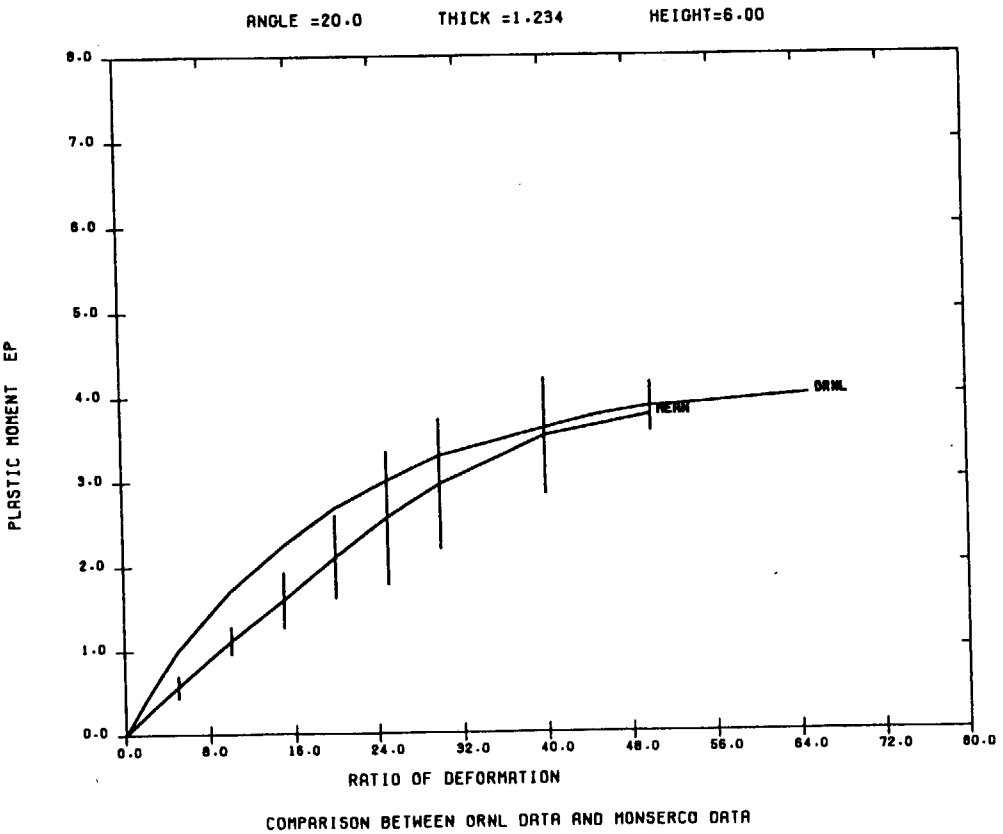

Fig. 9.18 Graphical Output of FINILB(16)

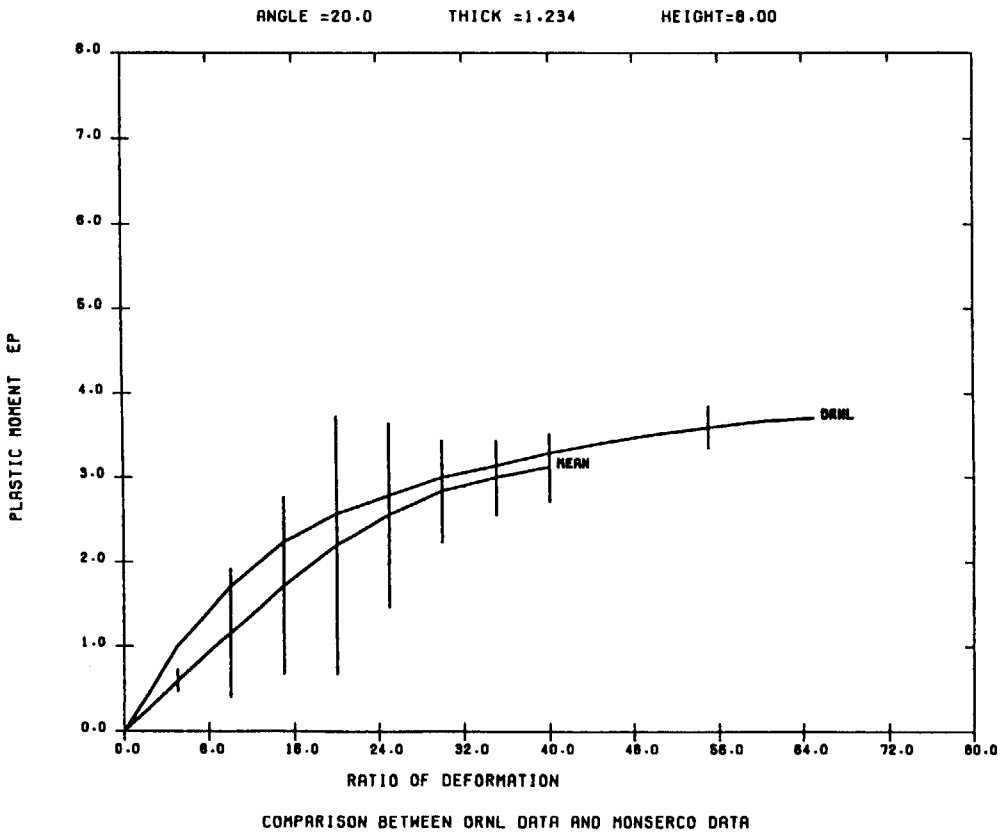

Fig. 9.19 Graphical Output of FINILB(17)

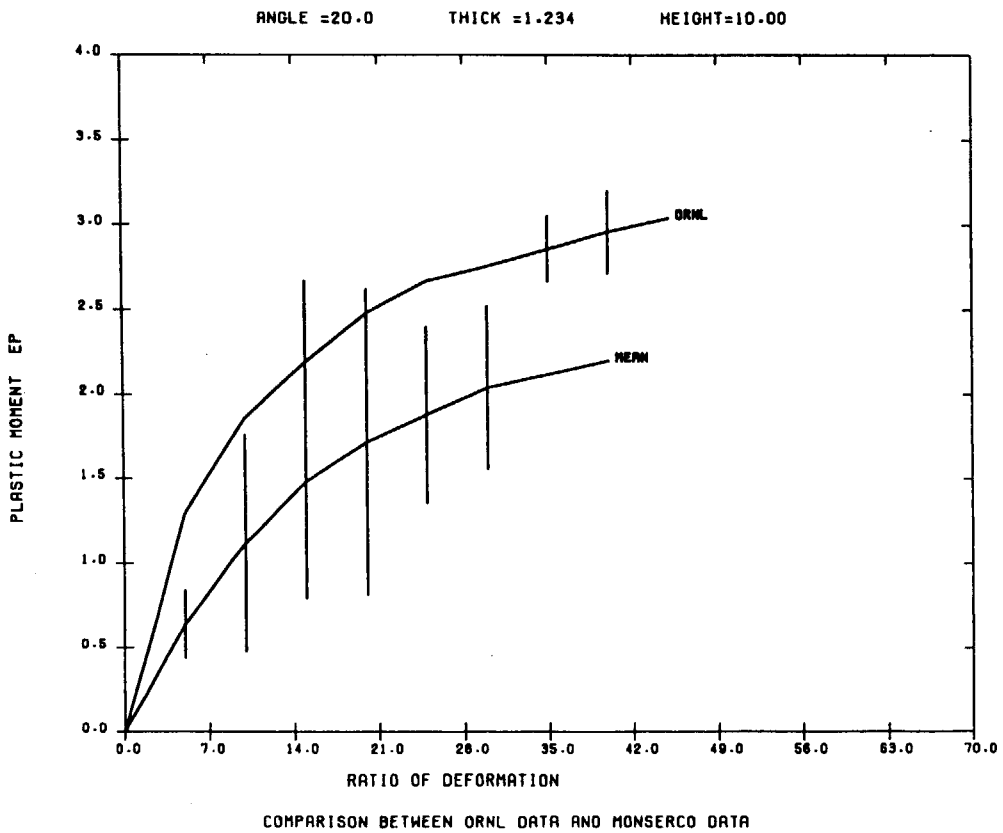

Fig. 9.20 Graphical Output of FINILB(18)

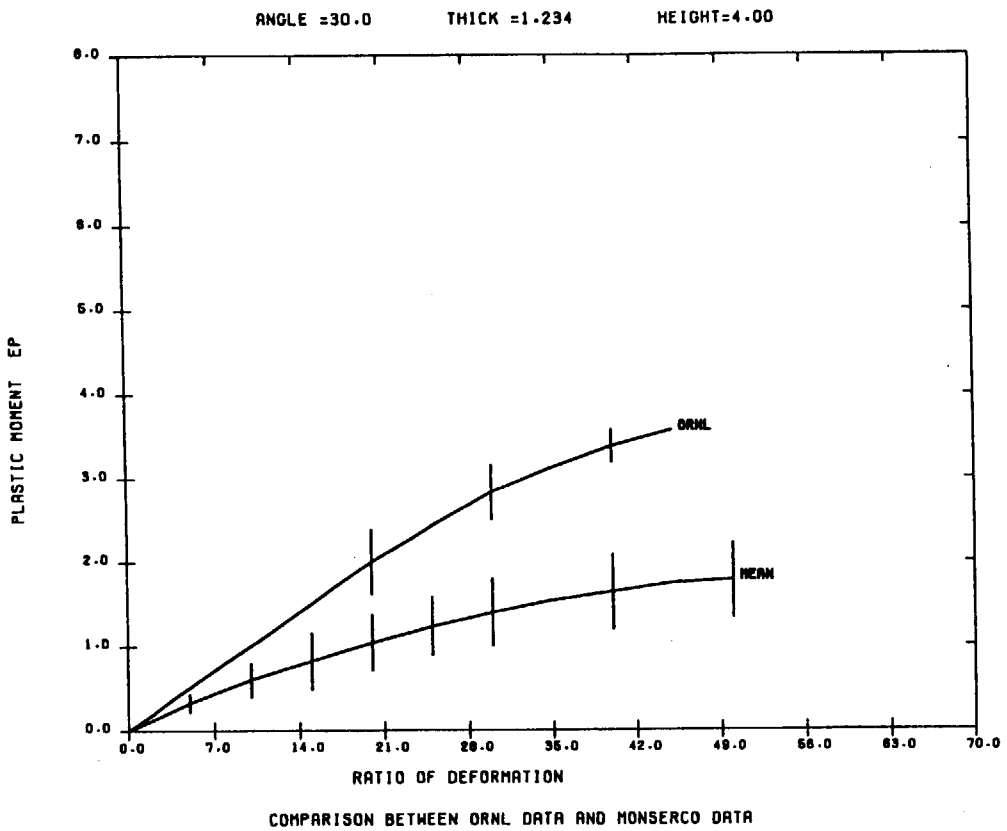

Fig. 9.21 Graphical Output of FINILB(19)

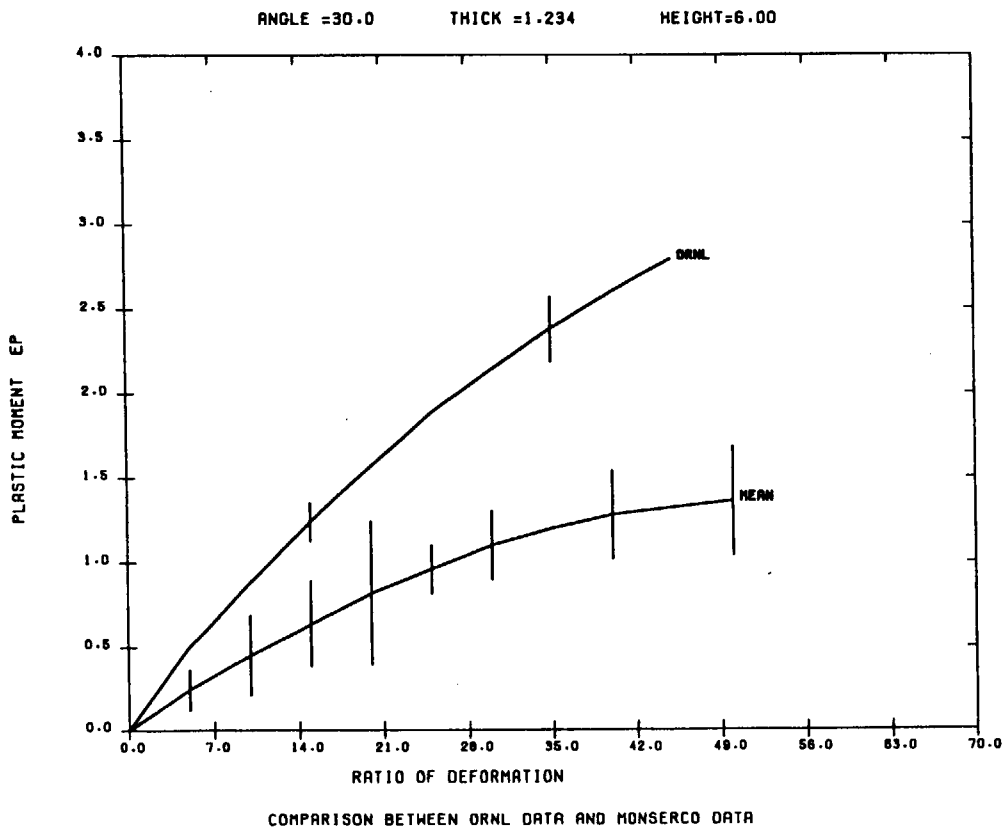

Fig. 9.22 Graphical Output of FINILB(20)

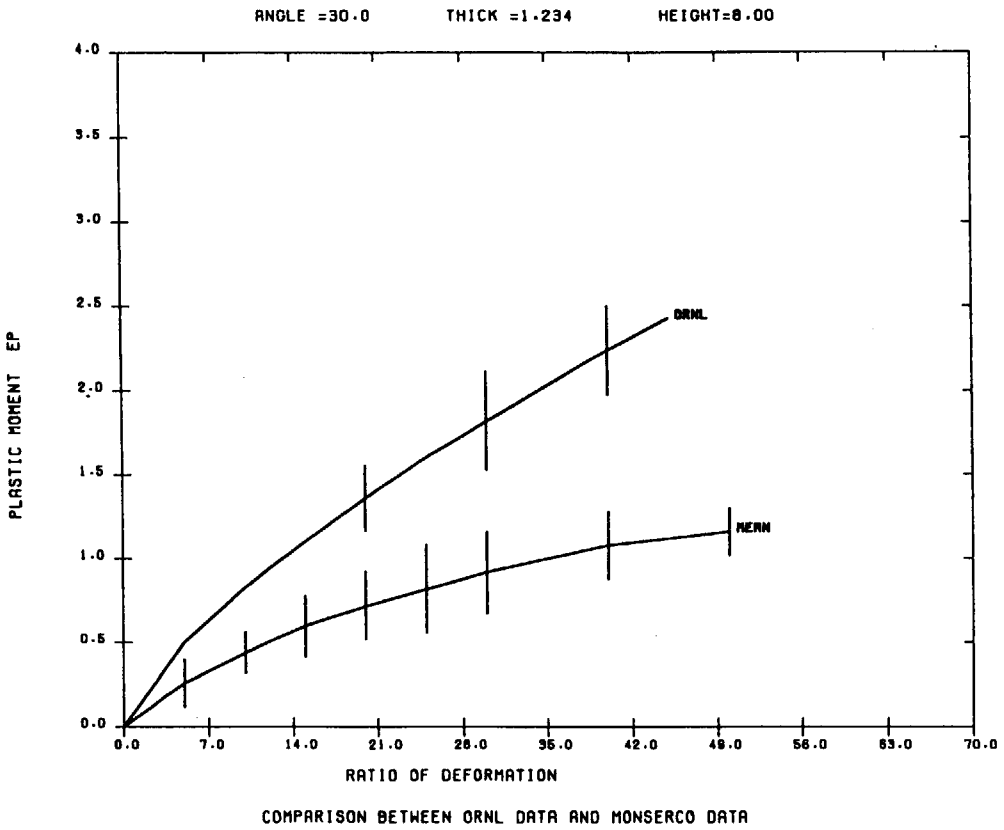

Fig. 9.23 Graphical Output of FINILB(21)

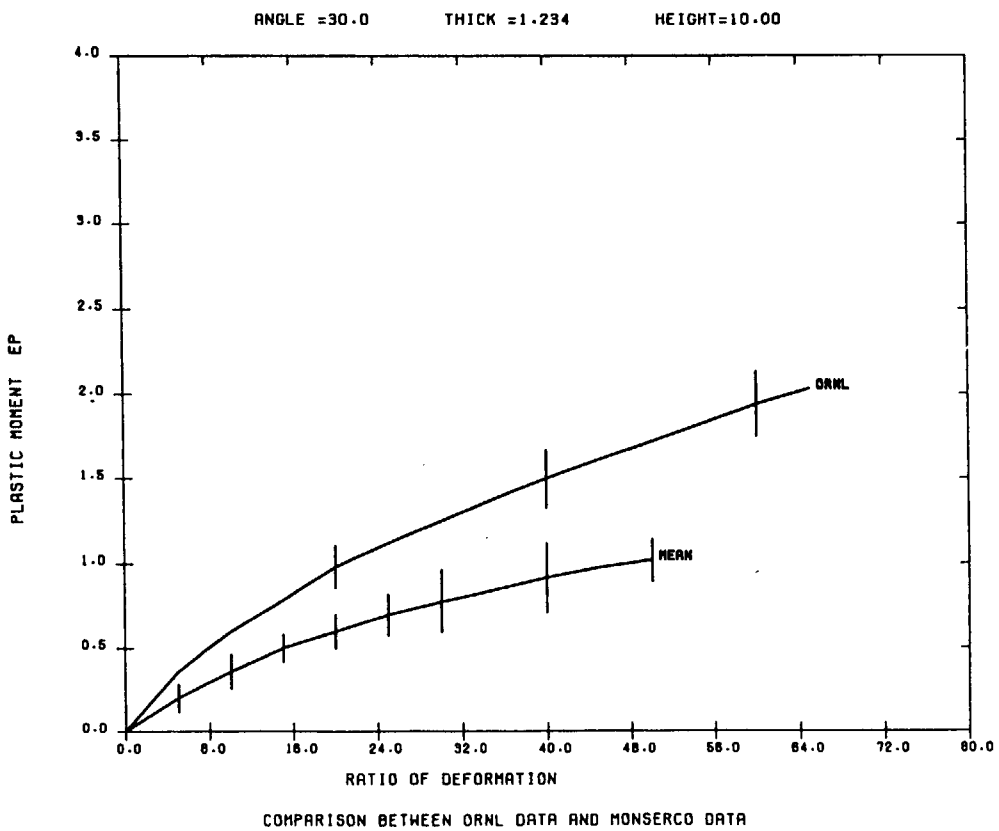

Fig. 9.24 Graphical Output of FINILB(22)

10. Conclusions

With regard to the evaluation of the maximum acceleration and deformation of the cask bodys in the case of the drop impact, the simplified computer code system CASKET will analyze it economically and save computer time as compared with the other detailed computer programs with a analysis method of dynamic interactions. The CASKET is further being utilized satisfactorily in safety analysis and designing not only spent fuel transport casks but also those for various radioactive transport casks.

Ackowledgements

The author is indebted to Dr. Kazuo Asada of Mitubishi Heavy Industries, Ltd. for providing the sample problems and valuable discussions. He is also indebted to Mr. Yutaka Hasegawa, Junji Oshika and Takashi Ishiwata of CRC Research Institute, Inc. for assistance of making the computer programs. Ackowledgments are due to Dr. Masatoshi Futakawa of Japan Atomic Energy Research Institute to review the articles and correcting the manuscripts.

References

(1) Halliquist, J. O., "User's Manual for DYNA2D - An Explicit Two-dimensional Hydro-dynamic Finite Element Code with Interactive Rezoning and Graphical Display", UCID-18756, Rev.3 (1988).

(2) Halliquist, J. O., "User's Manual for DYNA3D (Nonlinear Dynamic Analysis of Structures in Three Dimensions)", UCID-19592, Rev.5 (1989).

(3) Halliquist, J. O., "NIKE2D : An Implicit, Finite-Deformation, Finite Element Code with Analyzing the Static and Dynamic Response of Two-Dimensional Solids", UCID-52678 (1978).

(4) Halliquist, J. O., "NIKE3D : An Implicit, Finite-Deformation, Finite Element Code with Analyzing the Static and Dynamic Response of Three-Dimensional Solids", UCID-18822 (1981).

(5) Trigg, M., et al., "PISCES User's Manual", Physics International (1980).

(6) Key, S. W., Beisinger, Z. E. and Krieg. D., "HONDO II - A Finite Element Computer Program for the Large Deformation Dynamic Response of Axisymmetric Solids", SAND 78-0422 (1978).

(7) Ikushima, T. et al., "Simplified Computer Codes for Cask Impact Analysis", 10th Int. Symposium on the Packaging and Transportation of Radioactive Materials, pp.1419-1426, Japan(Yokohama) (1992).

(8) Ikushima, T., Ohshika, J. and Ishiwata, T., "Computer Codes System for Structural Analysis of Radioactive Materials Transport", 11th Int. symposium on the Packaging and Transportation of Radioactive Materials, pp.1174-1181, U.S.A(Las Vegas) (1995).

(9) Shapiro, A. B., "TOPAZ2D - A Two-Dimensional Finite Element Code for Heat Transfer Analysis, Electrostatic and Magnetostatic Problems", UCID-20824 (1986).

(10) Wilson, E. L., "SAP - A General Structural Analysis Program", SESM Report, Dept. of Civil Engineering, University of California, Berkeley, 70-20 (1970).

(11) Hallquist, J. O., "MAZE - An Input Generator for DYNA2D and NIKE2D", UCID-19029 Rev.1 (1982).

(12) Hallquist, J. O., "ORION - An Interactive Post-Processor for the Analysis Code, NIKE2D, DYNA2D and TACO2D", UCID-19310 (1982).

(13) Ikushima, T., "CRUSH1 : A Simplifed Computer Program for Impact Analysis of Radioactive Material Transport Casks", JAERI-Data/Code 96-025 (1996).

(14) Ikushima, T., "CRUSH2 : A Simplifed Computer Program for Impact Analysis of Radioactive Material Transport Casks", JAERI-Data/Code 97-001 (1997).

(15) Asada, K. et al.,"Development of Simplified Analysis Codes for Nine Meter Drop and One meter Puncture Tests for a Radioactive Material Transport Cask",Waste Management '88 (Tuscon) (1988).

(16) Ikushima, T., "FINCRUSH : A Computer Program for Impact Analysis of Radioactive Material Transport Cask with Fins", JAERI-Data/Code 97-018 (1997).

(17) Davis, F. C., "Structural Analysis of Shipping Casks, Vol.9: Energy Absorption Capabilities of Plastic Deformed Struts under Specified Loading Conditions", ORNL TM-1312 Vol.9 (1971).

(18) Torr, K. G., "Verification of the Performance of Impact Limiting Fins for Transportation Containers", INFO-0146 (1984).

(19) Torr, K. G., "Verification of the Performance of Impact Limiting Fins for Transportation Containers, Part-II", INFO-0146-2 (1986).

(20) Ikushima, T., "PUNCTURE : A Computer Program for Puncture Analysis of Radioactive Material Transport Casks", JAERI-Data/Code 97-036 (1997).

(21) Onat, E. T. and Haythornthwaite,R.M.,"The Load-Carrying Capacity of Circular Plates at Large Deflection",Trans. of ASME, Journal of Applied Mechanics,

(22) Larder, R. A. and Arthur, D., "Puncture of Shielded Radioactive Material Shipping Containers - Analysis and Results",NUREG/CR-0930 UCRL/52638 Vol.1 RT (1980).

(23) Saegusa, T., Ito, C., Imaeda, H., etal., "Cask Storage of Spent Fuel at Reactors", CRIEPI U27 (1993).

(24) Sirai, K. Ito, C. and Ryu, H., "Development of Seismic Response Analysis Code of Cask", 10th Int. Symposium on the Packaging and Transportation of Radioactive Materials, pp.1427-1434, Japan(Yokohama), (1992).

(25) Ikushima, T., "ROCKING : A Computer Program for Seismic Response Analysis of Radioactive Material Transport Casks", JAERI-Data/Code 95-017 (1995).

(26) Ikushima, T., "IMPACLIB : A Material Property Data Library for Impact Analysis of Radioactive Material Transport Casks", JAERI-Data/Code 97-049 (1997).

(27) Edwards, A. L., "TRUMP - Computer Program for Transient and Stesdy State Temperature Distributions in Multidimensional System", UCRL-14754 (1972).

(28) Turner, W. D., Elrod, D. C. and Siman-Toy, L. L., "HEATING5 - An IBM Heat Conduction Program", ORNL-CSD/TM-15 (1977).

(29) Elrod, D. C., Giles, G. E. and Turner, W. D., "HEATING6 - An Multi-dimensional Heat Conduction Analysis with the Finite-Difference Formulation", ORNL/NUREG/CSD-2/V2 (1986).

(30) Pilkey, W. et al. ed., "Structural Mechanics Computer Programs", University Press of Virginia (1986).

(31) Shapiro, A. B., "TOPAZ3D - A Three-Dimensional Finite Element Code", UCID-20481 (1985).

(32) Lawrence Livermore National Laboratory, "A Compilation of Thermal Property Data for Computer Heat-Conduction Calculations", UCRL-50589 (1968).

(33) Ikushima, T., "THERMLIB : A Material Property Data Library for Thermal Analysis of Radioactive Material Transport Cask with Fins", JAERI-Data/Code 98-009 (1998).

(34) Ikushima, T., "FINLIB : A Fin Energy Absorption Data Library for Impact Analysis of Radioactive Material Transport Cask with Fins", JAERI-Data/Code 97-035 (1997).

Appendix A Program Abstract

1. Name :

   CASKET.

2. Computer for which the program is designed and others upon which it is possible:

   FUJITSU-GS8400, SUN4 or IBM-PC.

3. Nature of physical problem solved:

   Computer code system for thermal structural analyses for radioactive material transport and/or storare cask

4. Method of solutions:

   -

5. Restrictions on the complexity of the problem:

   None.

6. Typical running time:

   FUJITSU-GS8400 : 10 seconds.
   SUN4 : 10 seconds.
   IBM-PC : 10 seconds.

7. Unusual features of the program:

   None.

8. Related and auxiliary program:

   None.

9. Status:

   -

10. References:

(1) Ikushima, T. et al.,"Simplified Computer Codes for Cask Impact Analysis", 10th Int. symposium on the Packaging and Transportation of Radioactive Materials, pp.1419-1426, Japan(Yokohama), (1992).

(2) Ikushima, T., Ohshika, J. and Ishiwata, T.,"Computer Codes System for Structural Analysis of Radioactive Materials Transport" , 11th Int. Symposium on the Packaging and Transportation of Radioactive Materials, pp.1174-1181, USA (Las Vegas) (1995).

(3) Shapiro, A. B., "TOPAZ : A Finite Element Heat Conduction Code for

Analyzing 2-D Solids", UCID-20045 (1984).

(4) Ikushima, T., "CRUSH1 : A Simplifed Computer Program for Impact Analysis of Radioactive Material Transport Casks", JAERI-Data/Code 96-025 (1996).

(5) Ikushima, T., "CRUSH2 : A Simplifed Computer Program for Impact Analysis of Radioactive Material Transport Casks", JAERI-Data/Code 97-001 (1997).

(6) Ikushima, T., "FINCRUSH : A Computer Program for Impact Analysis of Radioactive Material Transport Cask with Fins", JAERI-Data/Code 97-018 (1997).

(7) Ikushima, T., "PUNCTURE : A Computer Program for Puncture Analysis of Radioactive Material Transport Casks", JAERI-Data/Code 97-036 (1997).

(8) Ikushima, T., "ROCKING : A Computer Program for Seismic Response Analysis of Radioactive Material Transport Casks", JAERI-Data/Code 95-017 (1995).

(9) Ikushima, T., "IMPACLIB : A Material Property Data Library for Impact Analysis of Radioactive Material Transport Casks", JAERI-Data/Code 97-049 (1997).

(10) Lawrence Radiation Laboratory, "A Compilation of Thermal Property Data for Computer Heat-Conduction Calculations", UCRL-50589 (1968).

(11) Ikushima, T., "THERMLIB : A Material Property Data Library for Thermal Analysis of Radioactive Material Transport Cask with Fins", JAERI-Data/Code 98-009 (1998).

(12) Ikushima, T., "FINLIB : A Fin Energy Absorption Data Library for Impact Analysis of Radioactive Material Transport Cask with Fins", JAERI-Data/Code 97-035 (1997).

11.Machine requirement:

Required 1100 k bytes of core memory.

12.Program language used:

FORTRAN-77.

13.Operating system or monitor under which the program is executed:

FUJITSU-GS8400 : MSP.

SUN4 : Solaris 2.1.

IBM PC : Windows 3.1.

14.Any other programming or operating information or restrictions:

The program is approximately 25000 source steps (including data libraries and).

The graphical programs are as follows:

FUJITSU-GS8400 : CALCOMP plotter or the compatible ones.

SUN4 : X-windows.

IBM PC : windows 3.1.

15.Name and establishment of author:

T. Ikushima

Japan Atomic Energy Research Institute,

Tokai Research Establishment,

Department of Fuel Cycle Safety Research,

Tokai-mura, Naka-gun, Ibaraki-ken, 319-1195

Japan

16.Material available:

Program source and data library.

This is a blank page.

国際単位系 (SI) と換算表

表 1　SI 基本単位および補助単位

量	名称	記号
長さ	メートル	m
質量	キログラム	kg
時間	秒	s
電流	アンペア	A
熱力学温度	ケルビン	K
物質量	モル	mol
光度	カンデラ	cd
平面角	ラジアン	rad
立体角	ステラジアン	sr

表 2　SI と併用される単位

名称	記号
分，時，日	min，h，d
度，分，秒	°，′，″
リットル	l，L
トン	t
電子ボルト	eV
原子質量単位	u

$1\ \mathrm{eV} = 1.60218 \times 10^{-19}\ \mathrm{J}$

$1\ \mathrm{u} = 1.66054 \times 10^{-27}\ \mathrm{kg}$

表 5　SI 接頭語

倍数	接頭語	記号
10^{18}	エクサ	E
10^{15}	ペタ	P
10^{12}	テラ	T
10^{9}	ギガ	G
10^{6}	メガ	M
10^{3}	キロ	k
10^{2}	ヘクト	h
10^{1}	デカ	da
10^{-1}	デシ	d
10^{-2}	センチ	c
10^{-3}	ミリ	m
10^{-6}	マイクロ	μ
10^{-9}	ナノ	n
10^{-12}	ピコ	p
10^{-15}	フェムト	f
10^{-18}	アト	a

表 3　固有の名称をもつ SI 組立単位

量	名称	記号	他の SI 単位による表現
周波数	ヘルツ	Hz	s^{-1}
力	ニュートン	N	$m \cdot kg/s^2$
圧力，応力	パスカル	Pa	N/m^2
エネルギー，仕事，熱量	ジュール	J	N·m
工率，放射束	ワット	W	J/s
電気量，電荷	クーロン	C	A·s
電位，電圧，起電力	ボルト	V	W/A
静電容量	ファラド	F	C/V
電気抵抗	オーム	Ω	V/A
コンダクタンス	ジーメンス	S	A/V
磁束	ウェーバ	Wb	V·s
磁束密度	テスラ	T	Wb/m^2
インダクタンス	ヘンリー	H	Wb/A
セルシウス温度	セルシウス度	℃	
光束	ルーメン	lm	cd·sr
照度	ルクス	lx	lm/m^2
放射能	ベクレル	Bq	s^{-1}
吸収線量	グレイ	Gy	J/kg
線量当量	シーベルト	Sv	J/kg

表 4　SI と共に暫定的に維持される単位

名称	記号
オングストローム	Å
バーン	b
バール	bar
ガル	Gal
キュリー	Ci
レントゲン	R
ラド	rad
レム	rem

$1\ \mathrm{Å} = 0.1\ \mathrm{nm} = 10^{-10}\ \mathrm{m}$

$1\ \mathrm{b} = 100\ \mathrm{fm}^2 = 10^{-28}\ \mathrm{m}^2$

$1\ \mathrm{bar} = 0.1\ \mathrm{MPa} = 10^5\ \mathrm{Pa}$

$1\ \mathrm{Gal} = 1\ \mathrm{cm/s}^2 = 10^{-2}\ \mathrm{m/s}^2$

$1\ \mathrm{Ci} = 3.7 \times 10^{10}\ \mathrm{Bq}$

$1\ \mathrm{R} = 2.58 \times 10^{-4}\ \mathrm{C/kg}$

$1\ \mathrm{rad} = 1\ \mathrm{cGy} = 10^{-2}\ \mathrm{Gy}$

$1\ \mathrm{rem} = 1\ \mathrm{cSv} = 10^{-2}\ \mathrm{Sv}$

（注）

1. 表 1 − 5 は「国際単位系」第 5 版，国際度量衡局 1985 年刊行による。ただし，1 eV および 1 u の値は CODATA の 1986 年推奨値によった。
2. 表 4 には海里，ノット，アール，ヘクタールも含まれているが日常の単位なのでここでは省略した。
3. bar は，JIS では流体の圧力を表わす場合に限り表 2 のカテゴリーに分類されている。
4. EC 閣僚理事会指令では bar，barn および「血圧の単位」mmHg を表 2 のカテゴリーに入れている。

換　算　表

力	N(=10^5dyn)	kgf	lbf
	1	0.101972	0.224809
	9.80665	1	2.20462
	4.44822	0.453592	1

粘　度　1 Pa·s(N·s/m^2)=10 P(ポアズ)(g/(cm·s))

動粘度　1 m^2/s=10^4St(ストークス)(cm^2/s)

圧力	MPa(=10 bar)	kgf/cm^2	atm	mmHg(Torr)	lbf/in^2(psi)
	1	10.1972	9.86923	7.50062×10^3	145.038
	0.0980665	1	0.967841	735.559	14.2233
	0.101325	1.03323	1	760	14.6959
	1.33322×10^{-4}	1.35951×10^{-3}	1.31579×10^{-3}	1	1.93368×10^{-2}
	6.89476×10^{-3}	7.03070×10^{-2}	6.80460×10^{-2}	51.7149	1

エネルギー・仕事・熱量	J(=10^7erg)	kgf·m	kW·h	cal(計量法)	Btu	ft·lbf	eV
	1	0.101972	2.77778×10^{-7}	0.238889	9.47813×10^{-4}	0.737562	6.24150×10^{18}
	9.80665	1	2.72407×10^{-6}	2.34270	9.29487×10^{-3}	7.23301	6.12082×10^{19}
	3.6×10^6	3.67098×10^5	1	8.59999×10^5	3412.13	2.65522×10^6	2.24694×10^{25}
	4.18605	0.426858	1.16279×10^{-6}	1	3.96759×10^{-3}	3.08747	2.61272×10^{19}
	1055.06	107.586	2.93072×10^{-4}	252.042	1	778.172	6.58515×10^{21}
	1.35582	0.138255	3.76616×10^{-7}	0.323890	1.28506×10^{-3}	1	8.46233×10^{18}
	1.60218×10^{-19}	1.63377×10^{-20}	4.45050×10^{-26}	3.82743×10^{-20}	1.51857×10^{-22}	1.18171×10^{-19}	1

1 cal = 4.18605 J（計量法）
= 4.184 J　（熱化学）
= 4.1855 J　（15 °C）
= 4.1868 J（国際蒸気表）

仕事率　1 PS（仏馬力）
= 75 kgf·m/s
= 735.499 W

放射能	Bq	Ci
	1	2.70270×10^{-11}
	3.7×10^{10}	1

吸収線量	Gy	rad
	1	100
	0.01	1

照射線量	C/kg	R
	1	3876
	2.58×10^{-4}	1

線量当量	Sv	rem
	1	100
	0.01	1

（86 年 12 月 26 日現在）

CASKET:A COMPUTER CODE SYSTEM FOR THERMAL AND STRUCTURAL ANALYSES OF RADIOACTIVE MATERIAL TRANSPORT AND/OR STORAGE CASK